THE 6TH INTERNATIONAL WORKSHOP ON SIMULATION FOR ENERGY, SUSTAINABLE DEVELOPMENT & ENVIRONMENT

SEPTEMBER 17 - 19 2018
BUDAPEST, HUNGARY

EDITED BY
AGOSTINO BRUZZONE
JANOS SEBESTYEN JANOSY
LETIZIA NICOLETTI
GREGORY ZACHAREWICZ

PRINTED IN RENDE (CS), ITALY, SEPTEMBER 2018

ISBN 978-88-85741-17-1 (Paperback)
ISBN 978-88-85741-16-4 (PDF)

ISBN 978-88-85741-17-1 (Paperback)
ISBN 978-88-85741-16-4 (PDF)

THE 6TH INTERNATIONAL WORKSHOP ON SIMULATION FOR ENERGY, SUSTAINABLE DEVELOPMENT & ENVIRONMENT, SESDE 2018

SEPTEMBER 17 - 19 2018

BUDAPEST, HUNGARY

ORGANIZED BY

DIME – UNIVERSITY OF GENOA

LIOPHANT SIMULATION

SIMULATION TEAM

IMCS – INTERNATIONAL MEDITERRANEAN & LATIN AMERICAN COUNCIL OF SIMULATION

DIMEG, UNIVERSITY OF CALABRIA

MSC-LES, MODELING & SIMULATION CENTER, LABORATORY OF ENTERPRISE SOLUTIONS

HUNGARIAN ACADEMY OF SCIENCES CENTRE FOR ENERGY RESEARCH

AUTONOMOUS UNIVERSITY OF BARCELONA

MODELING AND SIMULATION CENTER OF EXCELLENCE (MSCOE)

LATVIAN SIMULATION CENTER – RIGA TECHNICAL UNIVERSITY

LOGISIM

LSIS – LABORATOIRE DES SCIENCES DE L'INFORMATION ET DES SYSTEMES

MIMOS – MOVIMENTO ITALIANO MODELLAZIONE E SIMULAZIONE

MITIM PERUGIA CENTER – UNIVERSITY OF PERUGIA

ISBN 978-88-85741-16-4; Bruzzone, Janosy, Nicoletti and Zacharewicz Eds.

BRASILIAN SIMULATION CENTER, LAMCE-COPPE-UFRJ

MITIM - MCLEOD INSTITUTE OF TECHNOLOGY AND INTEROPERABLE MODELING AND SIMULATION – GENOA CENTER

M&SNET - MCLEOD MODELING AND SIMULATION NETWORK

LATVIAN SIMULATION SOCIETY

ECOLE SUPERIEURE D'INGENIERIE EN SCIENCES APPLIQUEES

FACULTAD DE CIENCIAS EXACTAS. INGEGNERIA Y AGRIMENSURA

UNIVERSITY OF LA LAGUNA

CIFASIS: CONICET-UNR-UPCAM

INSTICC - INSTITUTE FOR SYSTEMS AND TECHNOLOGIES OF INFORMATION, CONTROL AND COMMUNICATION

NATIONAL RUSSIAN SIMULATION SOCIETY

CEA - IFAC

UNIVERSITY OF BORDEAUX

UNIVERSITY OF CYPRUS

DUTCH BENELUX SIMULATION SOCIETY

I3M 2018 INDUSTRIAL SPONSORS

CAL-TEK SRL

LIOTECH LTD

MAST SRL

SIM-4-FUTURE

ISBN 978-88-85741-16-4; Bruzzone, Janosy, Nicoletti and Zacharewicz Eds.

I3M 2018 MEDIA PARTNERS

INDERSCIENCE PUBLISHERS – INTERNATIONAL JOURNAL OF SIMULATION AND PROCESS MODELING

INDERSCIENCE PUBLISHERS – INTERNATIONAL JOURNAL OF SERVICE AND COMPUTING ORIENTED MANUFACTURING

IGI GLOBAL – INTERNATIONAL JOURNAL OF PRIVACY AND HEALTH INFORMATION MANAGEMENT (IJPHIM)

HALLDALE MEDIA GROUP: THE MILITARY SIMULATION AND TRAINING MAGAZINE

HALLDALE MEDIA GROUP: THE JOURNAL FOR HEALTHCARE EDUCATION, SIMULATION AND TRAINING

SAGE
SIMULATION TRANSACTION OF SCS

DE GRUYTER
INTERNATIONAL JOURNAL OF FOOD ENGINEERING

MDPI - SUSTAINABILITY

EUROMERCI: THE ITALIAN MONTHLY LOGISTICS JOURNAL

ISBN 978-88-85741-16-4; Bruzzone, Janosy, Nicoletti and Zacharewicz Eds.

EDITORS

AGOSTINO BRUZZONE
MITIM-DIME, UNIVERSITY OF GENOA, ITALY
agostino@itim.unige.it

JANOS SEBESTYEN JANOSY
MTA EK CENTRE FOR ENERGY RESEARCH HUNGARIAN ACADEMY OF SCIENCES, HUNGARY
Janos.S.Janosy@energia.mta.hu

LETIZIA NICOLETTI
CAL-TEK SRL
l.nicoletti@cal-tek.eu

GREGORY ZACHAREWICZ
IMS UNIVERSITÉ BORDEAUX 1, FRANCE
Gregory.zacharewicz@ims-bordeaux.fr

ISBN 978-88-85741-16-4; Bruzzone, Janosy, Nicoletti and Zacharewicz Eds.

THE INTERNATIONAL MULTIDISCIPLINARY MODELING AND SIMULATION MULTICONFERENCE, I3M 2018

GENERAL CO-CHAIRS

AGOSTINO BRUZZONE, *MITIM DIME, UNIVERSITY OF GENOA, ITALY*
MIQUEL ANGEL PIERA, *AUTONOMOUS UNIVERSITY OF BARCELONA, SPAIN*

PROGRAM CO-CHAIRS

FRANCESCO LONGO, *DIMEG, UNIVERSITY OF CALABRIA, ITALY*
YURY MERKURYEV, *RIGA TECHNICAL UNIVERSITY, LATVIA*

THE 6TH INTERNATIONAL WORKSHOP ON SIMULATION FOR ENERGY, SUSTAINABLE DEVELOPMENT & ENVIRONMENT, SESDE 2018

GENERAL CO- CHAIRS

JANOS SEBESTYEN JANOSY, *MTA EK CENTRE FOR ENERGY RESEARCH HUNGARIAN ACADEMY OF SCIENCES, HUNGARY*
GREGORY ZACHAREWICZ, *IMS UNIVERSITÉ BORDEAUX 1, FRANCE*

PROGRAM CHAIR

LETIZIA NICOLETTI, CAL-TEK SRL, ITALY

ISBN 978-88-85741-16-4; Bruzzone, Janosy, Nicoletti and Zacharewicz Eds.

SESDE 2018 INTERNATIONAL PROGRAM COMMITTEE

MICHAEL AFFENZELLER, *UPPER AUSTRIA UAS, AUSTRIA*
MATTEO AGRESTA, *UNIVERSITY OF GENOA, ITALY*
EMRE ARTUN, *MIDDLE EAST TECHNICAL UNIVERSITY, CYPRUS*
AGOSTINO BRUZZONE, *UNIVERSITY OF GENOA, ITALY*
DANIEL BUCHBINDER, *ALTERNA, GUATEMALA*
CATERINA FUSTO, *UNIVERSITY OF CALABRIA, ITALY*
RICCARDO DI MATTEO, *UNIVERSITY OF GENOA, ITALY*
STEPHAN HUTTERER, *UPPER AUSTRIA UNIVERSITY OF APPLIED SCIENCES, AUSTRIA*
JANOS SEBESTYEN JANOSY, *MTA EK CENTRE FOR ENERGY RESEARCH HUNGARIAN ACADEMY OF SCIENCES, HUNGARY*
MASSIMO LA SCALA, POLYTECHNIC UNIVERSITY OF BARI, ITALY
LUIS LE MOYNE, *UNIVERSITY OF BOURGOGNE, FRANCE*
ARNIS LEKTAUERS, *RIGA TECHNICAL UNIVERSITY, LATVIA*
FRANCESCO LONGO, *UNIVERSITY OF CALABRIA, ITALY*
GIANLUCA MAGLIONE, *UNIVERSITY OF GENOA, ITALY*
MARINA MASSEI, *UNIVERSITY OF GENOA, ITALY*
LETIZIA NICOLETTI, *CAL-TEK SRL, ITALY*
ANTONIO PADOVANO, *UNIVERSITY OF CALABRIA, ITALY*
M.R. RIAZI, *UNIVERSITY OF KUWAIT , KUWAIT*
GREGORY ZACHAREWICZ, *IMS UNIVERSITÉ BORDEAUX 1, FRANCE*

TRACKS AND WORKSHOP CHAIRS

TRANSPORTATIONS
CO-CHAIRS: ARNIS LEKTAUERS, RIGA TECHNICAL UNIVERSITY. LATVIA; LUIS LE MOYNE, UNIVERSITY OF BOURGOGNE, FRANCE

SMART GRID PLANNING, OPTIMIZATION AND CONTROL - SPOC
CHAIRS: MICHAEL AFFENZELLER, UPPER AUSTRIA UNIVERSITY OF APPLIED SCIENCES, AUSTRIA; STEPHAN HUTTERER, UPPER AUSTRIA UNIVERSITY OF APPLIED SCIENCES, AUSTRIA

SUSTAINABLE LAND USE AND TRANSPORT ADOPTING M&S
CHAIR: DANIEL BUCHBINDER, ALTERNA, GUATEMALA

CONSUMERISM
CHAIR: DANIEL BUCHBINDER, ALTERNA, GUATEMALA

SUSTAINABILITY
CHAIR: DANIEL BUCHBINDER, ALTERNA, GUATEMALA

SIMULATION AND MODELING IN THE HYDROCARBON INDUSTRY
CHAIRS: M. R. RIAZI, KUWAIT UNIVERSITY (KUWAIT); EMRE ARTUN, MIDDLE EAST TECHNICAL UNIVERSITY, NORTHERN CYPRUS CAMPUS, CYPRUS

ISBN 978-88-85741-16-4; Bruzzone, Janosy, Nicoletti and Zacharewicz Eds.

WELCOME MESSAGE 2018

These words cover a very broad and difficult topic addressing the most severe problem of our age. Thanks to our scientific and technological development, we are now probably capable already to completely destroy our environment: the ecosystem of our Earth, where our children and grandchildren should grow up and thrive.
As I was born, there were around 2 billion people on the Earth. Now we approaching 8 billion. Overpopulation is just one cause: we are even per capita consuming too much at the same time. This year all the renewable resources provided per year by our globe were completely consumed up already before September.
We are accustomed to the relatively cheap energy. All the electrical energy generated for a Hungarian family of four is equivalent to the physical work of around 50 slaves. One kWh energy equivalent to lifting 3600 times close to 100 kg weight to the height of 1 meter. We pay for this work around 10 eurocents. The most in Europe: 30 eurocents. In the meantime it looks like that the climate change really has been started already.
Something has to be done. Scientist should show the present situation in detail to the population in order to comprehend: where this approach leads. We should find ways to overcome the troubles of the present situation and to assist to the inconvenient and tiresome changes we should encounter.
We got nine excellent papers from eight countries including China and Mexico. It seems not too much but already something to consider and think over. New methods and technologies helps us to reduce the need and consumption of fossil fuels. New methods are to be worked out to find the way out of this situation.
The only way to show the possible solutions: simulation. Modeling and simulation. Tools that already became indispensable. Modeling should help us to understand the „what and how", and simulation shows „where that leads".
I wish a good stay with us in Budapest, on the Margarethe Island, in the middle of the Danube river, on the shores of which everything happens in Budapest.

Janos Sebestyen Janosy

MTA EK Centre for Energy Research Hungarian Academy of Sciences, Hungary

Gregory Zacharewicz

Ims Université Bordeaux 1 France

Letizia Nicoletti

Cal-Tek Srl, Italy

ISBN 978-88-85741-16-4; Bruzzone, Janosy, Nicoletti and Zacharewicz Eds.

ACKNOWLEDGEMENTS

The SESDE 2018 International Program Committee (IPC) has selected the papers for the Conference among many submissions; therefore, based on this effort, a very successful event is expected. The SESDE 2018 IPC would like to thank all the authors as well as the reviewers for their invaluable work.
A special thank goes to Prof. Miquel Angel Piera from Autonomous University of Barcelona, as Local Organizer and to all the organizations, institutions and societies that have supported and technically sponsored the event.

I3M 2018 INTERNAL STAFF

MATTEO AGRESTA, *SIMULATION TEAM, ITALY*
AGOSTINO G. BRUZZONE, *DIME, UNIVERSITY OF GENOA, ITALY*
ALESSANDRO CHIURCO, *DIMEG, UNIVERSITY OF CALABRIA, ITALY*
RICCARDO DI MATTEO, *SIMULATION TEAM, ITALY*
JESSICA FRANGELLA, *CAL-TEK SRL, ITALY*
CATERINA FUSTO, *DIMEG, UNIVERSITY OF CALABRIA, ITALY*
LUCIA GAZZANEO, *DIMEG, UNIVERSITY OF CALABRIA, ITALY*
FRANCESCO LONGO, *DIMEG, UNIVERSITY OF CALABRIA, ITALY*
MARINA MASSEI, *DIME, UNIVERSITY OF GENOA, ITALY*
LETIZIA NICOLETTI, *CAL-TEK SRL, ITALY*
ANTONIO PADOVANO, *DIMEG, UNIVERSITY OF CALABRIA, ITALY*
ANTONIO REDA, *CAL-TEK SRL, ITALY*
CATALDO RUSSO, *CAL-TEK SRL, ITALY*
KIRILL SINELSHCHIKOV, *SIMULATION TEAM, ITALY*
CARMINE TOTERA, *CAL-TEK SRL, ITALY*
MARCO VETRANO, *CAL-TEK SRL, ITALY*
BEATRICE ZACCARO, *SIMULATION TEAM, ITALY*

ISBN 978-88-85741-16-4; Bruzzone, Janosy, Nicoletti and Zacharewicz Eds.

This International Workshop is part of the I3M Multiconference: the Congress leading **Simulation around the World and Along the Years**

ISBN 978-88-85741-16-4; Bruzzone, Janosy, Nicoletti and Zacharewicz Eds.

Index

ISBN 978-88-85741-16-4; Bruzzone, Janosy, Nicoletti and Zacharewicz Eds.

MODELLING OF A SOLAR AIR CONDITIONING PILOT PLANT

S. Lugo[(a)] and W. Rivera[(b)]

[(a),(b)]Instituto de Energías Renovables, Universidad Nacional Autónoma de México, Temixco, Morelos, México.

[(a)]Email: sulu@ier.unam.mx, [(b)]Email: wrgf@ier.unam.mx

ABSTRACT

The present work repots the modelling of a solar air conditioning pilot plant to be installed in the Centro de Tecnología Avanzada (CIATEQ) in the city of Queretaro, México. The modelling was carried out by using the software *Transient System Simulation Tool-16* (TRNSYS-16). The pilot plant mainly consists of an absorption cooling system, a solar collector's field, a hot water storage tank, a cooling tower and an air handler. The office of the CIATEQ were first modelling without an air conditioning unit and then with the proposed solar air conditioning pilot plant. The results showed that without air conditioning, temperatures higher than 28 ºC can be reached between the 12:00 and the 19:00 hours during spring and summer, while with the proposed pilot plant temperatures not higher than 25 ºC can be obtained during the whole year during the working hours.

Keywords: solar cooling, solar air conditioning, absorption systems, ammonia-lithium nitrate

1. INTRODUCTION

Currently, many industries worldwide deliver waste heat to the atmosphere at low temperatures reducing with this the efficiency of the plant. The BCS of the U. S. Department of Energy (2008), estimated that just in the USA the unrecovered waste heat is 900 Trillion Btu/year at low temperatures. Absorption cooling systems (ACS) are some of the most attractive systems to recover industrial waste heat, because absorption systems consume negligible amounts of primary energy. Also, ACS may operate with renewable energies, such as solar or geothermal. According to Abdullah and Hieng (2010), in general, ACS uses natural refrigerants as water or ammonia, which do not contribute to global warming or ozone depletion.

Up to now, ammonia/water and water/lithium bromide have been the most used mixtures in ACS since they possess great advantages; however, they have some well-known disadvantages. According to the literature reviews carried out by Best and Rivera (2015) and Rivera et al. (2015), the ammonia/lithium nitrate mixture possesses some advantages over the conventional ones. For instance, contrary to the systems operating with ammonia/water, absorption systems operating with an ammonia/lithium nitrate mixture do not require a rectifier and may operate at lower generator temperatures and higher condensation temperatures and achieve higher coefficients of performance, as reported by Wu et al. (2012), and Boman et al. (2017). On the other hand, systems operating with an ammonia/lithium nitrate mixture do not operate in vacuum conditions such as the systems operating with water/lithium bromide mixture do. For cooling applications, the proposed mixture may be used for air conditioning and refrigeration, while water/lithium bromide can be only used for air conditioning since water is the refrigerant and is limited to operating at temperatures greater than 0°C.

Some of the relevant studies related to solar absorption cooling systems using the ammonia/lithium nitrate mixture are the following:

Wang et al. (2000) reported the results of an improved absorption refrigeration system operating with ammonia-lithium nitrate that uses a series of absorbers, among which one absorber is cooled by the external medium and the other absorbers are cooled by refrigerant at staged pressures between the evaporation and condensation pressures. The system was able to operate at temperatures as low as 65°C and produce refrigeration temperatures as low as -40°C. Rivera et al. (2011), developed an intermittent solar absorption refrigeration system operating with the $NH_3/LiNO_3$ mixture using a cylindrical parabolic collector instead a typical generator to provide the energy to the system and to produce the refrigerant, simultaneously. The system operated at generation temperatures between 75°C and 110°C and achieved evaporator temperatures as low as -11°C. The authors reported that the proposed system can produce as much as 8 kg of ice per day. Moreno-Quintanar et al. (2012),

compared the results of the system developed by Rivera et al. (2011), operating with $NH_3/LiNO_3$ and $NH_3/LiNO_3/H_2O$ mixtures. The authors reported that with the ternary mixture, the solar coefficients of performance were as much as 24% greater than those obtained using the binary mixture. Llamas et al. (2014), reported the results of a solar absorption air conditioning system of 10 kW of cooling capacity operating with the ammonia/lithium nitrate mixture. The system was able to produce chilled water at temperatures as low as 0°C with coefficients of performance of approximately 0.5. Zamora et al. (2014), reported the results of two pre-industrial absorption cooling systems operating with an ammonia/lithium nitrate mixture. One system was air-cooled, and the other was water-cooled. The second prototype was built with PHE as the main component. The system produced chilled water at 15°C for generation temperatures of 90°C. The maximum cooling capacity was approximately 12 kW. Zamora et al. (2015), also reported the results of a partial-load operation for the systems presented by Zamora et al. (2014). Hernández-Magallanes et al. (2014), reported the experimental assessment of an absorption cooling system operating with an ammonia/lithium nitrate mixture. The generator and absorber were shell and tube heat exchangers with a coil configuration for tubes, while the condenser, evaporator, and economizer were plate heat exchangers (PHE). Domínguez-Inzunza et al. (2016), presented the results of de evaluation of an absorption cooling system operating with the ammonia/lithium nitrate mixture. The generator and the absorber were shell and tubes falling film heat exchangers while the rest of the components were compact plate heat exchangers. The generator temperatures varied between 80 °C and 100 °C, while the cooling water temperatures varied from 20 °C to 34 °C. Cooling capacities up to 4.5 kW and evaporator temperatures as low as 4 °C were achieved with the system. The internal coefficients of performance varied between 0.3 and 0.62 depending on the system operating temperatures.

Although there have been some studies related with the development of an absorption cooling systems there have not been studies related with the development of an entire solar air conditioning pilot plant utilizing an absorption system operating with the ammonia/lithium nitrate mixture. On these bases, a project was submitted and approved by the Consejo Nacional de Ciencia y Tecnología (CONACyT) to model, develop and install a demonstrative solar air conditioning pilot plant at the Centro de Tecnología Avanzada (CIATEQ) office. The first step of this project, which is related with the modelling and dimensioning of the solar air conditioning pilot plant is presented in this work.

2. METHODOLOGY

To carry out the analysis of the energy requirements of the pilot plant, it was first necessary to study the space to be cooled. The office to be cooled is part of a building of the CIATEQ located in the city of Queretaro. The office has an area of 25 m^2, with a total volume of 75 m^3. The occupation is from 8:00 a.m. to 6:00 p.m. from Monday to Friday. Figure 1 shows the architectural plan of the studied area.

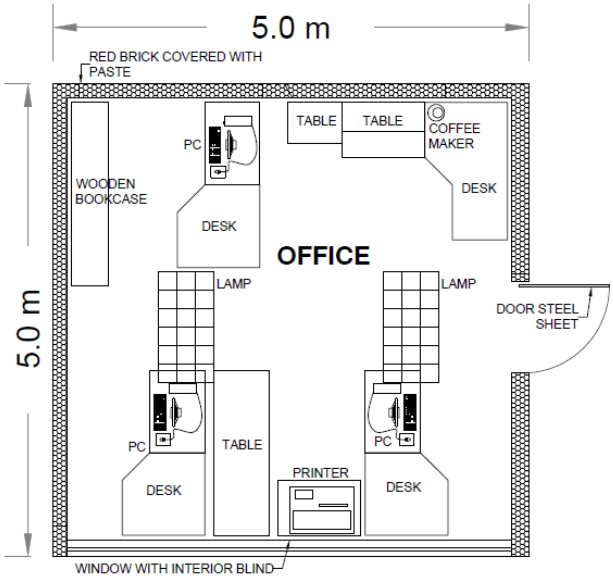

Figure 1: Architectural Plant of the Office Analysed

The walls of the office are constructed of red brick covered with paste. The ceiling is made of 15 cm thick concrete slab with reinforced dipstick. The doors are made of steel sheet and the windows are of common glass with a thickness of 0.5 mm. Figure 2 shows a diagram of the composition of the walls (or envelopes) of the analysed office.

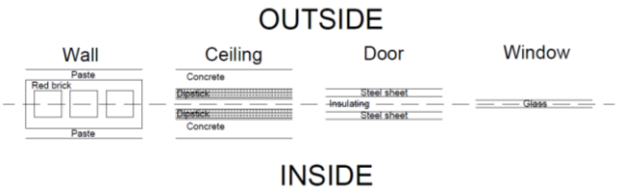

Figure 2: Walls composition of the Office Analyzed

The CIATEQ office were first modelled taking into account, the local weather, the orientation, dimensions, windows, construction materials, occupancy, etc., but without using an air conditioning unit. The modelling was carried out in transient mode by using the software *Transient System Simulation Tool-16 (*TRNSYS-16) each ten minutes during a whole year.

With this information and with the experience acquired on the development of this kind of systems, preliminary dimensions of the solar collector's field, hot water storage tank and absorption cooling machine were proposed. With the obtained results, the office was again modelled to see if with the proposed system climate comfort conditions could be reached. If the comfort conditions were not achieved, then a parameter such as the number of solar collectors or any other parameter was then changed. So, and iterative procedure was carried out until the comfort conditions were achieved, as well as the optimization of the solar collectors area, the size of the storage tank and the cooling capacity of the absorption cooling machine.

In order to carry out the modelling of the system it is necessary to know diverse information which is supply to the TRNSYS. The main information is that related with the office to be cooled, weather conditions, solar collector's field and the absorption cooling system among other information. Figure 3 shows the schematic diagram of the pilot plant components modelled by using TRNSYS.

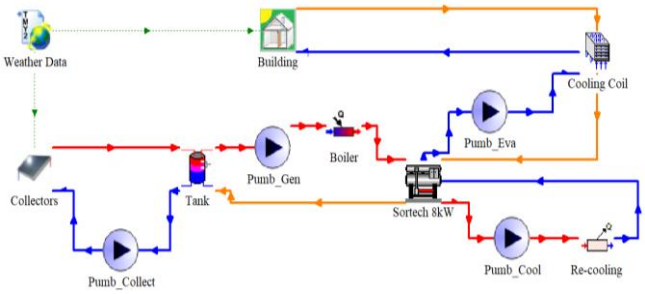

Figure 3: Schematic Diagram of the Pilot Plant Components Modelled by Using TRNSYS.

2.1 Weather conditions for the modelling

The place of interest is located in the municipality of El Marqués in the state of Querétaro, with coordinates 20.57 ° N and 100.27 ° W.

The climatic data have been obtained from a database generated by the UNAM with copyright registered in 2011, which contains meteorological information for Mexican populations of more than 10,000 inhabitants.

Table 1 shows for the twelve months the average values of the ambient temperature (Ta), the minimum ambient temperature (Tmin), the maximum ambient temperature (Tmax), the relative humidity (RH), the air velocity (Vair), and the horizontal solar radiation (H) for the nearest available locality (La Cañada, Querétaro):

Table 1: Monthly Average Weather Data for La Cañada, Queretaro.

Month	Ta [°C]	Tmin [°C]	Tmax [°C]	RH [%]	Vair [m/s]	H [MJ/m^2 day]
Jan	15.0	7.3	22.8	58.9	3.29	16.45
Feb	16.2	7.8	24.5	51.7	3.56	19.14
Mar	18.6	9.8	27.4	42.0	3.96	22.00
Apr	20.7	12.0	29.3	42.2	3.81	23.60
May	22.4	14.3	30.6	50.1	3.50	23.19
Jun	21.9	14.6	29.2	69.4	3.20	21.20
Jul	20.3	13.9	26.7	71.1	3.07	21.71
Aug	20.1	13.7	26.6	70.6	2.84	21.10
Sep	19.4	13.3	25.6	75.2	2.75	18.57
Oct	18.5	11.2	25.7	73.9	2.85	18.19
Nov	17.0	9.0	25.1	68.7	3.07	16.83
Dec	15.5	7.6	23.5	63.7	3.10	15.03
Mean	18.8	11.2	26.4	61.5	3.25	19.75

2.2 Solar collectors

For the modelling of the solar collector's field of the pilot plant, real data from the manufacturer's data sheet were used which are shown in Table 2. The solar collector modelled is the MS 2.5 Black from the company Módulo Solar.

Table 2: Parameters Used for Modelling the Flat Plate Solar Collectors

Parameter	Value
Aperture area [m^2]	2.326
Specific heat of the water [kJ/(kg K)]	4.19
Mass flow rate per unit area [kg/(h m^2)]	0.023
Stagnation temperature [°C]	195
Optical efficiency [dimensionless]	0.7535
Coefficient of thermal losses of first order [W/(m^2 K)]	2.9132
Coefficient of thermal losses of second order [W/(m^2 K)]	0.0099

2.3 Absorption cooling system

The absorption cooling system was modelled using the subroutines available in TRNSYS but adjusted with real data obtained from a system developed by Domínguez-Inzunza et al. (2016), at the Instituto de Energías Renovables of the Universidad Nacional Autónoma de México which is the absorption cooling system that would be installed in the CIATEQ office. The modelling parameters of the cooling system are shown in Table 3.

Table 3: Nominal Requirements of the Cooling System SORTECH ACS 08

Parameter	Value	Units
Inlet temperature	72	[°C]
Outlet temperature	65	[°C]
Volumetric flow	1.6	[m^3/h]
Thermal power supplied	13.03	[kW]
Cooling power	8	[kW]

3. RESULTS

Although there are currently several parameters to consider if a person is in comfortable conditions from the climatic point of view, the temperature, the relative humidity and the wind velocity are still recognized as the most common parameters. From these three parameters only the temperature and the relative humidity are analysed in the present study since for the wind velocity it was not possible to have reliable information.

Figure 4 shows the office indoor temperatures without using an air condition unit along the year. In this figure it can be seen that temperatures higher than 28 ºC can be reached between the 12:00 and the 19:00 hours during spring and summer seasons are out of the climate comfort zones which is in general considered to be between 22 °C and 27 °C.

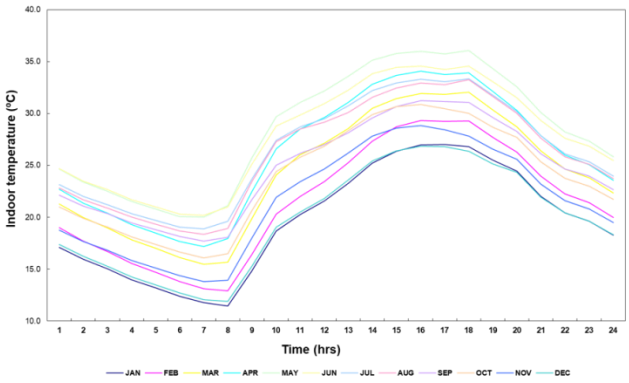

Figure 4: Indoor Temperatures along the Year without Using an Air Conditioning Unit

On the other hand, Figure 5 shows the average monthly relative humidity along day for a whole year. It can be seen that the highest relative humidities take place in August, September and October coinciding with the rainy season while the dryest months from February to April. Considering that most of the people feel comfortable at relative humidities between 40% and 60 %, it can be observed that in the months from February to May it is necessary to humidify the air in order to get the comfort conditions during the working hours.

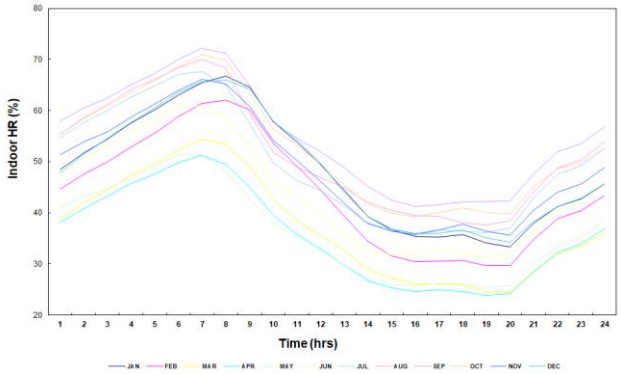

Figure 5: Distribution of the Average Monthly Relative Humidity along Day

Figure 6 shows the cooling power required to achieve the climate comfort inside the office. In this figure it can be observed that the maximum cooling capacities are required during the months from May to August between the 12:00 and 19:00 hours. As can be seen the maximum power required is 3.2 kW and the lowest is about 1.0 kW in December.

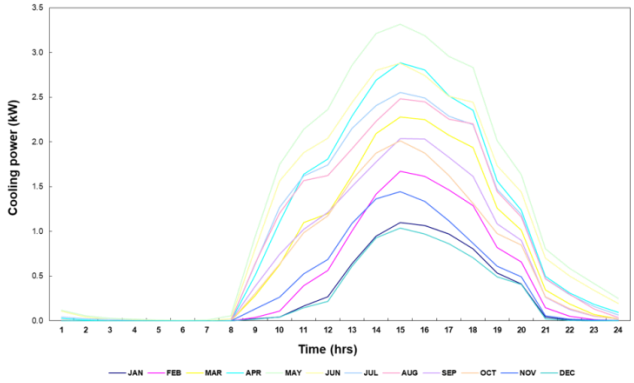

Figure 6: Cooling Power Required to Achieve the Climate Comfort Inside the Office

Figure 7 shows the indoor temperatures achieved by using the solar air conditioning system. It can be seen that after to have carried out an iterative modelling process of the pilot plant, the climate comfort was achieved since temperatures not higher than 25ºC were obtained during the whole year inside the modelled office during the working hours.

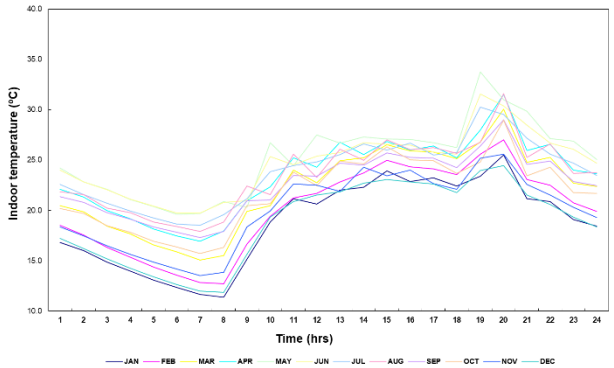

Figure 7: Indoor Temperatures along the Year by Using the Solar Air Conditioning Pilot Plant.

On the other hand, Figure 8 shows the distribution of the average monthly relative humidity along day by using the solar air conditioning system. As can be observed by using the solar absorption cooling pilot plant it is possible to achieve the comfort conditions the whole year during the working hours with exception of spring season between 14:00 and 18:00 hours since the relative humidity varies between 32% and 35%. However, although the comfort conditions were not completely met during spring, the relative humidity increases compared with the values obtained without the air conditioning unit which were between 22% and 27% at the same hours during spring as can be seen in Figure 5.

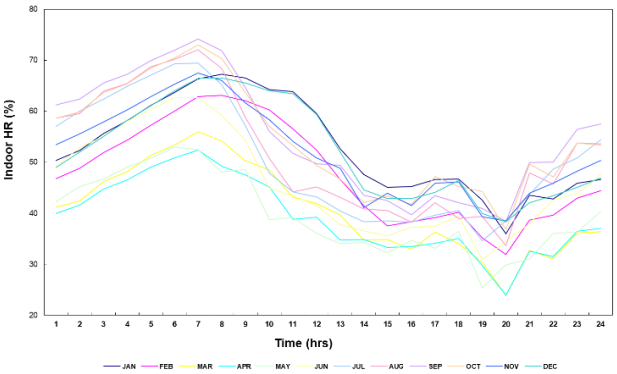

Figure 8: Distribution of the Average Monthly Relative Humidity along Day by Using the Solar Cooling Air Conditioning Pilot Plant.

Table 4 summarizes the results of the modelling and dimensioning of the solar air conditioning pilot plant. As can be seen in order to produce the cooling capacity of 3.5 kW it is necessary to use 27 solar collectors from the company Modulo Solar Model MS2.5, an storage heat water tank of 1500 litters and an absorption cooling system.

Table 4: Main Characteristics of the Solar Air Conditioning Pilot Plant

Concept	Company	Model	Quantity	Capacity
Absorption cooling system	Developed by the IER	-	1	3.5 [kW]
Solar collectors	Módulo solar	MS2.5	27	-
Hot water storage tank	MASS	THN-2	1	1500 [litters]

4. CONCLUSIONS

The modelling and dimensioning of a solar air conditioning pilot plant was carried out. From the modelling it was showed that climate comfort conditions could be achieved during the whole year inside the CIATEQ office by using an absorption air conditioning system powered by solar energy.

ACKNOWLEDGMENT

The authors are grateful for the support provided by the *Fondo sectorial CONACYT-SENER-Sustentabilidad Energética*, through the *Centro Mexicano de Innovación en Energía Solar (CeMIE-Sol)*, under the strategic project number 09, titled: *"Desarrollo de Sistemas de Enfriamiento Operados con Energía Solar"*.

REFERENCES

Abdullah M.O., Hieng T.C., 2010. Comparative analysis of performance and techno-economics for an H_2O-NH_3-H_2 absorption refrigerator driven by different energy sources. Applied Energy 87(5), 1535-45.

BCS, Incorporated, Waste Heat Recovery: Technology and Opportunities in U. S. Industry, prepared for the U.S. Department of Energy, Industrial Technologies Program. Available from https://www1.eere.energy.gov/manufacturing/intensiveprocesses/pdfs/waste_heat_recovery.pdf. March 2008.

Best R., Rivera W., 2015. A review of thermal cooling systems. Applied Thermal Engineering 75, 1162-1175.

Boman D.B., Hoysall D.C., Staedter M.A., Goyal A., Ponkala M.J., Garimella S.. 2017. A method for comparison of absorption heat pump working pairs. Int. J. of Refrigeration 77, 149-175.

Domínguez-Inzunza L.A., Hernández-Magallanes J.A., Soto P., Jiménez C., Gutiérrez-Urueta G., Rivera W., 2016. Experimental assessment of an absorption cooling system utilizing a falling film absorber and generator. Applied Thermal Engineering, 103, 1105-1111.

Hernández-Magallanes J.A., Domínguez-Inzunza L.A., Gutiérrez-Urueta G., Soto P., Jiménez C., Rivera W., 2014. Experimental assessment of an absorption cooling system operating with the ammonia/lithium nitrate mixture. Energy 78, 685-692.

Llamas S.U., Cuevas R., Best R., Gómez V.H., 2014. Experimental results of a direct air-cooled ammonia-lithium nitrate absorption refrigeration system. Applied Thermal Engineering 67, 362-369.

Moreno-Quintanar G., Rivera W., Best R., 2012. Comparison of the experimental evaluation of a solar intermittent refrigeration system for ice production operating with the mixtures NH_3-$LiNO_3$ and NH_3-$LiNO_3$-H_2O. Renewable Energy 38, 62-68.

Rivera W., Best R., Cardoso M.J., Romero R.J., 2015. A review of absorption heat transformers. Applied Thermal Engineering 91, 654-670.

Rivera W., Moreno-Quintanar G., Rivera C.O., Best R., Martínez F., 2011. Evaluation of a solar intermittent refrigeration system for ice production operating with ammonia/lithium nitrate. Solar Energy 85, 38–45.

Wang J.F., Gao G.C., Chen G.M., 2000. An improved absorption refrigeration cycle driven by unsteady thermal sources below 100°C. Int. J. of Energy Research 24, 633-640.

Wu W., Zhang X.L., Li X.T., Shi W.X., Wang B.L., 2012. Comparisons of different working pairs and cycles on the performance of absorption heat pump for heating and domestic hot water in cold regions. Applied Thermal Engineering 48, 349-58.

Zamora M., Bourouis M., Coronas A., Vallès M.. 2014. Pre-industrial development and experimental characterization of new air-cooled and water-cooled ammonia/lithium nitrate absorption chillers. Int. J. of Refrigeration 45, 189-197.

Zamora M., Bourouis M., Coronas A., Vallès M.. 2015. Part-load characteristics of a new ammonia/lithium nitrate absorption chiller. Int. J. of Refrigeration 56, 46-51.

AUTHORS BIOGRAPHY

In 1985, Dr. Rivera graduated from the Universidad Autonoma Metropolitana with a degree in Energy Engineering. He obtained a Masters degree in Solar Energy from the Universidad Nacional Autonoma de Mexico and in 1996 a Ph.D. in Chemical Engineering from Salford University in the U.K. Today, he is a senior researcher at the U.N.A.M Energy Research Center and a member of the National System of Researchers; with a Level III category, the highest given by the National System. Dr.Rivera has been sometimes responsible and others participant in various national and international projects, with internal and external support, related to heat pumps, energy conservation, and solar refrigeration systems. He has published more than 80 international articles in specialized journals which can be found in the Science Citation Index; has directed several doctoral and master theses, has been cited more than 1600 times, and is the owner of a patent with two more in revision. In 1997 was appointed Coordinator of the Solar Energy graduate program and in January of 2003 received the appointment of U.N.A.M.'s Coordinator of all Doctoral and Masters engineering programs from the Rector of the U.N.A.M.Being chosen as Mexico's representative of the International Energy Agency in the field of solar refrigeration and heating from 1999 to 2013 as well as obtaining the National Award in Innovation regarding Renewable Energies from the Energy Department are among his main honors.

Sergio Lugo obtained a Ph.D. degree in Engineering from the Universidad Nacional Autónoma de México in 2018, where he has worked as an associate researcher in the FORDECYT project. He is a specialist in the use of the TRNSYS software for dynamic simulation of thermal processes. He has worked on multiple projects with the use of this software to generate heat with solar energy and applications in solar cooling. Also, He specializes in the area of solar thermal energy with experience in the design, sizing and installation of systems for process heat. He has worked as project engineer and supervisor in companies focused on renewable energies mainly in solar thermal and photovoltaic energy, managing to improve their processes and project quality and higher sales. He has collaborated in projects of CONACYT and SENER as, for example: FORDECYT, FONCICYT, CIE-SENER. He has taught TRNSYS courses and has supported in some classes of the college career in Renewable Energies of the UNAM.

HYPERSPECTRAL DATA PROCESSING AND ADAPTIVE MODELLING FOR THE NATURAL OBJECTS PROPERTIES DETECTION

Olga V. Grigoreva [a], Viktor F. Mochalov[b], Vjasheslav A. Zelentsov [c]

[a],[b] Military Space Academy named after A.F. Mozhaisky, Zhdanovskaya embankment, 41, 197198 St.Petersburg, Russia
[c] St.Petersburg Institute for Informatics and Automation of RAS, 14 line 39, 199178 St.Petersburg, Russia

[a]alenka12003@mail.ru, [b]vicavia@yandex.ru, [c] v.a.zelentsov@gmail.com

ABSTRACT
The article proposes a method for assessing the state of natural objects that is based on the complex use of heterogeneous models and hyperspectral Earth remote sensing data used to estimate the parameters of these models. The base model is an artificial neural network, for the training of which multiparametric models of radiation transfer, gradient search algorithms, as well as regression empirical models supplementing them, can be used and adaptively adjusted. The advantage of the method is the ability to determine the state of water bodies and vegetation under conditions of uncertainty with the possibility of making more precise estimates for the limited volume of ground measurements at reference points. Examples of approbation of the method in determining the state of coastal waters of the Black Sea with the use of hyperspectral imaging materials from "Resurs-P" satellite, as well as in assessing the state of vineyards, are shown.

Keywords: remote monitoring of the environment, radiative transfer model, regression models, artificial neural networks, nonlinear optimization, multi- and hyperspectral data

1. INTRODUCTION

At present, the use of Earth remote sensing data, obtained with the help of aerospace surveying, is becoming increasingly widespread for assessing the state of natural objects (NOs). The use of materials from aerospace survey conducted in a large number of spectral ranges (from 8-10 to several hundred) makes it possible to increase the reliability of the estimation of the NOs' state parameters during the construction and implementation of models of the change of NOs' state on large territories. This significantly reduces the cost of the analysis of natural objects in agricultural production, in monitoring the state of the environment, in forest management, in emergency situations (Zelentsov 2017), etc. The key concepts in conducting such an analysis are the concepts of models for estimating the NOs' state parameters and the methods for estimating these parameters using space survey materials.

In this paper, the issues of estimating the parameters of the state of NOs are considered from the point of view of propagation, scattering, absorption and reflection of the light flux for different wavelengths of the electromagnetic spectrum of the optical range. Formally, these processes are described using multiparametric models of radiation transfer in different natural media - water, vegetation (Lee, Carder, Hawes, Steward, Peacock, and Davis 1994; Jacquemoud, Zarco-Tejada, Verhoef, Asner, Ustin, Baret, and François 2006; Gastellu-Etchegorry, Demarez, Pinel, and Zagolki 1996; Rosema, Verhoef, Noobergen, Borgesius 1992; Borel and Gerstl 1994). However, the practical application of these radiative transfer models (RTM) is often hampered by a significant number of parameters, which in most cases are unknown. In this case, as a rule, the more complex the model and the higher its potential adequacy to the object of study, the more initial data is required for its implementation. Therefore, at present, the method of direct estimation based on the analysis of statistical dependencies between the characteristics (features) extracted from a snapshot and the parameters of the object of study itself is often used to estimate the parameters of the state of natural objects (Brovkina, Novotnya, Cienciala, Zemeka, and Russ 2017; Grigoryeva, Zhukov, Markov, and Mochalov 2016; Grigoryeva, Shilin 2012; Biospheric Aspects 1993; Biftu and Gan T.Y. 2001; Fefilov 2003). In order to construct such regression models, information about the properties of the object at reference points (in situ) present on the image should be known, and, in most cases, either spectral characteristics in separate spectral ranges or derived indices are used as the signs in the image.
In these conditions, it is advisable to use a combined approach, in which RTM that are more accurate, but require a large amount of input data could be adaptively supplemented with simpler regression models that do not require large volumes of full-scale measurements. This approach can be implemented by using additional information for RTM, which can be extracted from materials of multi- and hyperspectral imaging. The development of technologies for obtaining and processing hyperspectral imaging data, as well as the

creation of multispectral systems with a large number of channels in the visible and near infrared spectral ranges, provide opportunities for restoring environmental properties (for example, estimating biomass and nitrogen in plants, determining physicochemical and organic parameters of water). Such remote sensing equipment can include equipment installed on the "Resurs-P" satellite (Zelentsov, Sokolov, Grigorieva, Mochalov, Potryasaev, and Shumeiko 2016), which is now actively used in Russia for various natural-resource problems.

Using the information capabilities of hyperspectral data, as well as the principles of multimodal analysis (Sokolov, Zelentsov, Yusupov, and Merkuryev 2014), it is possible to implement a new approach to assessing the NOs' state based on adaptive modeling in conducting such an assessment. The proposed approach and the corresponding method of its implementation are based on the application of the mathematical apparatus of artificial neural networks (ANNs) and methods of multiparametric non-linear optimization of RTM for the training of ANNs, in particular, the gradient descent algorithm, or the Levenberg-Markravdt method (Hagan, Demuth, Beale, and Jesus 1996). In this case, the final tuning of the ANN is performed using regression empirical models. The limited amount of ground-based data required to implement the algorithm is compensated by the possibility to remotely measure the reflective properties of objects for tens or hundreds of wavelengths of the visible and near infrared spectral ranges. It is expected that in this case the use of hyperspectral data will provide a reduction in errors during the operation of the ANN for the solution of the task. In turn, the quality of the models used can be improved by adjusting the training of the ANNs. The advantage of the ANN is that it allows several models to be used at once to study the relationship between the reflective properties of objects and their state. Therefore, for its training, it is proposed to use in situ data at reference points, thereby compensating for deficiencies or enhancing the advantages of some models over others.

2. METHODS

The proposed method of adaptive modeling for assessing the properties of natural objects is based on the use of multispectral and hyperspectral remote sensing data that undergoes the atmospheric correction phase and is then used to classify landscape elements and estimate the values of the parameters of the NOs' state.

The main idea of the last stage is to use an ANN, trained with the use of a complex of models. At the same time for direct training, multiparametric radiative transfer models are used, and the training is tuned by regression empirical models. The block diagram of the algorithm implementing the proposed method is shown in Figure 1.

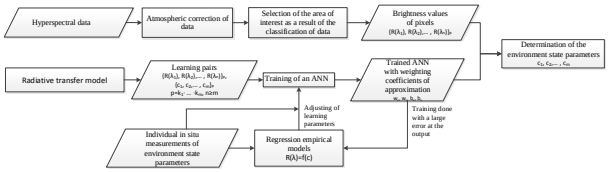

Figure 1: An algorithm for analyzing the NO's state

Thus, a multi-model approach to the estimation of the parameters of the NOs' state is implemented. It allows combining the advantages of the RTM approach, which provides a detailed account of the reflective characteristics of the analyzed objects, and regression methods that reduce the requirements for the composition of the initial parameters.

The qualitative preliminary processing of the multispectral and hyperspectral data related to the elimination of distortions introduced by the atmosphere into the brightness values recorded by the equipment significantly influences the accuracy of the determination of the NOs' state. Atmospheric correction of aerospace survey data can be performed using the atmospheric radiative transfer modeling program MODTRAN.

The next stage is the classification of data, the purpose of which is determined by the features of the problem being solved and by the object of the study itself. For example, in the study of shallow coastal areas of the water area, for which a reflection from the bottom significantly contributes to the brightness of the water surface, the bottom classification of the water areas is carried out using specially developed indices (Grigorieva, Markov, Zhukov, Mochalov, and Nikolenko 2016). When studying the properties of land objects, classification implies segmentation of the territory, allowing one to analyze only those fragments of images that correspond to the objects under study (agricultural fields or forests).

After the classification, a direct determination of the parameters of the NOs' state is carried out as a result of the training of the ANN using the radiation transfer equation RTM in the investigated media.

To train the ANN using the RTM, a set of value vectors, the so-called pairs of input and output data, is calculated:

$$R(\lambda_j)=f(c_1,\ldots,c_i,\ldots c_n), \quad (1)$$

where $R(\lambda_j)$ - the brightness values of the studied landscape element in the j-th spectral channel; c_i - the values of the required parameters of the state of the natural object.

The accuracy of the estimation of the parameters of the NOs' state is influenced, in the first place, by the choice of the RTM and their parameters. In addition, as practice has shown, in most cases, when training only by the RTM, the network is retrained, and this leads to errors in real data. The advantage of the ANN is that the input of the network can also be supplied with the known data, obtained as a result of in situ measurements, additionally train the network and adjust the weighting coefficients in the direction of reducing the error at the output of the network. Therefore, the proposed algorithm introduces

the adaptation stage, which consists in tuning the training of the ANN on the regression models and (or) on the results of in situ observing of the parameters of the NOs state. This stage of adaptation is especially relevant for vegetation, since it is not as volatile as the water surface for which in situ measurements should exactly match the time of passage of the satellite.

The analysis of the input data occurs in the hidden and output layers of the neural network. The analysis results are contained in the output layer, which is a data array containing information about the estimated state parameter of the object c_i. After the training of the neural network is done, a set of weights is determined, which are the result of approximation of the radiation propagation model and are iteratively corrected in the direction of the configuration that allows the network to distinguish between the prototype images of interest.

It is important to choose the ANN configuration for each task to be solved. By configuration of an ANN we mean the number of input neurons, hidden layers and neurons in it. The effectiveness of using the learning process is also determined by the chosen method of training: the method of back propagation of the error, which can be referred to the methods of gradient descent, the Levenberg-Markvardt method (Hagan and Menhaj 1994), the conjugate gradient method, etc. However, the universal method of selecting the ANN architecture does not exist and it is defined, mainly, by the research task. It is known that the architecture of a neural network is optimal if the network is trained with minimal errors at the output. In turn, the number of input neurons depends on the number of informative spectral channels of the multispectral and hyperspectral imaging equipment.

Below we consider in detail the model descriptions of radiation generation processes by the examples of the aquatic environment and vegetation used to implement an algorithm for estimating their state from hyperspectral remote sensing data. When assessing the state of the water area, under defined parameters we mean the concentration of chlorophyll and its derivatives in water, which characterize the trophic status of the reservoir; the content of mineral suspended matter and organic "yellow" substance; as well as the depth of the water area. For vegetation, the leaf area index LAI, the content of chlorophyll "a", biomass and other parameters that describe the state of forests and crops are estimated.

3. MODELS

3.1. Model of radiation transfer in an aquatic environment

The model of radiation transfer in an aquatic environment is described by the spectral characteristics of the reflection of the bottom, the absorption and scattering of the water column and the water surface. The absorption and backscattering indices of the aquatic environment determine the presence of dissolved matter, phytoplankton pigments and various suspensions in water. In this case, the model of radiative transfer in the water column can be represented in the form of the following equation (Lee, Carder, Hawes, Steward, Peacock, and Davis 1994):

$$R_{dp}(\lambda)[1-e^{-2fk_d(\lambda)H}]+R_b(\lambda)e^{-2fk_d(\lambda)H}=R_a(\lambda), \quad (2)$$

where $R_a(\lambda)$ is coefficients of spectral brightness of the sea, obtained from materials of hyperspectral aerospace survey;

$R_b(\lambda)$ is the spectral value of the albedo of the bottom;

$R_{dp}(\lambda)$ is the spectral coefficient of diffuse reflection of the water column for an infinitely deep sea

$k_d(\lambda) = b_w(\lambda) + b_{bp}(\lambda) + a_w(\lambda) + a_{ph}(\lambda)+a_g(\lambda)$ is the spectral index of the vertical attenuation of radiation (back and forth), m^{-1};

$a_w(\lambda)$ and $b_w(\lambda)$ are the known absorption and backscattering indices of pure sea water;

$a_g(\lambda)$ is the absorption index of the dissolved organic matter;

$a_{ph}(\lambda)$ is the absorption index of phytoplankton pigments;

$b_{bp}(\lambda)$ is the index of backscattering of radiation by suspension.

H is depth of the bottom, m;

$f = 1.04/\cos(Q)$ is an index that depends on the angle of refraction of the sun's rays Q.

The absorption indices of phytopigments, yellow substance and backscattering by suspension are expressed through specific absorption indices at reference wavelengths λ_0 or through their concentration C (Grigoryeva, Zhukov, Markov, and Mochalov 2016).

To implement the proposed algorithm in the modeling process, the set of vectors of values, used for training the ANN, is calculated: $R(\lambda)=f(C_g, C_{ph}, C_{bp}, H)$. Determination of one of the parameters of the aquatic environment (the depth of the reservoir, the concentration of chlorophyll, suspended and dissolved organic substances) is carried out by the weight coefficients obtained during the training of the network.

The adjustment of the ANN training is carried out according to known statistical dependencies, expressed in the form of regression models, between the hydrooptical parameters (the content of chlorophyll "a" and suspended substances) and the brightness values of the radiation rising from the surface for selected wavelengths obtained from in situ observations. For example, the following empirical relationship between the concentration of suspended solids and the brightness at a wavelength of 660 nm has proved to be well-established in practice (Grigoryeva, Shilin 2012):

$$R_{590\text{-}710}=0.043\ln(C_{bp})-0.044. \quad (3)$$

To estimate chlorophyll "a" C_{ph} content, it is possible to use bio-optical regression models that are based on measuring water leaving radiance, and intended for the analysis of satellite products SeaWiFS (Fefilov 2003).

3.2. Models of radiation transfer in plant environment

Plant landscapes refer to complex natural complexes, for which the transfer of radiation is characterized by a re-reflection between the underlying surface and the tiers of vegetation. Therefore, the use of a strict relationship between the parameters of the state of the forest (for example, biomass) and its spectral brightness is possible only for vegetation with the same structure of the canopy. To date, special RTM have been developed for the study of crops and grass cover. One of these widely used models is the PROSAIL model (Jacquemoud, Zarco-Tejada, Verhoef, Asner, Ustin, Baret, and François 2006), which is a combination of the leaf optical properties model PROSPECT and canopy bidirectional reflectance model SAIL. Variable parameters of this model for calculating the brightness of spectral radiation are: soil reflectance, conditions of the geometry of the survey (solar zenith angle, viewing zenith angle, relative azimuth angle, leaf area index, leaf inclination distribution function, chlorophyll a + b concentration, equivalent water thickness, dry matter content). For more complex plant complexes, such as forests, it is recommended to use other canopy reflectance models: DART (discrete anisotropic radiative transfer) model (Gastellu-Etchegorry, Demarez, Pinel, and Zagolki 1996), forest-light interaction model FLIM (Rosema, Verhoef, Noobergen, Borgesius 1992) and others. They take into account such parameters as the density of trees, the damping coefficient, the diameter and height of the crown, as well as other parameters for simulating the open-canopy geometry, including the effect of crown and soil in the shade and in the sunlight. In this case, we talk about a nonlinear model of mixing of radiation recorded by remote sensing equipment, where the PROSPECT model can also be integrated. The nonlinear model is based on the biophysical parameters of the multilayer vegetation-soil system and provides for a sequential calculation of the transmission and reflection of direct and scattered, descending and ascending radiation by each layer in different directions, as well as the determination of the total fluxes due to single reflection from leaves and soil and multiple scattering radiation in the layers of vegetation, reflected by plant elements and soil. One of such models is the model Borel and Gerstl, which is an analytical solution of the bi-directional reflectance distribution function BRDF, calculated taking into account the presence of shades in the field of view of the equipment and the geometry of the survey. For a two-layer surface, it is expressed by the following equation (Borel and Gerstl 1994):

$$\mathrm{BRDF}_\lambda(\mathrm{Q},\mathrm{h};\ \varphi_\mathrm{Q},\varphi_\mathrm{h}) = \frac{1}{\pi \mathrm{E}_\mathrm{o}}\left[\mathrm{P}_\mathrm{l}^{\mathrm{sun}}\left(\frac{\mathrm{B}_1}{\mathrm{L}}\right) + \mathrm{P}_\mathrm{s}^{\mathrm{sun}}(\rho_\mathrm{s}\mathrm{E}_\mathrm{o} + \rho_\mathrm{s}\mathrm{B}_2) + \mathrm{P}_\mathrm{s}^{\mathrm{shad}}\rho_\mathrm{s}\mathrm{B}_2\right], \quad (4)$$

where $\mathrm{R}_\lambda = \pi\mathrm{BRDF}_\lambda$ is the coefficient of the pixel's spectral brightness;

$\mathrm{P} = \mathrm{f}(\mathrm{L},\ \mathrm{Q}_\mathrm{h}, \mathrm{h}, \varphi_\mathrm{Q}, \varphi_\mathrm{h})$ is probability of observing illuminated leaves $\mathrm{P}_\mathrm{l}^{\mathrm{sun}}$ and soil $\mathrm{P}_\mathrm{s}^{\mathrm{sun}}$, shaded soil $\mathrm{P}_\mathrm{s}^{\mathrm{shad}}$;

$\mathrm{B} = \mathrm{f}(\mathrm{L}, \rho_\mathrm{s}, \rho, \tau)$ is spectral brightness of the upper surface of the leaf layer (1), the lower side (2), the earth's surface (3);

$$\mathrm{B}_1 = \mathrm{E}_\mathrm{o}\left[\mathrm{L}\rho + \mathrm{L}\tau\rho_\mathrm{s}\left(\frac{1+\mathrm{L}(\tau-1)}{1-\rho\rho_\mathrm{s}\mathrm{L}}\right)\right];$$

$$\mathrm{B}_2 = \mathrm{E}_\mathrm{o}\left[\mathrm{L}\left(\frac{\tau+\rho\rho_\mathrm{s}(1-\mathrm{L})}{1-\rho\rho_\mathrm{s}\mathrm{L}}\right)\right];$$

$$\mathrm{B}_3 = \mathrm{E}_\mathrm{o}\left[\rho_\mathrm{s}\left(\frac{1+\mathrm{L}(\tau-1)}{1-\rho\rho_\mathrm{s}\mathrm{L}}\right)\right];$$

E_o is total incident radiation per unit area, W/m^2;

ρ and τ are coefficient of reflection and transmission of radiation by leaves;

ρ_s is coefficient of reflection of soil or other underlying surface;

Q is sighting angle;

h is height of the Sun;

φ_Q and φ_h are azimuth of sight and the Sun;

L is projective vegetation cover.

The element of the reflection function $\left[\frac{1}{1-\mathrm{L}\rho\rho_\mathrm{s}}\right]$ in B causes its non-linear character and accounts for multiple reflection between leaves and soil.

A feature of the application of the model is that, because of its computational complexity, the calculation of the projective coverage is possible only with the help of methods of nonlinear optimization, especially for a multilayered surface. In addition, for large areas the use of one model is not enough, i.e. it is required to use several models for different types of vineyards and age, since they differ significantly in their spectral characteristics. In connection with this, in the problem of estimating the projective covering of multilayer plant surfaces by hyperspectral data, the use of the ANN apparatus is best. In this case, the ANN training is carried out with the help of the models discussed above, and the training adjustment can be carried out by regression dependencies, e.g., of the following kind:

$$\mathrm{LAI}=1.71\mathrm{NDVI}+0.48 \quad (5)$$

for grassy vegetation (Biospheric Aspects 1993);

$$\mathrm{LAI}=-2.5\ln(1.2-2\mathrm{NDVI}) \quad (6)$$

for crops (Biftu and Gan 2001).

Thus, we can talk about a fairly large list of models, the choice of which is determined by the object of study, the number of parameters of its state, and the quality of the model itself.

4. RESULTS

The method of adaptive modeling, proposed by the authors, was applied when restoring the following properties of the environment from the hyperspectral data from "Resurs-P" satellite:

- the depth of coastal areas of the Black Sea from the data of the hyperspectral imaging from [18];
- distribution of organic and inorganic impurities in coastal waters, including determination of suspended matter concentration, the content of

chlorophyll "a" and its derivatives, dissolved organic matter;

- the index of the leaf area of vineyards, which is a reflection of such an important crop parameter as biomass.

At the same time, the best ANN configuration was selected for each task. The number of layers and the number of elements in each layer are determined by the complexity of the RTM function (Khaikin 2008; Kalan 2001; Schowengerdt 2007; Egorov, Ilyin, Kalinin, Rodionov, and Rodionov 2011). The number of input neurons for solving the inverse problem of reconstructing the properties of an object from radiative transfer models is determined by the number of spectral information channels, including those limited by the capabilities of multispectral observing means. So, to monitor the ecological state of the water areas the most informative are the spectral intervals taken only in the visible range of the spectrum (Zhukov 2016), and for the study of vegetation - in the visible and near infrared spectral ranges. The size of the output layer depends on the range of variation and the increment of the object's state parameter being determined. The step size is important in terms of accuracy of the parameter estimation. For example, in order to determine the trophicity of a reservoir in terms of the chlorophyll content, the size of the output layer with 30 elements for a range of concentrations from 1 to 30 mg / m^3 can be specified with increment and the accuracy of estimation of 1 mg m^3. If the number of input and output neurons depends on the type of object under study, the greatest difficulties arise when choosing the optimal number and size of hidden layers. One of the heuristic rules is that the number of observations should be ten times greater than the number of connections in the network (http://www.statsoft.ru/HOME/TEXTBOOK/modules/stneunet.html). In this case, networks with a large number of weights model more complex functions but are prone to retraining, while a network with a small number of weights may not be flexible enough to model the existing dependence (for example, a network without intermediate layers actually simulates a conventional linear function).

In accordance with this approach, it was found that to approximate a semi-analytical model of radiation transfer in water, it would be best to use a network with 10 neurons in one hidden layer in the case of 12 spectral channels, and to solve the multiparameter problem of non-linear optimization of RTM vegetation, it is enough to have no more than two intermediate layers. In this case, the ANN with the training by Levenberg-Marquardt method was used. To assess the state of the water area, 12 elements corresponding to the spectral channels in the range of 450-660 nm were fed to the input; the output layer consisted of 16 elements determining the concentration of chlorophyll in the range of 5-20 mg/m^3 with increment of 1 mg/m^3. To determine the properties of the vegetation cover, 18 elements corresponding to the spectral channels in the range of 480-850 nm were fed to the input; the output layer consisted of 7 elements for the LAI range from 0.1 to 0.7 with increment of 0.1.

The setting of ANN learning is carried out by the regression dependences between the brightness values (or special indices) and the parameters to be determined, so that the error on the control sample, which does not intersect with the training, stops growing. If the control error begins to grow (in the case of re-training), several hidden elements or layers are gradually removed.

Figure 2 shows the change in the network error with ten neurons in one hidden layer when training the network by RTM to estimate the chlorophyll content in the Black Sea at the Sevastopol Bay by the hyperspectral data from Resource-P with the ANN tuning on regression models. The dependence, presented in formula 3, was used as a regression model for estimating the content of suspended solids in water. Concentration of chlorophyll "a" was determined with the use of the SeaWiFS model adapted to the spectral channels of the hyperspectral camera of the Resource-P satellite:

$$C_{ph}=a(L_{450}/L_{570})^{-b}, \quad (7)$$

where a and b are the approximation coefficients obtained from in situ;

L_{450} and L_{570} - the normalized brightness of radiation from under the water surface at wavelengths of 450 and 570 nm, respectively.

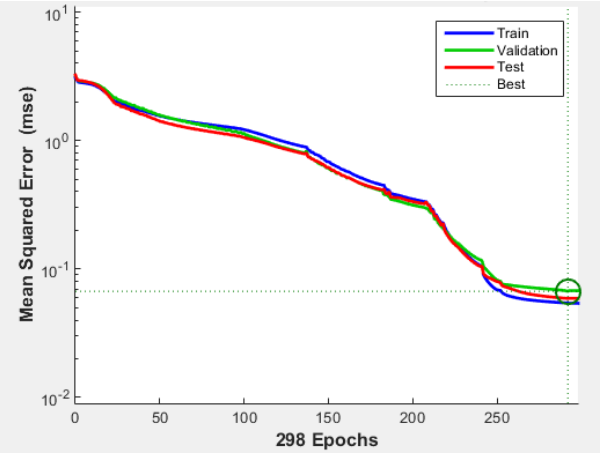

Figure 2: Reduction of the network error depending on the number of epochs at the output with 10 neurons in one hidden layer

The result of the evaluation is shown in Figure 3 in comparison with the result without tuning, where there was re-training of the network only when using the RTM. In the latter case, the result does not correspond to the actual in situ observations.

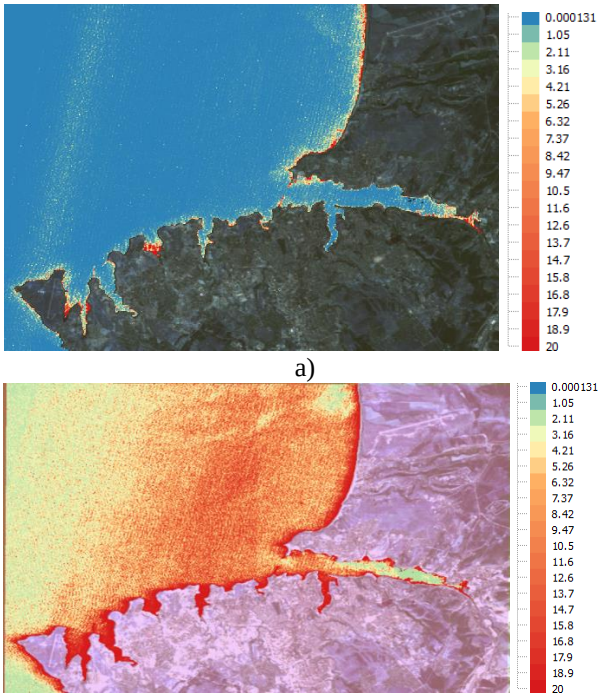

a)

b)

Figure 3: Content of chlorophyll "a" and its derivatives, mg/m^3, in the water area of the Sevastopol bay of the Black Sea (a – with the use of adaptive modeling, b - without the use of adaptive modeling)

The indicator of the efficiency of the adapted ANN for estimating the state of the water area in the form of a false-positive rate distribution (plot receiver operating characteristic, ROC) is shown in Figure 4 and reveals that the classifier tends to be almost ideal. As validation data of the classification accuracy estimation, the results from shipboard measurements of the chlorophyll "a" concentration in the near-surface layer of water at more than dozens of points within one of the surveyed bays were used, with simultaneous registration of spectral reflectance by the FieldSpec®4 spectroradiometer (ASD) in spectral range of 350 - 2500 nm.

The results showed that elevated concentrations of chlorophyll "a" and its derivatives are recorded in the eastern part of the Sevastopol Bay, as well as in the Kruglaya and Dvoynaya bays. The most polluted areas of the Sevastopol Bay, characterized by difficult water exchange, include the mouth of the Chernaya River, which brings many biogenic organic substances from the entire catchment area.

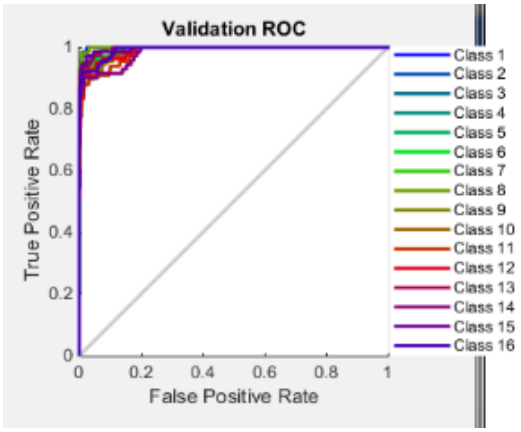

Figure 4: Plot ROC for assessing the effectiveness of the classification of the water area state according to the content of chlorophyll "a" into 16 classes from 5 to 20 mg/m^3 with increment of 1 mg/m^3

Figure 5 shows the result of the implementation of the developed method in the task of assessing the projective coverage of vineyards in the Crimean peninsula, where the model Borel and Gerstl was used (Borel and Gerstl 1994). Since this model is applicable only for one bush, it was modified to estimate the projective coverage of the field and take into account the planting scheme, and the data from the in situ measurements was used to configure the network. Field spectrometric measurements were carried out on one of the fields by the FieldSpec®4 spectroradiometer. Figure 6 shows examples of the obtained spectral signatures of vineyards for different LAI used to configure the network. Similar data were used to evaluate the functioning of the network. For example, the mean squared deviation of network outputs from validate data was only 6.14e-9, which indicates a rather high efficiency of the developed algorithm.

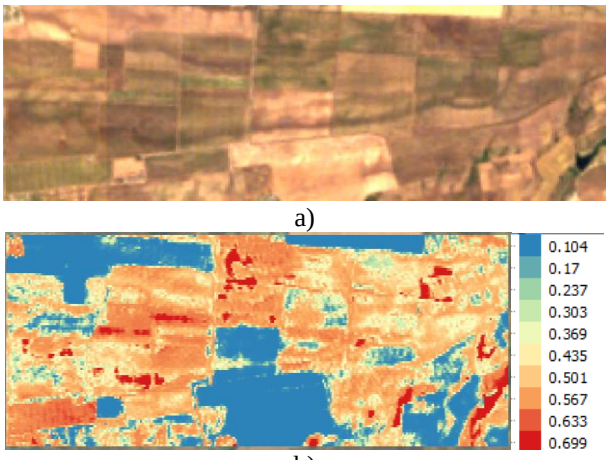

a)

b)

Figure 5: Map of the estimation of the projective coverage of vineyards using adaptive modeling (a – the image synthesized in natural colors according to hyperspectral data from the “Resurs-P” satellite, b – the result of the evaluation)

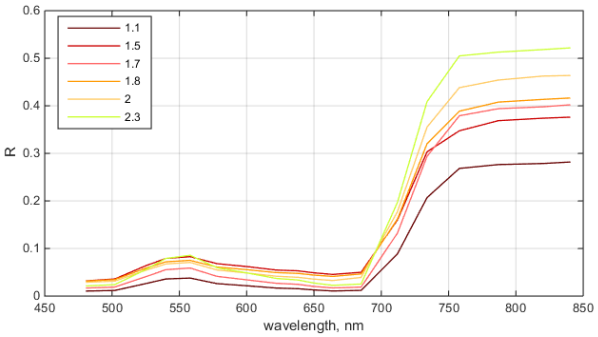

Figure 6: Spectral signatures of vineyards for different LAI, used for configuring and verifying the ANN

Implementation of methods for processing multispectral and hyperspectral data was carried out using specialized software that allows creating digital maps of the state of water bodies and vegetation. The presentation of the results was based on thematic services using earth remote sensing data (Zelentsov and Potriasaev 2017).

5. DISCUSSIONS

Application of the method of adaptive modeling to adjust the training of ANN by spectral characteristics of natural objects (vegetation and water bodies) showed that neural networks in conjunction with the description of multimodal facilities allow us to solve the inverse problem of reconstructing their properties by hyperspectral remote sensing data. The main advantage achieved through multimodality, adaptivity and the use of hyperspectral data is the reduction of the probability of errors.

It is planned to improve the algorithm for optimization of ANN parameters and the choice of its configuration by modification and hybridization of evolutionary optimization algorithms (such as swarm intelligence algorithm or stochastic genetic algorithm), wherein as the objective function the error of determining the object's state by in situ measurements is used. The use of ANNs is also promising for solving the problem of determining the relative abundances of the finite elements in pixels and subpixels in the case of the analysis of medium spatial resolution data, when the pixel comprises both vegetation and inter-crown objects (the problem of subpixel mixture separation and al.).

ACKNOWLEDGEMENTS

The research described in this paper is partially supported by the Russian Foundation for Basic Research (grants 16-08-00510, 17-06-00108,) state research 0073–2018–0003 (№ state registr. AAAA-A16-116030250074–1), International project ERASMUS+, Capacity building in higher education, № 73751-EPP-1-2016-1-DE-EPPKA2-CBHE-JP, Innovative teaching and learning strategies in open modelling and simulation environment for student-centered engineering education.

The research devoted to multimodel approach development is supported by the Russian Science Foundation (project 17-11-01254).

REFERENCES

Brovkina O., Novotnya J., Cienciala E., Zemeka F., Russ R., 2017. Mapping forest aboveground biomass using airborne hyperspectral and LiDAR data in the mountainous conditions of Central Europe. Ecological Engineering, 100, 219–230. Available from: www.elsevier.com/locate/ecoleng.

Hagan M.T., Demuth H.B., Beale M.H., Jesus O., 1996. Neural Network Design. 2nd ed. Boston, MA: PWS Publishing.

Kay S., Hedley J., and Lavender S., 2009.Sun glint correction of high and low spatial resolution images of aquatic scenes: A review of methods for visible and near-infrared wavelengths. Remote Sens., 1(4), 697–730.

Grigorieva O.V., Markov A. V., Zhukov D.V., Mochalov V.F., Nikolenko A.A., 2016. Possibility of the use of visible and near infrared multispectral and hyperspectral sensors for the bottom classification of shallow seas. Problems of military-applied geophysics and control of the state of the natural environment, 111-116. Petersburg: A.F. Mozhaysky's Military-Space Academy.

Hagan M.T., Menhaj M.B., 1994. Training feedforward network with the marquardt algorithm. IEEE Transactions on neural networks, 5(6), 989-993.

Lee Z., Carder K. L., Hawes S. K., Steward R.G., Peacock T.G., Davis C.O., 1994. A model for interpretation of hyperspectral remote-sensing reflectance. Appl. Opt., 33, 5721– 5732.

Grigoryeva O.V., Zhukov D.V., Markov A.V., Mochalov V.F., 2016. Reconstruction of the depths of coastal waters from data of multi- and hyperspectral imaging. Optics of the Atmosphere and the Ocean, 29(7), 553-559.

Jacquemoud S., Zarco-Tejada P.J., Verhoef W., Asner G.P., Ustin S.L., Baret F., François C., 2006. PROSPECT+SAIL: 15 Years of Use for and Surface Characterization. Proceedings IEEE International geoscience and remote sensing symposium, 31 July – 4 August, Denver, Colorado.

Gastellu-Etchegorry J.P., Demarez, V.Pinel V., Zagolki F., 1996. Modeling radiative transfer in heterogeneous 3-D vegetation canopies. Remote Sensing of Environment, 58, 131-156.

Rosema A.W., Verhoef W., Noobergen H., Borgesius J.J., 1992. A new forest light interaction model in support of forest monitoring. Remote Sensing of Environment, 42, 23-41.

Borel C.C., Gerstl S.A.W., 1994. Nonlinear spectral mixing models for vegetative and soil surfaces. Remote Sensing of Environment, 47, 403-416.

Khaikin S., 2008. Neural Networks: Full Course. Williams Publishing House.

R. Kalan, 2001. Basic Concepts of Neural Networks. Williams Publishing House.

Schowengerdt R.A., 2007. Remote Sensing, Third Edition: Models and Methods for Image Processing. Burlington, MA, Academic Press.

Egorov V.V., Ilyin A.A., Kalinin A.P., Rodionov A.I., Rodionov I.D., 2011. Biometrical features estimation of narcotic vegetation on the data of aircraft hyperspectral survey. Current problems in remote sensing of the Earth from space, 8(2), 195-200.

Zhukov D.V., 2016. Spectral features for identification of typical examples of pollution of seas according to aerial and space survey data. Optics of the Atmosphere and the Ocean, 29(7), 560-565.

Grigoryeva O.V., Zhukov D.V., Markov A.V., Mochalov V.F., 2016. Reconstruction of the depths of coastal waters from data of multi- and hyperspectral surveys. Optics of the Atmosphere and the Ocean, 29(7), 553-559.

Grigoryeva O.V., Shilin B.V., 2012. Experience in assessing the ecological characteristics of marine areas of seaports according to video spectral survey data. Modern problems of Earth remote sensing from space, 9(1), 156-166.

Biospheric Aspects of the Hydrological Cycle (BAHS), 1993. Report №27. Ed. By BAHC Core Project Office. Institut fur Meteorologie, Freie Universitat Berlin, Germany.

Biftu G.F., Gan T.Y., 2001. Semi-distributed, physically based, hydrologic modeling of the Paddle River basin, Alberta, using remotely sensed data. Journal of Hydrology, 244, 137-156.

Fefilov Yu.V., 2003. Development and creation of information technology for remote determination of parameters of primary productivity in ocean monitoring systems: Abstract from. disseration of Cand. tech. sciences. Moscow: Moscow Institute of Electronics and Mathematics.

Zelentsov V. et al., 2017. River Flood Forecasting System: An Interdisciplinary Approach. In: Refice A., D'Addabbo A., Capolongo D. (eds) Flood Monitoring through Remote Sensing. Springer Remote Sensing: Photogrammetry. Springer, Cham.

Zelentsov V., Sokolov B., Grigorieva O., Mochalov V., Potryasaev S., Shumeiko V., 2016. "Resurs-P" satellite hyperspectral data: preliminary evaluation of information capacities. Proc. 'Living Planet Symposium 2016', 1789. May 9-13 (ESA SP-740, August 2016), Prague, Czech Republic.

Sokolov B., Zelentsov V., Yusupov R., Merkuryev Yu., 2014. Multiple models of information fusion processes: Quality definition and estimation. Journal of Computational Science, 5(3), 380-386.

Zelentsov V.A., Potriasaev S.A., 2017. Architecture and Examples of Implementing the Informational Platform for Creation and Provision of Thematic Services Using Earth Remote Sensing Data. SPIIRAS Proceedings, 55, 86-113.

DESIGN METHODOLOGY CONSIDERING ENVIRONMENTAL IMPACT AND CRITICAL RAW MATERIALS, APPLICATION ON INDUCTION HOBS

Patricia Gómez[a], Daniel Elduque[b], Carmelo Pina[c], Carlos Javierre[d]

[a],[c] BSH Electrodomésticos España, S.A. Avda de la Industria, 49, Zaragoza (Spain)
[b],[d] i+, University of Zaragoza, C/ María de Luna 3, Zaragoza (Spain)

[a]patricia.gomez@bshg.com, [b]delduque@unizar.es, [c]carmelo.pina@bshg.com
[d]carlos.javierre@unizar.es

ABSTRACT
The target of this paper is to show a methodology developed to establish the influence of material composition on the environmental impact, considering the presence of critical and strategic raw materials.
A Life Cycle Assessment (LCA) has been performed to calculate the environmental impact, analyzing all the life cycle stages of the product. In order to achieve a more precise environmental impact analysis, EcoInvent database has been updated with primary data from product supplier's data. Also, a new software tool, "Sustainable Electronics" was developed and used to calculate the environmental impact and raw material consumption.
This methodology has been implemented on an induction hob, as it is a multipart product made of several components from electronics boards to metallic and plastic parts. The application of this methodology shows the huge influence of material composition on the environmental impact of the product, helping engineers to design more sustainable products.

Keywords: Critical Raw Materials, Life Cycle Assessment, Environmental Impact, Design Methodology, Induction Hobs.

1. INTRODUCTION

During the last decade, there is a huge concern among the European society about materials supply risk and their economical vulnerability. That was the reason why in 2008, the European Commission established the European Raw Materials Initiative. The main purpose of this initiative was to ensure the access to raw materials in the European Union, since more than 30 millions of industrial jobs depend on their availability (European Commission 2017).
Those raw materials with high economic importance and supply vulnerability are considered as critical. In order to ensure and improve citizen's quality of life, they need to be taken into consideration (Andrea et al. 2017), not only in Europe (European Commission 2017) but also globally (ESRC 2015).
The methodology to determine the criticality of a material takes into account data along last 5 years and parameters such as priority, quality or availability. It establishes that a raw material is consider as critical when the combination of two parameters, economic importance and supply risk, are above the limit defined by the European Commission (European Commission 2017).
As a result of the initiative and following the explained methodology, in 2011 the European Commission created the first list of critical raw materials from the non-energy and non- agricultural candidate materials considered as strategic. This document is updated approximately every three years. In 2011, 14 materials were considered as critical out of 41 potential candidates. While in the 2014 report, 20 critical materials were determined out of 54 strategic materials analyzed. Finally, in the last report, presented in 2017, 43 from 78, comprising 24 individual and 3 grouped materials (European Commission 2017).
Critical materials suppose a negative contribution not only for the economic vulnerability or supply risk but also for environmental risk. So in order to perform an exhaustive environmental impact assessment, the influence of all materials needs to be considered.
The supply of these raw materials is often necessary to develop better eco-efficient technologies and innovations. In addition, nowadays the design of products should be more environmentally responsible (Pina et al. 2015) (Camañes et al. 2014). The ecodesign trend emerged at the beginning of 90s in Europe, and it was over the last decade when the design of products has been hugely influenced by environmental legislation. Several laws have emerged in order to reduce the environmental impact of products and services by mean of ecodesign (ISO 2011) (European Parliament 2005) (European Parliament 2009), to reduce the use of hazardous or toxic substance and chemical control (European Parliament 2006) (European Parliament 2003); other laws are focused on the reduction of electrical and electronic equipment waste (European Parliament 2012).
Recent studies have shown that a key aspect when ecodesigning a product, is considering its material composition, as it has a significant influence on the environment. That is why this paper is focused on materials composition and their specific influence on the environmental impact.

In the household appliance industry, the reduction of products environmental impact supposes a huge contribution for market competitiveness. Any decrease of environmental impact can produce significant improvements in the companies, increasing their profits and their market competitiveness (Muralikrishna and Manickman 2017) (Plouffe et al. 2011).
Induction technology is an emerged cooking technology, where one of the most contributions to household appliances industry is its innovative technology, as heat is created directly in the pot from the generation of magnetic fields.

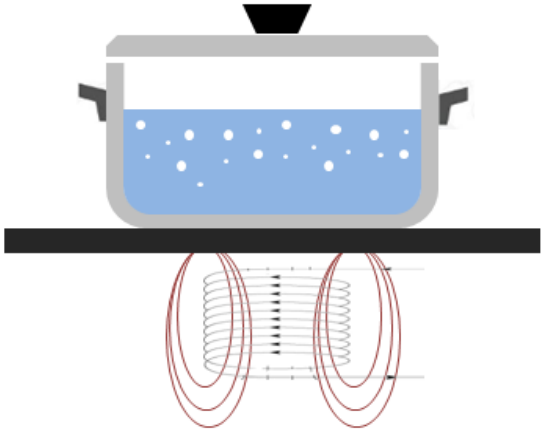

Figure 1: Magnetic Fields

Despite induction is not the most popular technology between electric hobs, the number of units sold from 2002 to 2008 increases around 24% per year. Increasing the number of units sold since it was developed and included into the market. Last 2007, more than a million of induction hobs were sold, 19.8% of the total market. During 2008, the number of units was increased in 22% and in 2010, 2.5 millions of units were sold in Europe; they rose 18% in 2012 and in 2017 around 12% (European Commission 2011).

2. ENVIRONMENTAL ASSESSMENT METHODOLOGY

Many Life Cycle Assessment (LCA) models are performed by means of professional databases as EcoInvent, developed by Swiss Centre for life cycle inventories, and one of the most used LCA databases (Martínez et al. 2015). Nevertheless, the main weakness of mentioned databases is that they include generic data that sometimes is not adjusted and adequate for specific products (Elduque et al. 2015a) (Elduque et al. 2015b).

2.1. General approach

The methodology explained in this paper is based on a LCA model updated with customized datasets. Although many materials and components are included on EcoInvent database, these are generic compositions, which usually do not match the composition of the product to be analyzed. This generates uncertainty on the environmental assessment results. Our methodology considers, not only the materials present in the final product but also the overall consumption of material and waste generation required. This innovative methodology allows engineers to calculate the environmental impact while developing their products, considering the exact composition, and knowing in each moment how changes in material composition affect the overall environmental impact. Also, it has been applied to components such as SMD transistors, diodes, aluminum parts and ceramic glasses. The results show that the presence of some precious metals like gold and critical raw materials as neodymium highly increases the environmental impact, despite being in low quantities.
Over the years, LCA methodology has been applied to analyze the environmental impact of several products from buildings (Pérez and Cabeza 2017) (Fraile-Garcia, et al. 2016) (Fraile-Garcia, et al. 2015), mobile telephones (Moberg et al. 2014) or waste containers (Galve et al 2016) to denim cloths (Periyasamy et al. 2017), food packaging (Fernández et al. 2013) or wine production (Jiménez et al. 2014).
There are several studies assessing life cycle environmental impacts of house hold appliances such as refrigerators (Monfared et al. 2014), washing machines (Ardente and Mathieux 2014), microwaves (Gallego-Schmid et al 2018) or dishwahsers (Johansson and Björklund 2010), however no single study exists in the field of induction hobs, focused on the material composition and critical raw materials as a key influence on the environmental impact.

2.1.1. Life Cycle stages

LCA methodology is performed in this paper to calculate the environmental impact, considering it throughout the all life cycle of the product. In order to perform an exhaustive LCA, it is really important to analyze in detail materials, processes, power consumption, transports, use, end of life… that affects the whole product and its entire life.

3. DESIGN METHODOLOGY APPLIED TO INDUCCTION HOBS (METHODOLOGY DEVELOPED)

In this paper, a new design methodology is proposed. It consists on updating EcoInvent database making it more precise by introducing data obtained from suppliers or manufacturers.

3.1. Dataset improvement methodology

The main objective is to consider the specific composition of each component to analyze the total environmental impact, following EcoInvent methodology but considering the real composition of products and components. In addition, several scenarios are considered in order to calculate the quantity of critical raw materials.

3.2. Inventory data and Assumptions

The life cycle inventory for this study has been performed by means of EcoInvent v3.4, one of the most

used databases and developed by Swiss Centre for Life Cycle Inventories.
SimaPro 8.4, developed by Pré Consultants, has modeled the LCA. Following ReCiPe methodology and Carbon Footprint, the LCA has been executed. Where the first one, ReCiPe combines midpoint and endpoint method to validate CML and Eco Indicator 99 systems and the second one, Carbon Footprint establishes the correspondence between the emissions of gas which generates greenhouse effect and CO_2 amount with same effect.

3.3. Software development

In order to implement the methodology developed and focusing on electronic components, a new software tool has been developed (Gómez et al. 2016). The Software "Sustainable Electronics" developed by the authors has the purpose of calculating the environmental impact and raw material consumption, determining the quantity of Critical Raw Materials on electronic components. It also allows the users to compare between several designs considering the exact composition, depending not only on the environmental impact but also assessing the consumption of critical and strategic raw materials.

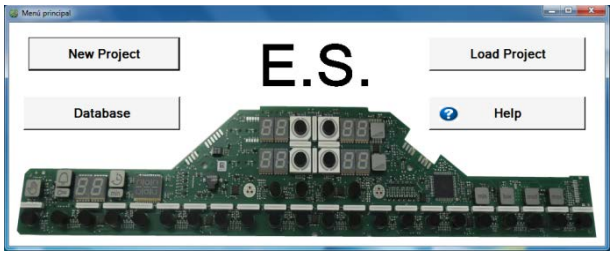

Figure 2: Software Screen

In comparison to other software, this allows the user to analyze the environmental impact of several design scenarios customizing Life Cycle Inventory included in the database.
As explained previously, nowadays there is an increasing concern over Critical Raw Materials; that is the reason why the software evaluates the environmental impact and shows the quantity of critical and strategic materials contained in the electronic component analyzed. There is a screen where the 27 critical materials considered by the EU are shown and the screen also includes the rest strategic materials evaluated by the EU in 2017.

4. METHODOLOGY APPLICATION

In this study, the innovative methodology previously explained has been applied on a specific multipart product: an induction hob. In addition, LCA was performed with the purpose of determining the influence of the materials composition.

4.1. Induction hob

Induction hobs are complex products, composed by many parts and components such as electronics boards, metallic parts, plastic housings, ceramic glass or wires.


Figure 3: Top Side Induction Hob

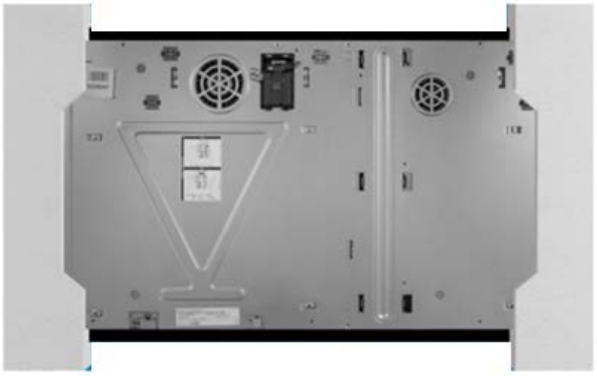
Figure 4: Bottom Side Induction Hob

Figure 5: Packaging, Wires and Documentation Induction Hob.

The environmental burden produced by all the components of an induction hob (electrical, electronic and mechanical ones) will be assessed to examine the percentage of each part in the total impact of the appliance and also in order to analyze the influence of the material composition on the environmental impact.
On one side, among electronics of an induction hob are included components such as printed circuit boards, diodes, transistors or resistors; on the other side, metallic parts comprise aluminum, stainless steel, iron or cooper parts. Besides, as mentioned before exist plastic or ceramic glass parts, which all together create the complex structure of the induction hob assembly.
Due to the complexity of the product and also because of the significant amount of parts and different materials used to manufacture each induction hob the design

methodology previously explained has been applied on induction hobs, considering the material composition and the presence of critical raw materials in electronics and mechanical components included in an induction hob.

4.2. Electronics Inventory

Due to the technological change among our society the use and consumption of electrical and electronic components is emerging, in consequence the sales of those components are increasing exponentially. The increase of electrical and electronic demand together with low costs of electronic devises generates a fast advancement in technology and in consequence, huge amounts of waste of electrical and electronic equipment (WEEE).

The study of electronic components in this paper is focused on diodes and transistors, both integrated in the electronic boards and included in the analyzed induction hob.

4.2.1. Electronics Inventory: Diodes

Diodes are simple semiconductor components, non lineal dispositive made of two electrodes, anode and cathode. An induction hob uses several types of diodes and also a high quantity of them, but here the study is focused on Zener diodes. They are two-terminal diodes that allow electrical current only in one direction, giving a stable voltage between terminals.

This subsection is focused on Zener diodes included in the induction hob, their weight is around 8miligrams and the main target of the study is to analyze the influence of their material composition on the environmental impact.

The composition of the studied diodes includes materials such as tin, silver, gold, nickel, antimony, manganese… where the higher environmental impact is caused mainly by gold, follow by silver and manganese.

The impact created by these materials on the environmental is really harmful, even although small quantities of them are included in the diode's composition.

4.2.2. Electronics Inventory: Transistors

Transistors are one of the most important electronic elements, due to the importance advance that their invention supposed for the electronic industry. They are considered as essential component for electronic devices due to their low electric power consumption.

Most of the main manufacturers of transistors are focused on the size reduction, whereas the environmental impact reduction supposes for the manufacturers an increase of market competitiveness, an improvement of their benefits and costs saves.

This study is focused on surface-mount device (SMD) transistors included in induction hobs, with dimensions in the region of 3 mm x 1.74 mm x 1.3 mm and 8 miligrams of weight.

Several SMD transistors have been analyzed, and it has been concluded that transistors that generate higher impact for the environment are the ones with higher quantities of gold in their composition (Gómez et al. 2015). Also, there are materials considered as critical by the European Union included in the composition of studied SMD transistors, they are cobalt, silicon and chromium; whose presence in the composition of the transistors suppose supply risk and they are affected by the economical importance of the material.

4.3. Mechanical Inventory

Mechanical components are essential for any type of induction hob, the main purpose of mechanical parts is placing each component, electronic and non electronic ones (electronic boards, wires, inductors…) and fix them during the whole life of the product.

Induction hobs include an extensive range of non electronic or mechanical components, such as aluminum or steel parts, ceramic glass, ferrites… In this section all of these parts and materials have been analyzed, studying also their environmental impact contribution.

4.3.1. Mechanical Inventory: Aluminum

Six cast aluminum alloys have been analyzed in order to study the influence of composition on the environmental impact (Gómez et al. 2016). They are Al Si9, Al Si9Cu3(Fe)(Zn), Al Si10Mg(Fe), Al Si9Cu3Zn3Fe, Al Si5Mg and Al Si12Cu1(Fe).

Once they have been analyzed and compared, it can be confirmed the importance of the selection of material composition not only for cost saving and mechanical properties improvement, but also for the impact that they generate on the environment.

The highest environmental impact in Recipe methodology is obtained by alloy Al Si9Cu3Zn3Fe with 1.01 pts per kg, in contrast the lowest impact belongs to Al Si9 alloy with 0.61 pts per kg. Analyzing all the alloys, it can be concluded that environmental impact is highly influenced by the materials included in the composition, where copper and tin are the materials with higher influence.

4.3.2. Mechanical Inventory: Steel

Steel is hugely included in the mechanical inventory, because most of the structural elements are made of it: in components such as the cover frame, screws and springs. There are five different types of steel included in the induction hob; all of them have been analyzed considering their composition and following the explained methodology.

In the 5 types of steel studied, the environmental impact varies from 0.2380 points per Kg to 0.6763 points per Kg in Recipe methodology; where the highest impact is created by stainless steel. The elements included in the analyzed steels that mainly contribute to increase the environmental impact are silica, chrome and boron.

4.3.3. Mechanical Inventory: Ceramic Glass

Ceramic glass part is the outer component of the induction hob; main characteristics of this part are hardness, temperature resistance and ease of cleaning.

There are several types of ceramic glass depending on the composition. Also the aesthetic of this piece is changeable and the client can choose between a large amount of them; there are several types of beveled surfaces and a huge variety of colors available.
As in the previous components, the environmental impact has been analyzed from real material composition of the seven types of ceramic glass analyzed.
Once the analysis of the ceramic glass types was performed, it can be established that tin and neodymium are the elements that highly contribute to increase the environmental impact. In addition, some critical raw materials considered by the European Union such as barite and magnesium together with neodymium are included in the composition.

4.3.4. Mechanical Inventory: Ferrite

Ferrites are ceramic compounds made of iron oxides and metallic cations like cobalt, manganese-zinc alloys or iron. They are mainly used in electronic devices such as transformers, electromagnets or electronic inductors. The main properties of ferrites are their low coercitivity with a high resistivity, high permeability and low losses.
In this study, the main purpose consists on showing the importance of considering the exact material composition of a component when analyzing environmental impact. That can be achieved comparing the results between EcoInvent ferrite dataset and the customization of it considering the exact material composition of manganese-zinc soft ferrites (MnZn).
The environmental impact in Recipe methodology varies from around 1570 mPt/Kg to more than 2220 mPt/kg, depending on material selection. Whereas the environmental impact calculated from EcoInvent dataset is more than 2700 mPt/Kg, which suppose a result 72% higher than the minimum environmental impact, obtained from a composition based on Iron Oxide and 21.5% more than the maximum, with a composition based on Manganese Oxide. The variation of the environmental impact results is created by the difference on the quantity of Manganese included in the dataset, which is higher on EcoInvent.

5. SOFTWARE APPLICATION

As it has been previously exposed, "Sustainable Electronics" software allows the users to consider environmental impact and critical raw materials content while designing or selecting new components or parts.
The software has been developed by means of Visual Basic .NET, trying to create a friendly interface for the users. It is made of three main blocks: new project/load project, databases and results; following the software structure shown in Figure 6.
By means of block "new project" the user is able to create and name a new project, whereas in block "load project" an existing project can be selected. Finally, in "BBDD Components" section the user can manage the database available in the tool.

Although this software has been firstly developed for electronic components, it was enlarged to include mechanical and structural components such as aluminum or glass ceramic components. In that way, the user is able to perform an exhaustive life cycle assessment, considering the whole life cycle stages. It allows the user to know the exact quantity of critical raw materials included in the analyzed product and also the impact they generate on the environment. Once the inventory data is updated, it seems to be easy for the user to get results and calculate the environmental impact of the components.

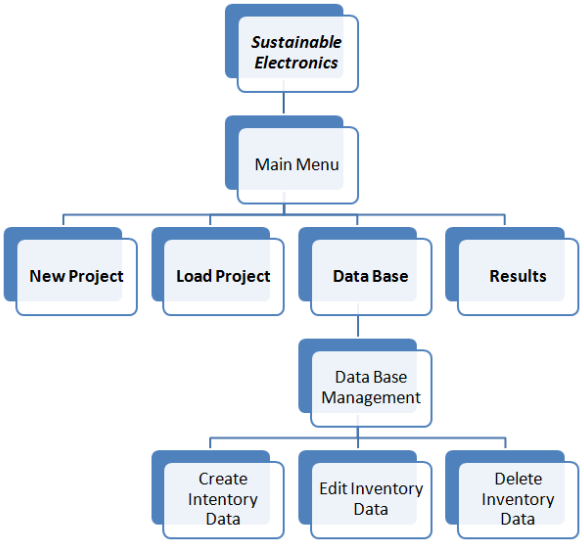

Figure 6: Software Structure

6. RESULTS AND DISCUSSION

Once implemented the methodology on the components included on an induction hob (electronic and mechanic), it is shown the huge influence of material composition on the environmental impact. Besides the impact created by the materials on the environment, the presence of critical raw materials has been assessed.
Material engineers are able to compare materials based not only on cost and properties but also taking into account materials' environmental impact.
Through the entire paper, it has been proved that the presence of certain materials highly contribute the increase of environmental impact values, specially in electronics components. That is the case of gold, cobalt, silicon and chromium included in transistors. And tin, silver, gold, nickel, antimony and manganese included on diodes composition.
In the case of mechanical inventory, the elements with higher environmental impact values are cooper and tin in the studied aluminum alloys; silica, chrome and boron in components made of steel; tin and neodymium on glass ceramics analyzed and finally in ferrites the environmental impact is mainly created by manganese.
Materials such as manganese, barite, and magnesium are included in the 2017 list of critical and strategic materials due to its high economic importance and supply risk in the European Union industry.

7. CONCLUSIONS

The article highlights the relevance of considering the exact materials composition in the calculation of the environmental impact.

In order to achieve more accurate environmental impact results and higher sensitivity when designing, it is really important to contemplate the exact material composition. Thereby, engineers are able to assess how few modifications on the composition and properties of materials such as steel, aluminum or ceramic glasses generate changes on the environmental impact. The influence of these changes can be calculated in detail by means of the methodology explained in this paper. In contrast, the influence of material composition on the environmental impact cannot be calculated by means of generic databases, where the material composition is not considered.

ACKNOWLEDGMENTS

The research in this paper has been partially supported by the Spanish MINECO under Project RETO RTC-2014-1847-6, and has been developed by members of the I+AITIIP (DGA-T08_17R) research group of the FEDER 2014-2020 "Construyendo Europa desde Aragón" program, recognized by the Regional Government of Aragon.

REFERENCES

Andrea Blengini A., Nuss P., Dewulf J., Nita V., Talens Peirò L., Vidal-Legaz B., Latunussa C., Mancini L., Blagoeva D., Pennington D., Pellegrini M., Van Maercke A., Solar S., Grohol M., Ciupagea C., 2017. EU methodology for critical raw materials assessment: Policy needs and proposed solutions for incremental impovements. Resources Policy, 53, pp. 12-19.

Ardente F., Mathieux F., 2014. Environmental assessment of the durability of energy-using products: Method and application. Journal of Cleaner Production, 74, pp. 62-73.

Camañes V., Elduque D., Javierre C., Fernández A., 2014. The Influence of Different Recycling Scenarios on the Mechanical Design of an LED Weatherproof Light Fitting. Materials, 7, pp. 5769-5788.

Elduque A., Elduque D., Javierre C., Fernández A., Santolaria J., 2015. Environmental impact analysis of the injection molding process: analysis of the processing of high-density polyethylene parts. Journal of Cleaner Production, 198, pp. 80-89.

Elduque A., Javierre C., Elduque D., Fernández A., 2015. LCI Databases Sensitivity Analysis of the Environmental Impact of the Injection Molding Process. Sustainability, 7, pp. 3792-3800.

ESRC Centre for Climate Change Economiics and Policy, 2015. Critical minerals today and in 2030: an analysis of OECD countries. Gramar Research Institute on Climate Change and Environment.

European Commission, 2011. Lot 23 Domestic and commercial hobs and grills, included when incorporated in cookers. Task 2: Economic and Market Analysis. Brussels: European Commission.

European Commission, 2017. Methodology for establishing the EU list of Critical Raw Materials. Guidelines. Luxembourg: Publications Office of the European Union.

European Commission, 2017. Study on the review of the list of Critical Raw Materials. Criticality Assessments, Luxembourg: Publications Office of the European Union.

European Parliament, 2003. Directive 2002/95/EC of the European Parliament and of the Council of 27 January 2003 on the restriction of the use of certain hazardous substances in electrical and electronic equipment (RoHS). EU Publications Office, Luxembourg. Official Journal of the European Union.

European Parliament, 2005. Directive 2005/32/EC of the European Parliament and of the Council of 6 July 2005 Establishing a Framework for the Setting of Ecodesign Requirements for Energy-Using Products, EU Publications Office, Luxembourg: Official Journal of the European Union.

European Parliament, 2006. Regulation (Ec) No 1907/2006 of the European Parliament and of the Council of 18 December 2006 concerning the Registration, Evaluation, Authorisation and Restriction of Chemicals (REACH), establishing a European Chemicals Agency. Official Journal of the European Union. EU Publications Office, Luxembourg.

European Parliament, 2009. Directive 2009/125/EC of the European Parliament and of the Council of 21 October 2009 Establishing a Framework for the Setting of Ecodesign Requirements for Energy-Related Products, EU Publications Office, Luxembourg: Official Journal of the European Union.

European Parliament, 2012. Directive 2012/19/EU of the European Parliament and of the Council of 4 July 2012 on Waste Electrical and Electronic Equipment (WEEE). EU Publications Office, Official Journal of the European Union. Luxembourg.

Fernández A., Javierre C., González J., Elduque D., 2013. Development of thermoplastic material food packaging considering technical, economic and environmental criteria. Journal of Biobased Materials and Bioenergy, 7(2), pp. 176-183.

Fraile-Garcia E., Ferreiro-Cabello J., Martínez-Camara E., Jiménez-Macias E., 2015. Adaptation of methodology to select structural alternatives of one-way slab in residential building to the guidelines of the European Committee for Standardization (CEN/TC 350). Environmental Impact Assessment Review, 55, pp. 144-155.

Fraile-Garcia E., Ferreiro-Cabello J., Martínez-Camara E., Jiménez-Macias E., 2016. Optimization based on life cycle analysis for reinforced concrete

structures with one-way slabs. Engineering Structures, 109, pp. 126-138.
Gallego-Schmid A., Mendoza J.M.F., Azapagic A., 2016. Environmental assessment of microwaves and the effect of European eco-design and waste management legislation. The Science of the total environment, 618, pp. 487-499.
Galve J.E., Elduque D., Pina C., Javierre C., 2016. Sustainable Supply Chain Disposal Scenarios on the Environmental Impact of a 2400 L Waste Container. Sustainability, 6, pp. 564-576.
Gómez P., Elduque D., Sarasa J., Pina C., Javierre C., 2016. Influence of the material composition on the environmental impact of cast aluminum alloy. Materials, 9, pp.1-14.
Gómez P., Elduque D., Sarasa J., Pina C., Javierre C., 2015. Influence of the material composition on the environmental impact of surface-mount device (SMD) transistors. Journal of Cleaner Production, 107, pp.722–730.
Gómez P., Pina C., Elduque D., Clavería I., Javierre C., Sarasa J., 2016. Environmental assessment tool to analyse the presence of critical and valuable raw materials. International Journal of Service and Computing Oriented Manufacturing, 2, pp.205–225.
Jiménez E., Martínez E., Blanco J., Pérez M., Graciano C., 2014. Methodological approach towards sustainability by integration of environmental impact in production system models through life cycle analysis: Application to the Rioja wine sector. SIMULATION, 90(2), pp. 143-161.
Johansson J.G., Björklund A.E., 2010. Reducing life cycle environmental impacts of waste electrical and electronic equipment recycling. Journal of Industrial Ecology. 14(2), pp. 258-269.
Martínez E., Blanco J., Jiménez E., Saenz-Diez J.C., Sanz F., 2015. Comparative evaluation of life cycle impact assessment software tool through a wind turbine case study. Renewable Energy. 74, pp. 237-246.
Moberg A., Borggren C., Ambell C., Finnveden G., Guldbrandsson F., Bondesson A., Bergmark P., 2014. Simplifying a life cycle assessment of a mobile phone. The International Journal of Life Cycle Assessment, 19 (5), pp. 979-993.
Monfared B., Furberg R., Palm B., 2014. Magnetic vs. Vapor-compression household refrigerators: a preliminary comparative life cycle assessment. International journal of refrigeration, 42, pp. 69-76.
Muralikrishna I.V., Manickman V., 2017. Environmental Impact Assessment and Audit. Environmental Management, Chapter Six, pp. 77-111.
Pérez G., Cabeza L.F., 2017. Buildings Life Cycle Assessment. Encyclopedia of Sustainable Technologies, pp. 275-290.
Periyasamy A.P., Wiener J., Militky J., 2017. Life cycle assessment of denim. Sustainability in Denim, chapter 4, pp. 83-110.
Pina C., Elduque D., Javierre C., Martinez E., Jiménez E., 2015. Influence of mechanical design on the evolution of the environmental impact of an induction hob. The International Journal of Life Cycle Assessment, 20, pp. 937-946.
Plouffe S., Lanoie P., Berneman C., Vernierd M.-F., 2011. Economic benefits tied to ecodesign. Journal of Cleaner Production, 19, pp. 573-579.
UNE-EN ISO 14006:2011, 2011. Sistemas de gestión ambiental. Directrices para la incorporación del ecodiseño. AEN/CTN 150 – GESTIÓN AMBIENTAL.

AUTHORS BIOGRAPHY

Patricia Gómez finished her degree in Industrial Engineering at the University of Zaragoza in 2013. She works at BSH Home Appliances Group – Spain. Since September 2014 she is a PhD candidate in Mechanical Engineering at the University of Zaragoza. Her work focuses on ecodesign taking into account materials composition and critical materials. She has researched on the influence of material composition of SMD transistor on the environmental impact.

Carmelo Pina is a part-time professor at the University of Zaragoza in the Department of Design and Manufacturing. He works, as well, at BSH Home Appliances Group – Spain and is the Head of Mechanical Platform Development of Induction Cooktops. He received his PhD in 2015. His main research interests include mechanical engineering, life cycle assessment and environmental impact.

Daniel Elduque is an Assistant Professor at the University of Zaragoza in the Mechanical Engineering Department and PhD Co-Director of Patricia Gómez. He is part of the I+ research group. He received his PhD in 2014. His main research interests include mechanical engineering, life cycle assessment and environmental impact. Some of his latest publications are the analysis of the environmental impact of the injection moulding process, and the influence of the composition on the environmental impact of SMD.

Carlos Javierre is a Professor at the University of Zaragoza in the Mechanical Engineering Department and PhD Co-Director of Patricia Gómez. He is part of the I+ research group. His main research interests include mechanical engineering, life cycle assessment and environmental impact. Some of his latest publications are the study of the influence of environmental conditions on the dimensional stability of components injected with PA6 and PA66; or the analysis of the environmental impact of the injection moulding process of high-density polyethylene parts by carrying out a life cycle assessment.

SIMULATION OF AN ISOLATED WIND POWER SYSTEM WITH BATTERY ENERGY STORAGE AND DUMP LOAD

R. Sebastián[(a)], J. Quesada[(b)]

[(a)] Department of Electrical, Electronic and Control Engineering (DIEEC), Spanish University for Distance Education, UNED 28040 Madrid, Spain
[(b)]University of the Basque Country UPV/EHU, E.U.I. Vitoria-Gasteiz, Nieves Cano 12, 01006 Vitoria-Gasteiz, Spain

[(a)]rsebastian@ieec.uned.es, [(b)]jeronimo.quesada@ehu.es

ABSTRACT
This study presents the modelling and dynamic simulation of an Isolated Wind Power System (IWPS) consisting of a Wind Turbine Generator (WTG), a synchronous machine (SM), consumer load, dump load (DL) and a Battery Energy Storage System (BESS). First the IWPS architecture and the dynamic models of the IWPS components are described. Second, the control requirements for frequency regulation of the IWPS are studied and a PID regulator to govern the active power stored+dumped by the BESS+DL combination or supplied by the BESS along with a power sharing algorithm between the BESS and DL is presented. Finally the IWPS is simulated facing to variations to load and WTG power. The simulation results are given showing graphs of the main electrical variables in the IWPS: system frequency and voltage and active power in each component. The results show how the BESS or BESS+DL combination regulates correctly the isolated system frequency. The results also show that the BESS improves the IWPS reliability when compared with the frequency control obtained using only the DL.

Keywords: Wind Turbine Generator, Battery energy storage, Isolated microgrid, Power systems Simulation

1. INTRODUCTION

Remote microgrids (RMG) are microgrids [Lasseter 2002] and [Basak et al. 2012] located in remote geographical areas which can be either isolated from the distribution grid or with an intermittent or low-reliability connection to it. Among the different possibilities, this article deals with the isolated wind power system (IWPS) presented in Fig.1. It consists of a synchronous machine (SM) working as a grid forming Synchronous condenser (SC) which provides the isolated grid voltage waveform, one wind turbine generator (WTG) which supplies uncontrolled active power, consumer load which consumes uncontrolled active power, a dump load (DL) which consumes controlled active power and a battery energy storage system (BESS) which consumes/generates controlled active power. The IWPS of Fig. 1 can be considered a High Penetration Wind Diesel Power System (WDPS) in Wind Only mode where the Diesel Generators are not running and only the WTGs supply active power to the system (Sebastián 2016). The Diesel generator (DG) in a WDPS is in charge of regulating the isolated system frequency and voltage. In the IWPS of Fig.1 the system voltage is controlled by the SM voltage regulator and the system frequency is regulated by balancing the active power of the system using the DL and BESS components as the next section 3 explains.

WDPSs are isolated power systems with low inertia, so that the benefits obtained by adding a short term Energy Storage System (ESS) to a WDPS such as frequency support, voltage stabilization, increasing reliability (Sebastián 2017) are more effective than in the case of large power systems with much higher inertia. The IWPS of Fig, 1 has no controlled generator and even lower inertia than a WDPS, so that the included BESS in it is fully justified to improve the IWPS power stability. Examples of ESS providing system frequency support in low inertia power systems are (Serban and Marinescu 2014), and (Sebastián 2016) with BESS, (Tarkeshwar and Mukherjee 2015) with capacitive ESS and (Sebastián, and Peña 2015) with a flywheel ESS.

2. THE IWPS MODELING

The IWPS of Fig 1 has been modeled using MATLAB-Simulink software. The models of the IWPS components are described in the following paragraphs.

The SM generates the voltage waveform of the isolated grid and its automatic voltage regulator controls the system voltage to be within the prescribed levels. The SM has a rated power ($P_{SM\text{-}NOM}$) of 300 KVA and works with zero input torque. The SM electrical part is represented by a sixth-order model and the voltage regulator model is an IEEE type 1. The SM inertia constant H_{SM} is 1 s (typical SM-H_{SM} values are between 1 and 1.5 seconds (Kothari 2003)).

The WTG consists of a Wind Turbine (WT) driving an Induction Generator (IG) directly connected to the autonomous grid forming a constant speed stall-controlled WTG (no pitch control). The mechanical power produced by a WT (Rodriguez Amenedo et al 2003) is:

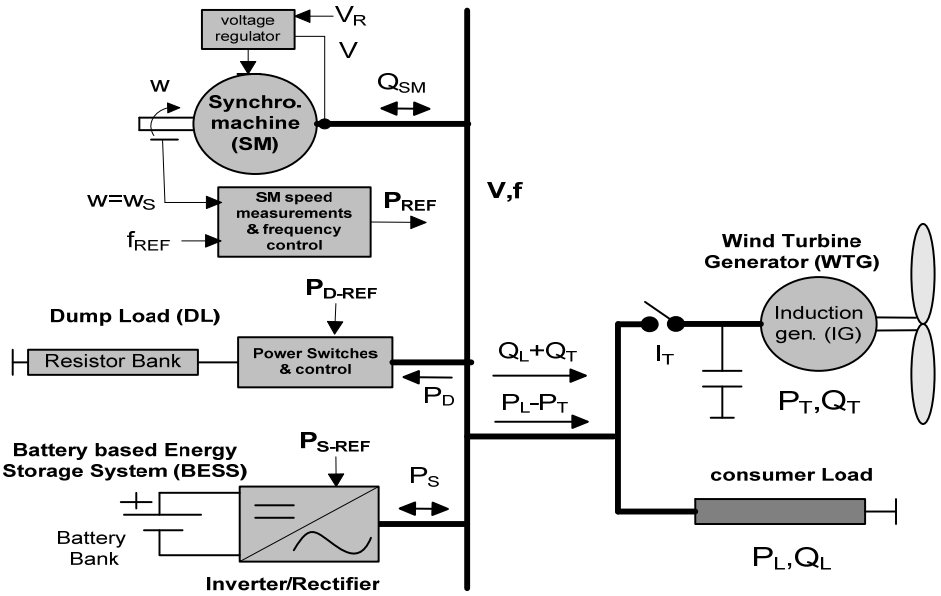

Fig. 1. Layout of the isolated Wind Power System

$$P_{T-MEC} = \frac{1}{2}\rho A v^3 C_P \quad (1)$$

where ρ is the air density, v is the wind speed, A is the area swept by the turbine blades and C_P is the power coefficient. C_P is a function of the Tip Speed Ratio (TSR=$R\omega_r/v$, where R is the blade length and ω_r is the WT shaft speed) and the blade pitch. Since the WTG used in this paper has no pitch control, C_P is only a function of TSR. In addition, the IG speed range variation in the WTG is very limited and thus C_P can be considered in first approximation as a function only of the wind speed. As the wind speed is quasi-random there is no way to control the active power that the WTG produces, so the WTG behaves as an uncontrolled source of active power. Ref. (Li and Chen 2008) shows other WTG types that allow better control of WTG produced power, but less robust and with more maintenance than the constant speed stall-controlled WT-IG type used in this article, The IG consumes reactive power so a capacitor bank has been added in Fig. 1 to compensate the power factor. The simulated constant speed stall controlled WTG model follows the one in (Gagnon et al. 2002) and consists of an Induction Generator (IG) of 275 kW (WTG rated power $P_{T\text{-}NOM}$ = 275 kW) and the Wind Turbine (WT) block described later. The electrical part of the IG is represented by a fourth-order model. Typical inertia constant H_W values for WTGs are between 2 and 6 seconds (Knudsen and Nielsen 2005). As the WTG used in the article is a low power one, the low limit of the previous range, 2 seconds, is assigned to H_W.

The Dump Load (DL) consists of a set of semiconductor power switches and a bank of resistors. By closing/opening these power switches, the DL consumed active power can be controlled behaving as a controlled sink of active power. The DL of (Sebastian 2011) is used and consists of eight three phase resistors connected in series with GTO switches. The resistors values follow an 8 bit binary progression so that the power consumed by the DL, assuming that the voltage in the isolated grid is nominal, can be expressed in the form:

$$(I_0+I_1\cdot 2^1+..+I_7\cdot 2^7)\cdot P_{STEP} = X_{D\text{-}REF}\cdot P_{STEP} \quad (2)$$

(2) means that the power can be varied discretely from 0 to $255\cdot P_{STEP}$, where P_{STEP} is the power corresponding to the least significant bit and I_J is "1" when the associated GTO is turned on and "0" when the GTO is turned off. For this article P_{STEP} = 1.4 kW and therefore $P_{D\text{-}NOM}$ = 357 kW. The DL is used in the IWPS to consume power when there is an excess of generated active power.

The BESS is based on a 240 V Ni-Cd battery bank, a battery side LC filter, an IGBT three-phase bidirectional Current Controlled Inverter (CCI) of rated power $P_{S\text{-}NOM}$=150kW, a grid side L filter and a 150 kVA elevating transformer. The BESS is used to store/supply the WTG active power excess/deficit for frequency regulation. BESSs can also support voltage regulation (Krata and Saha 2018).

The CCI performs the DC/AC conversion to connect the battery bank to the grid. The CCI can operate as an inverter by supplying power to the isolated grid (discharging the battery) or as a rectifier by absorbing power from the isolated grid (charging the battery). In order to reduce the converter sizing its reactive power reference is null, so the CCI works with 1 power factor. The CCI uses IGBTs, with a 5 kHz IGBTs switching frequency. A description of this grid connection converter is given in (Sebastian and Peña 2015).

The model for the 240V Ni-Cd battery (Tremblay 2007) comprises a variable DC voltage source in series

with an internal constant resistance. The voltage source value depends on the battery state of charge (SOC) according to the battery discharge curve and the internal resistance has the same constant value for charging and discharging. Ref (Li, 2013) shows other possible battery model. The battery stored energy is 93.75 kWh. Details of the battery sizing can be seen in (Sebastian 2008). The Ni-Cd battery capacity C is 390.625Ah (93.75 kWh/240V= 390.625Ah).

3. THE IWPS FREQUENCY REGULATION

The IWPS of Fig.1 can only works if the average power coming from the WTG is greater than the power consumed by the load plus the system losses. The frequency is regulated by maintaining the instantaneous balance of the active power consumed and produced. To accomplish this active power balance, the BESS can store (P_S>0) or the DL can dump (P_D>0) the surplus active power from the WTG. Also the BESS can supply power (P_S <0) in the periods when the wind power is less than current load. If P_T and P_L are respectively the active power generated by the WTG (P_T>0) and consumed by the load (P_L>0), J is the inertia of the SM, and ω is the SM shaft speed in rad/s (related to the frequency of the voltage waveform f by ω=2πf/p, with p the SM number of pole pairs), the power equation of the SM if no losses are taking into account is:

$$P_T - P_L - P_S - P_D = J\omega\frac{d\omega}{dt} \quad (3)$$

$$\frac{d\omega}{dt} = 0 \Rightarrow P_T - P_L = P_S + P_D \quad (4)$$

Equation (4) shows that to obtain constant synchronous shaft speed (system frequency) (dω/dt=0), the BESS+DL combination must consume power when P_T exceeds P_L and the BESS must generate power when P_T is less than P_L. Eq. (3) is valid for the considered IWPS because the BESS-CCI works in the current control mode, so the CCI adapts to the voltage waveform and frequency imposed by the SM. For BESS inverters working as a voltage source inverter (VSI) with a fixed frequency, equation (3) does not apply (Drouilhet 1999).

To control system frequency a PID frequency regulator is applied (Sebastián 2016). The PID input is the frequency error (difference between the current frequency and the power system nominal frequency 50/60 Hz) and the PID output is the reference power P_{REF} needed to be absorbed (P_{REF} >0) by the BESS+DL or supplied (P_{REF} <0) by the BESS to balance the active power of the system.

When P_{REF}>0 a power sharing between DL and BESS must be calculated, computing the reference power to be dumped by DL $P_{D\text{-}REF}$ and the reference power to be stored/supplied $P_{S\text{-}REF}$ by BESS, so that:

$$P_{REF} = P_{S-REF} + P_{D-REF} \quad (5)$$

$$0 \le P_{D-REF} \le P_{D-NOM}, \quad |P_{S-REF}| \le P_{S-NOM} \quad (6)$$

Eq. (6) is the DL rated power ($P_{D\text{-}NOM}$) and BESS rated power ($P_{S\text{-}NOM}$) limitations. The power sharing algorithm used in this article tries to maximize the energy storage of the available wind power excess in the BESS and to minimize the changes in the DL consumed power P_D. As commented before, P_D can only vary in discrete steps multiples of P_0 kW. To vary P_D the DL resistors must be switched on and off and these commutations produce system voltage variations and for this reason the BESS/DL load sharing algorithm tries to minimize the $P_{D\text{-}REF}$ changes. A detailed description of this algorithm can be seen in (Sebastian and Peña 2010).

4. SIMULATION RESULTS

The IWPS of Fig.1 were simulated using the MATLAB-Simulink multipurpose simulation software (Matlab 2018). The IWPS Simulink schematic can be seen in Fig. 2. Some of the components described previously and shown in Fig.2, such as the IG, the SM and its voltage regulator, the consumer load (main and extra load), etc. are blocks which belong to the SimPowerSystems library for Simulink.

The WT block of Fig. 2 contains the wind turbine power curves which define the mechanical power in the WT shaft $P_{T\text{-}MEC}$ as a function of the wind speed and the WT shaft speed as it is described in eq. (1) This $P_{T\text{-}MEC}$ is divided by the WT speed to calculate the mechanical torque applied to the WTG-IG.

The simulations cover the response of the IWPS to a 75 kW load disconnection/connection through the 3 Phase breaker (3PB) of Fig. 2 and to positive/negative wind steps. In all perturbations it is shown that the PID controller uses the BESS or the BESS+DL combination as actuators to regulate system frequency.

Four graphs are shown for the presented tests: the frequency per unit (Fig 3), the RMS voltage per unit (Fig 4), the active powers for the WTG and consumer load (Fig 5) and the active powers for the BESS and DL (Fig 6). For the WTG the active power is considered positive if generated and for the rest of components: BESS, DL and consumer load positive if consumed In the simulation initial state at t = 0, the IWPS is in steady state, the WTG is producing +143 kW (with 9 m/s wind speed), the load is consuming 100 kW, the BESS is consuming 43 kW and the DL power is 0 kW.

From the initial state, at t = 0.2 s the wind speed increases from 9 to 10 m/s and the WTG power increases from the initial 143 to the final 200 kW as Fig. 5 shows. The reference power P_{REF} is positive and below 0.9 $P_{S\text{-}NOM}$ (135 kW) during the whole transient and the initial DL power is zero, so according to the power sharing algorithm the BESS+DL load sharing is not performed, the DL is not actuated and the BESS stores all the active power excess (Fig. 6). During the transient the maximum frequency is 1.0014 and the voltage minimum is 0.995 pu. In the steady state the BESS consumes 100 kW.

At t= 3.2 s the 3PB of Fig. 2 is opened, so the 75 kW extra load is disconnected as can be seen in Fig. 5 which also shows a negative peak transient in the WTG power although the WTG steady state power has the same 200 kW initial value at t=3.2, since the wind speed does not change during the test.

As the active power excess is increased during this test in the same quantity as the load disconnection, soon the reference power P_{REF} is over 0.9 $P_{S\text{-}NOM}$ and the power sharing algorithm between BESS and DL is performed so the DL begins to consume power. Fig 6 shows that after the DL reaches a 50 kW constant value, the BESS assumes all the P_{REF} variability. In the steady state the BESS/DL consumption is 125/50 kW respectively.

During the -75 kW load transient the maximum frequency is 1.002 and the voltage minimum/maximum are 0.973/1.013 pu.

At t=6.2 the Fig2-3PB is closed, so the 75 kW extra load is re-connected as can be seen in Fig. 5, which also shows that the WTG power presents a positive peak transient. In steady state the WTG power has the same 200 kW initial value at $t = 6.2$ s, since the wind speed has not changed. The calculated reference power P_{REF} falls below 0.7 $P_{S\text{-}NOM}$ (105 kW) during this test, so according to the power sharing algorithm $P_{D\text{-}REF}$ is reduced until reaches 0 and the BESS assumes all the active power excess with a final value of 100 kW. The fpu minimum is 0.9981 pu and the voltage minimum/maximum are 0.9899/1.0019.

At t=9.2 a -2 m/s wind step is applied so the final wind speed is 8 m/s. The WTG reduces its supplied power to 92 kW in steady state which is less than the 100 kW consumer load consumption as Fig. 5 shows. Consequently the BESS changes from consuming the previous 100 kW active power excess to supplying the 8 KW active power deficit as Fig. 6 shows. The frequency decreases during the transient being its minimum 0.9973 and the voltage minimum/maximum are 0.9947/1.0042.

In Fig. 3 the system frequency resulting when only the DL is used to regulate frequency is plotted in dot style. The same PID regulator of the BESS+DL case is used and in this case $P_{REF} = P_{D\text{-}REF}$ as the BESS is turned off. In Fig. 3 the only DL-fpu waveform is very close to the BESS case until t= 9.2 s. From that instant the active power balance is not possible as the DL can not supply power, so the fpu falls continuously. Therefore, unless some load is shedding or another power source is quickly connected (Sebastian 2008), the IPWS will collapse.

5. CONCLUSSIONS

It has been shown how the BESS or the BESS + DL combination under the command of a PID controller and a BESS-DL power sharing algorithm balances the IWPS active power to regulate the IWPS frequency. The BESS also allows the IWPS to operate when the WTG power produced is lower than the consumed load, situation which it is not possible with the DL, so the IWPS reliability of the BEES+DL case is better than the frequency regulation in the DL only case.

ACKNOWLEDGMENTS

The authors would like to thank the DIEEC-UNED for supporting the attendance to the conference**.**

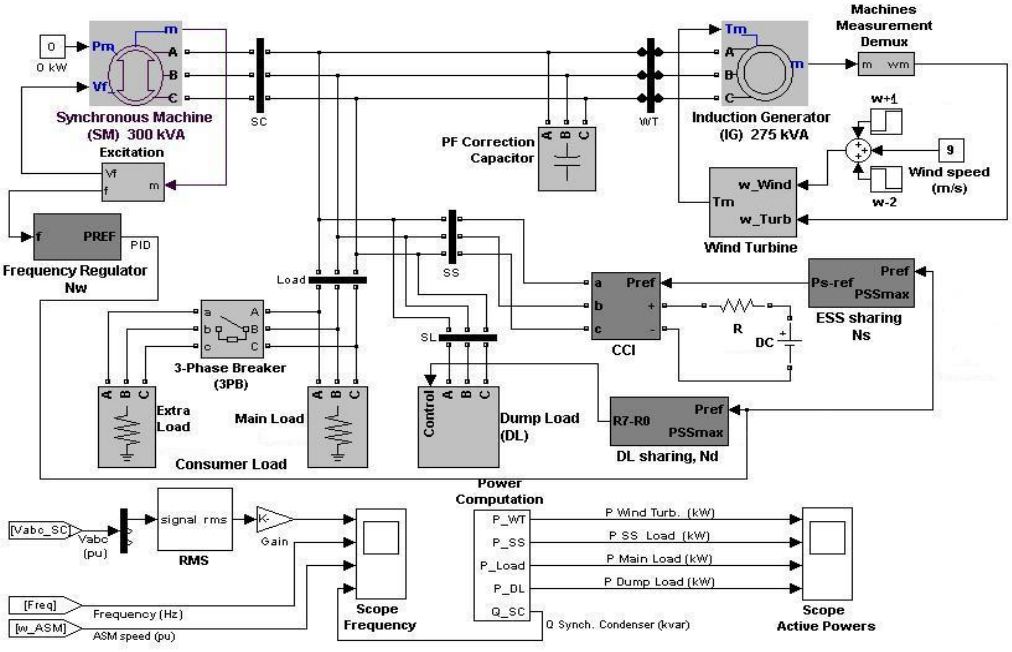

Fig. 2. Isolated Wind Power System with BESS and DL Simulink schematics

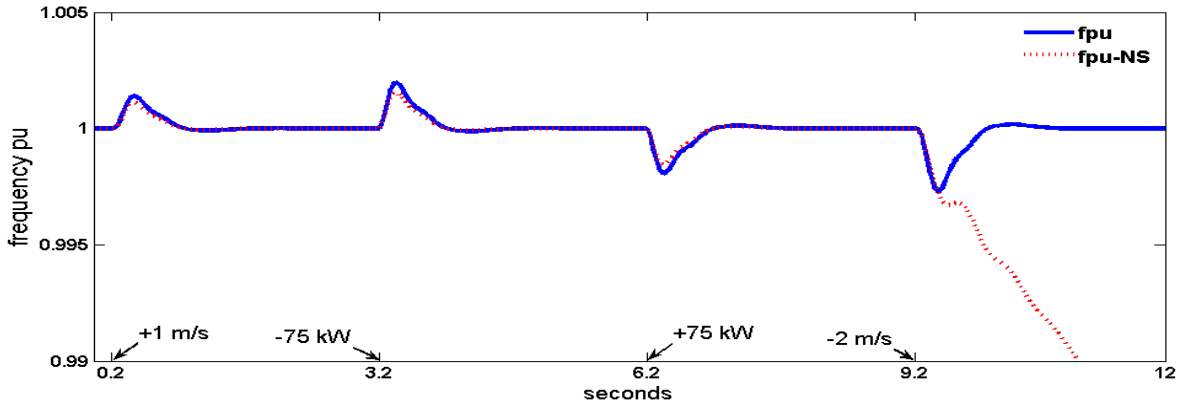

Fig. 3. Frequency per unit in the BESS+DL and only DL cases

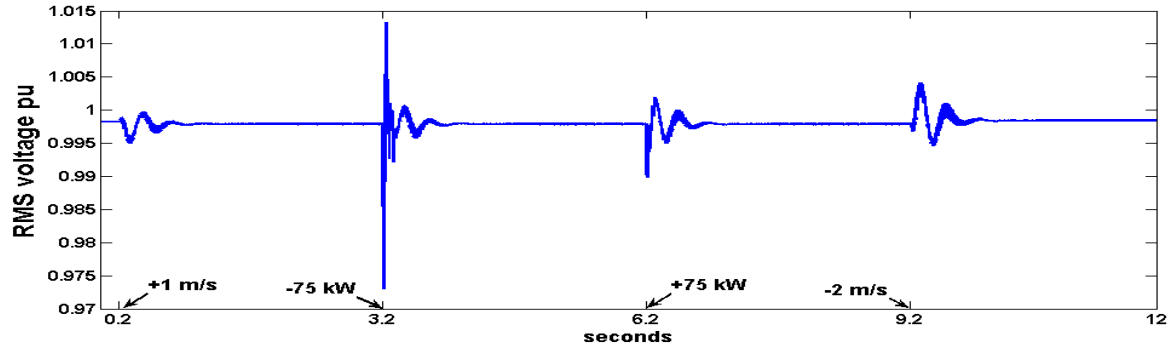

Fig. 4. RMS Voltage per unit (BESS+DL)

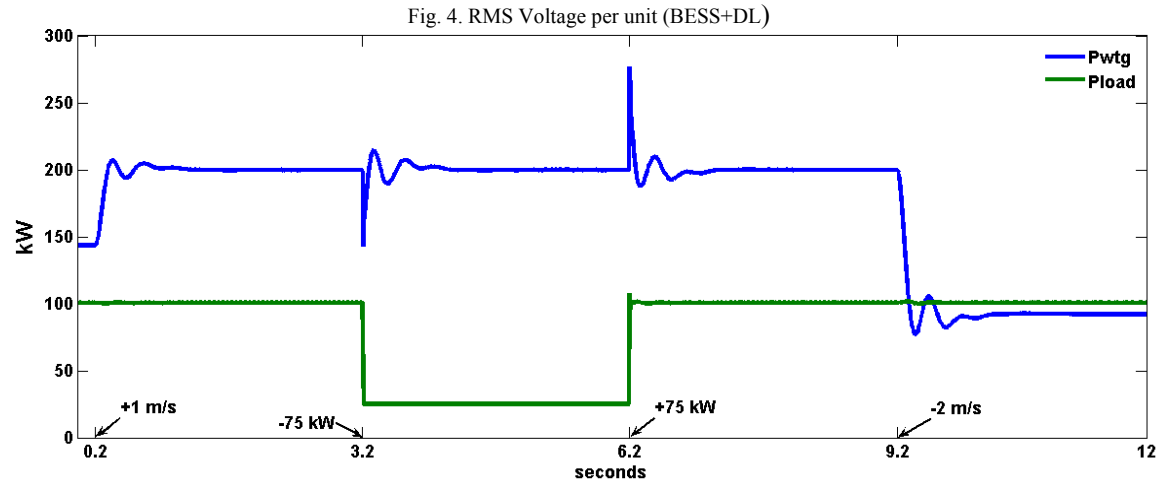

Fig. 5. Active powers for the WTG (generated) and load (consumed)

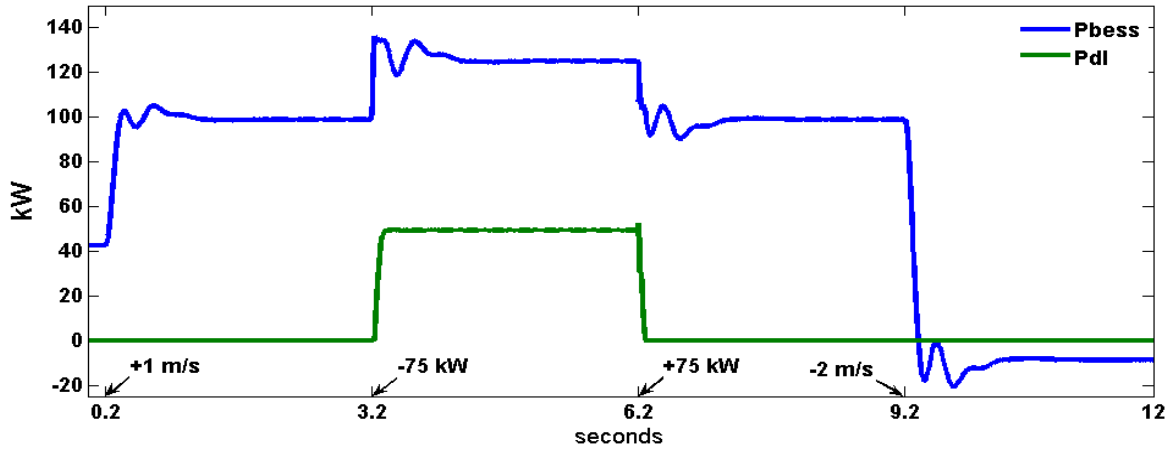

Fig. 6. Consumed Active powers for the BESS and DL

REFERENCES

Basak P., S. Chowdhury, S. Halder nee Dey, S.P. Chowdhury, A literature review on integration of distributed energy resources in the perspective of control, protection and stability of microgrid, Renew. Sustain. Energy Rev. 16 (2012) 5545–5556.

Drouilhet, S., "Power flow management in a high penetration wind-diesel hybrid power system with a short- term energy storage", Wind Power 99, June 1999, Vermont, USA

Gagnon, R.; Saulnier, B.; Sybille, G.; Giroux, P.: "Modelling of a Generic High-Penetration No-Storage Wind-Diesel System Using Matlab/Power System Blockset", 2002 Global Windpower Conference, April 2002, Paris, France

Knudsen H., Nielsen J. N., Introduction to the modeling of wind turbines, In *Wind Power in Power Systems*, T. Ackermann, Ed. Chicester, U.K. Wiley, 2005, pp. 525–585

Kothari, D. P. , Nagrath I. J., Modern power system analysis**,** Tata McGraw-Hill Education, 2003

Krata, J., Saha, T. K. Real-Time Coordinated Voltage Support with Battery Energy Storage in a Distribution Grid Equipped with Medium-Scale PV Generation, (2018), IEEE Transactions on Smart Grid. doi: 10.1109/TSG.2018.2828991

Lasseter R., Microgrids, in: Proceedings of the IEEE PES Winter Meeting, vol. 1, 2002, pp. 305–308.

Li, X., Hui, D., Lai, X.: 'Battery energy storage station (BESS)-based smoothing control of photovoltaic (PV) and wind power generation fluctuations', IEEE Trans. Sustain. Energy, 2013, 4, (2), pp. 464–473

Li H., Chen Z.: "Overview of different wind generator systems and their comparisons", IET Renewable Power Generation. vol. 2 no. 2, pp. 123-138, 2008.

Matlab 2018, The MathWorks Inc., "Matlab – Simulink documentation", available in: http://www.mathworks.es/es/help/index.html

Rodriguez Amenedo, J.L. , J.C. Burgos Diaz, S. Arnalte Gomez, Sistemas eólicos de producción de energía eléctrica, ISBN: 9788472071391, Madrid 2003.

Sebastian, R.: "Smooth transition from wind only to wind diesel mode in an autonomous wind diesel system with a battery-based energy storage system", Renewable. Energy, vol. 33, pp. 454-466, 2008.

Sebastián R., Peña Alzola R., 2010 , Effective active power control of a high penetration wind diesel system with a Ni–Cd battery energy storage, Renewable Energy, Volume 35, Issue 5, May 2010, Pages 952-965, ISSN 0960-1481, http://dx.doi.org/10.1016/j.renene.2009.11.029.

Sebastián R., 2011,"Modelling and simulation of a high penetration wind diesel system with battery energy storage" International Journal of Electrical Power & Energy Systems vol. 33 no. 3 pp. 767-774 March 2011 ISSN 0142-0615., http://dx.doi.org/10.1016/j.epsr.2010.10.033.

Sebastián R, Peña-Alzola R., 2015, Control and simulation of a flywheel energy storage for a wind diesel power system, International Journal of Electrical Power & Energy Systems, Volume 64, 2015, Pages 1049-1056, ISSN 0142-0615, https://doi.org/10.1016/j.ijepes.2014.08.017.

Sebastian R., 2016, "Application of a battery energy storage for frequency regulation and peak shaving in a wind diesel power system," in IET Generation, Transmission & Distribution, vol. 10, no. 3, pp. 764-770, 2 18 2016. doi: 10.1049/iet-gtd.2015.0435.

Sebastián R., 2017.: 'Battery energy storage for increasing stability and reliability of an isolated Wind Diesel power system', IET Renewable Power Generation, 2017, 11, (2), p. 296-303, DOI: 10.1049/iet-rpg.2016.0220

Serban I.and C. Marinescu, "Control Strategy of Three-Phase Battery Energy Storage Systems for Frequency Support in Microgrids and with Uninterrupted Supply of Local Loads," in IEEE Transactions on Power Electronics, vol. 29, no. 9, pp. 5010-5020, Sept. 2014

Tarkeshwar M. and V. Mukherjee, "Quasi-oppositional harmony search algorithm and fuzzy logic controller for load frequency stabilisation of an isolated hybrid power system", in IET Generation, Transmission & Distribution, vol. 9, no. 5, pp. 427-444, 4 2 2015. doi: 10.1049/iet-gtd.2014.0502

Tremblay O., L.-A. Dessaint, A.-I. Dekkiche: "A generic battery model for the dynamic simulation of hybrid electric vehicles", Vehicle Power and Propulsion Conference, 2007, VPPC 2007. IEEE 9–12 September (

INVESTIGATION OF PRESSURE LOSS COEFFICIENT OF HOT DUCT BREAK SCENARIO IN ALLEGRO REACTOR USING THE CATHARE THERMOHYDRAULIC CODE

Gusztáv Mayer[(a)], Attila Guba[(b)]

[(a),(b)]Hungarian Academy of Sciences Centre for Energy Research (MTA EK), P.O. Box 49, H-1525 Budapest, Hungary

[(a)]gusztav.mayer@energia.mta.hu, [(b)]attila.guba@energia.mta.hu,

ABSTRACT

Preliminary thermohydraulical calculations carried out for the ALLEGRO 75 MW CEA 2009 design (Mayer and Bentivoglio 2014) pointed out that the peak cladding temperature exceeded the required temperature limit in case of hot duct break scenario, when the aggravation event of the stop of the second blower was taken into account. The value of the pressure loss coefficient used in the hot duct break modeling plays pivotal role in the corresponding peak cladding temperature (PCT). In this study we investigate how this pressure loss value influences the peak cladding temperature in ALLEGRO reactor. We selected the French CATHARE thermohydraulical code as a simulation tool to describe the hot duct break transient and to determine the PCT values. We carried out several transient calculations by varying the pressure loss coefficient and the results confirmed its importance. It was found that if the pressure loss value is less than 1.4 the PCT limit exceeds the criterion of 850 ºC.

Keywords: ALLEGRO, gas cooled, fast reactor, CATHARE simulation, hot duct break, pressure loss

1. INTRODUCTION

The helium cooled GFR2400 fast reactor is one of the six concepts that were selected for future research by the GIF international forum. The main advantage of the 2400 MWth power nuclear reactor is its high coolant outlet temperature – providing high thermal efficiency – and the fast neutron spectrum – giving the possibility of the closure of the fuel cycle. Nevertheless, any gas cooled fast reactor has never been built so far. Therefore, a demonstrator reactor was envisaged to validate the new refractory carbide fuels and to prove the usability of helium technology. This reactor is called ALLEGRO and its currently expected thermal power is 75MW. The ALLEGRO reactor is currently being developed the in Czech Republic, France, Hungary, Slovakia and Poland. Previous studies revealed that the hot duct break scenario aggravated by blower failure is one of the most critical transients of ALLEGRO reactor. In this paper the pressure loss coefficient of the hot duct break is investigated using the CATHARE thermohydraulics code.

2. THE ALLEGRO 75MW 2009 CEA DESIGN

The ALLEGRO 75MW CEA 2009 design consists of two main primary loops and three additional decay heat removal (DHR) loops as it can be seen in Figure 1. The primary coolant is helium pressurized at 70 bar. Each primary loop contains a primary blower which drives the flow.

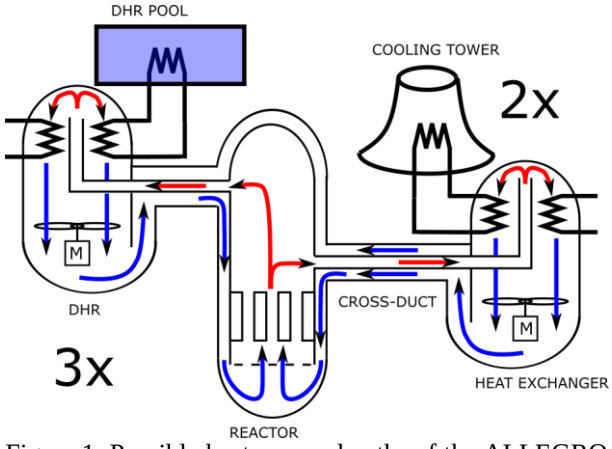

Figure 1: Possible heat removal paths of the ALLEGRO 75MW CEA 2009 design. During normal operation the three DHR loops (left) are closed.

In normal operation the heat is removed by the two main primary-secondary heat exchangers. The secondary side of them contains water pressurized at 65 bar. The water coolant is circulated by the two main water pumps and the heat is removed via the two air coolers, which are cooled directly by ambient air. As this concept suggests there is no electricity production envisaged for this demonstration reactor.

The three DHR loops (Figure 1. left hand side) are dedicated for accidental conditions and they are closed during normal operation. These loops are designed to remove decay heat in both natural and forced convection mode. Their secondary circuit is filled with pressurized water of 10 bar and they are designed to operate in

natural convection. The heat sink of the loops are three independent pools filled with water.
The whole primary system is encompassed by a cylindrical tank, which is called the guard vessel. The primary purpose of this vessel is to keep backup pressure in case of LOCA situations in order to decrease the power needed for the active core cooling.
Each shaft of the main primary blowers is equipped with two motors. The first is the main motor, which has the role to circulate the helium coolant in nominal conditions. The second is an auxiliary motor, which drives the flow as the scram is actuated. This second auxiliary motor is called "pony" motor and has significantly less power that the main motor.
This concept is called the "pony concept" and the primary idea behind it is to keep the nominal heat removal path after scram without starting the DHR loops. Of course, if the heat removal using the ponies and the primary heat exchangers is not sufficient anymore the ponies are stopped, the main primary valves are closed and the DHR loops are opened.
When the SCRAM is effective, only the decay heat has to be removed from the core, which is only a few percent of the original core power. In order to avoid the overcooling of the core the ponies are running only at 20% of the nominal rotation speed if the system is pressurized (Mayer and Bentivoglio 2015). When there is a loss of coolant accident (LOCA) and the primary pressure becomes low, the speed of the ponies is increased back to the original 100% rotational speed. In this case the helium is less dense than at nominal pressure. For that reason, the ponies require less electric power in LOCA situations than at pressurized conditions. According to this concept the current protection logic of ALLEGRO switches off the main motors after SCRAM and starts the pony motors immediately.

3. HOT DUCT BREAK SCENARIO

In conventional PWRs (Pressurized Water Reactors) the hot and cold legs (ducts) are separated from each other. Opposed to that, due to thermomechanical considerations the gas cooled ALLEGRO 75MW CEA 2009 design uses the so called cross duct technology, which means that the hot duct of the primary circuit is led inside the cold duct. In other words, the ALLEGRO uses a "pipe in a pipe" concept. As a consequence, in case of hot duct break scenario, there is no loss of primary coolant. However, there is a large flow which bypasses the core through the broken pipe (Figure 2). Consequently, the decreasing flow rate leads to an excessive temperature rise in the core, which threatens the integrity of the fuel claddings.
Since the maximal fuel cladding temperature plays a pivotal role during the design process of a nuclear power plant we investigated in detail the effect of the pressure loss coefficient through the break. The main focus is on how the pressure loss coefficient of the break influences the maximal peak cladding temperature during the hot duct break transient.
In nuclear reactors there is a technical limit for keeping the maximum fuel cladding temperature below a certain level. In case of hot duct break initial event of ALLEGRO the corresponding temperature limit is 850 ^{o}C – it is the beginning of lack of confining the cladding material. For initial events that are in the design basis of a nuclear power plant a single failure criterion has to be applied. This means that the hot duct break has to be aggravated by other failures. Previous studies pointed out that the failure of one of the blowers is the worst case single failure in this situation (Mayer and Bentivoglio 2014).

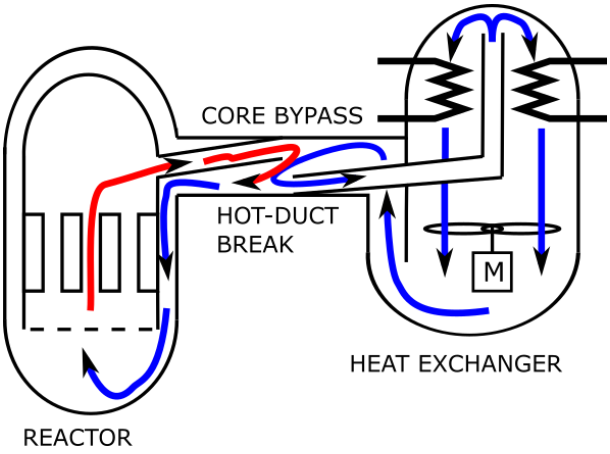

Figure 2: Graphical representation of the core bypass in case of hot duct break of ALLEGRO. The second loop is not depicted because its isolation valve is supposed to be closed after the stop of the 2nd blower.

4. THE CATHARE CODE USED FOR SIMULATION

In this study the French CATHARE thermohydraulic code was selected as a simulation tool for the hot duct break scenario of ALLEGRO. The CATHARE code was primarily developed for simulating two-phase flow phenomena in PWRs and BWRs (Boiling Water Reactors). Later, its validity was extended to sodium and gas cooled reactors as well.
The CATHARE code uses a one-dimensional 6-equation model (Bestion 1990), which is based on the conservation principles of the mass, momentum and energy for both liquid and gas phases. There is a possibility to model non condensable gases by adding an extra mass balance equation to the system. The full equations solved by the CATHARE are presented in (Bestion 1990). For a monophasic gas flow these equations can be written as:

$$\frac{\partial}{\partial t}\left(A\rho_G\right)+\frac{\partial}{\partial z}\left(A\rho_G V_G\right)=S_i \tag{1}$$

$$A\rho_G\left[\frac{\partial V_G}{\partial t}+V_G\frac{\partial V_G}{\partial z}\right]+A\frac{\partial p}{\partial z}= -\chi_f C_G\frac{\rho_V}{2}V_G\left|V_G\right|+A\rho_G g \tag{2}$$

$$\frac{\partial}{\partial t}\left[A\rho_G\left(H_G+\frac{V_G^2}{2}\right)\right]+$$
$$\frac{\partial}{\partial z}\left[A\rho_G V_G\left(H_G+\frac{V_G^2}{2}\right)\right]-A\frac{\partial p}{\partial t} \quad (3)$$
$$=\chi_c Q_{PG}+A\rho_G V_G g+SE_G$$

With ρ_G : gas density (kg.m^{-3}), V_G : gas velocity (m.s^{-1}), A : flow area (m^2), S_i : gas mass source term, p : pressure (Pa), χ_f : friction perimeter (m), C_G : friction coefficient, g : gravity (m.s^{-2}), H_G : gas enthalpy (J.kg^{-1}), χ_c : heating perimeter (m), Q_{PG} : heat transferred to the walls (W.m^{-2}), SE_G : source of energy (W.m^{-1}).
The gas (helium for this application) is considered as a perfect gas.
Solid structures are represented using so-called walls and friction and heat transfer between the gas and the walls are calculated using classical correlations.

5. THE HOT DUCT BREAK MODEL

5.1. Hot duct break model

The amount of flow which bypasses the core depends on the break size and the break geometry. Using conservative considerations in this study we supposed that there is a guillotine break in the middle of the hot duct.

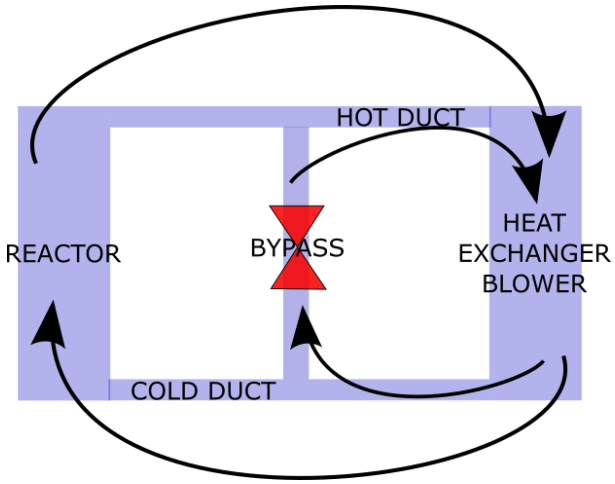

Figure 3: Hot duct break model of ALLEGRO. The hot and the cold ducts are connected by a pipe element. In case of hot duct break simulation, the valve is opened.

The CATHARE model of ALLEGRO contains several "pipe" elements. Since CATHARE is a one dimensional code, the hot duct break is simulated by simply inserting a pipe element between the hot and the cold duct as it is depicted in Figure 3. There is a valve in this connecting pipe, which is closed during normal operation and opened when the hot duct break occurs. When this valve opens a continuous gas flow is generated between the cold and the hot duct. As a result, the nominal mass flow rate of the core may drastically decrease causing a temperature increase in the reactor core. The most important parameter which influences the break mas flow rate is the pressure loss coefficient of the break valve. The lower pressure loss coefficient is selected the higher maximum cladding temperature develops.

5.2. Implementation of hot duct break

The nodalization of the ALLEGRO reactor is depicted in Figure 4. We built the reactor core by using an average, a hot and a bypass channel. The main heat exchangers were modeled by using two axial elements, one for the primary and one for the secondary side and then an exchanger module was defined between these two axials. The guard vessel consists of two axial elements and further volumes were added in order to connect it with the primary system in case of LOCA events.

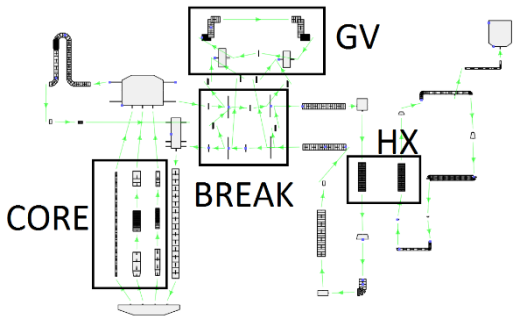

Figure 4: CATHARE nodalization scheme of the ALLEGRO reactor. HX represents the main heat exchanger, GV depicts the guard vessel.

6. CATHARE CALCULATIONS

The transient calculations were started from steady state conditions of the ALLEGRO 75MW 2009 CEA design. At the start of the transient the break valve (Figure 3. middle) is suddenly opened in the first loop and at the same time the blower in the second loop is tripped. The blower in the second loop coast down according to its inertia and friction. At around 60 seconds the blower stops and the primary valve in the cold leg of the second loop closes. According to the current Instrumentation and Control (I&C) the first blower continues to work at 20% of the original speed.
Series of CATHARE simulations were carried out by varying the pressure loss coefficient of the break valve from 0 to 1.4 and the maximum cladding temperature values were monitored.

7. RESULTS

The corresponding maximal cladding temperatures can be seen in Figure 5. When the pressure loss coefficient was set to zero, the core exceeded the temperature of 1300 ºC – which is the melting of the cladding – in less than 4 minutes. When the pressure loss value was set to 1.4 the PCT value was about 850 ºC, which is the maximum permissible limit for this transient. These results suggest that the ALLEGRO cladding remains confined in case of hot duct break if the pressure loss value is larger than 1.4. We emphasize here that these

computations were best estimate calculations so additional margin has to be taken into account.

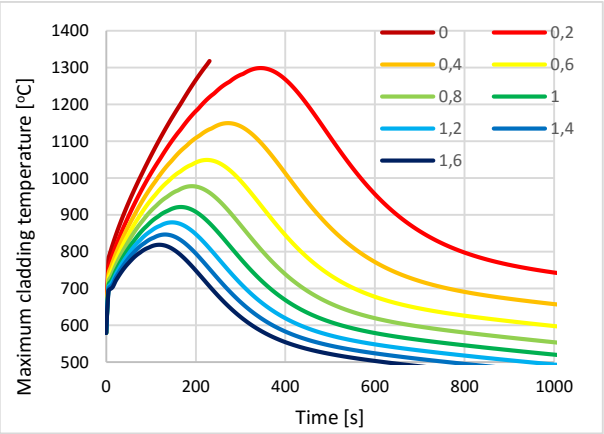

Figure 5: Time evolution of maximum cladding temperature for different pressure loss values.

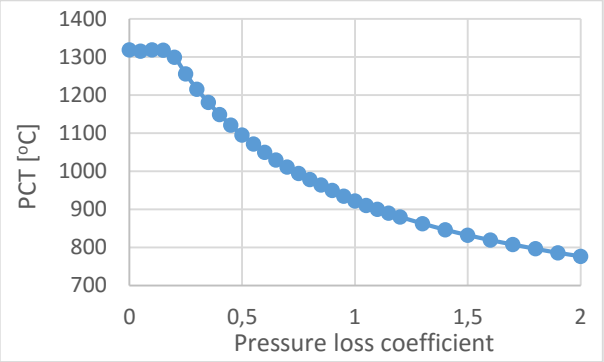

Figure 6: Effect of the pressure loss coefficient on the PCT value.

Nevertheless, previous Computational Fluid Dynamic (CFD) studies pointed out (Farkas and Farkas 2017) that the pressure loss values are at the range of ~1.0, which suggests that the in case of 75MW initial power the cladding temperature will exceed the 850 °C limit. In our previous CATHARE calculations (Mayer 2017) we used the 0.549 value for the pressure loss coefficient, which might be sufficiently conservative for further consideration steps. In those calculations, obviously, the PCT values are higher, which indicates that the initial core power of the ALLEGRO has to be decreased significantly in order to fulfill the criterion of 850 °C.

Of course, other solutions are possible to keep the PCT below 850 °C, for instance introducing a third primary loop to the ALLEGRO or redesign the I&C of ALLEGRO.

Figure 6. shows the PCT values in the function of the pressure loss coefficient. It can be seen that the cladding temperature exceeds the cladding melting temperature if the pressure loss coefficient is below 0.2. If the pressure loss values are higher than 1.4 the PCT is below 850 °C.

In Figure 7. the time instants of the PCT values are depicted. For the pressure loss values below 0.2 there is no PCT value calculated because the CATHARE code does not give results for melted core. Therefore, the instant of the reaching of the 1300 °C is depicted. The conclusion of Figure 7 is that as the pressure loss coefficient is increasing the duration of the peak cladding temperature is decreasing. This phenomenon can be seen in Figure 5. as well.

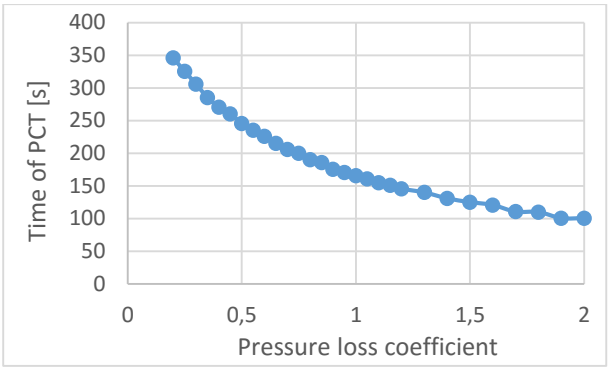

Figure 7: Effect of the pressure loss coefficient on the PCT value

8. CONCLUSION

The results showed that the PCT values are highly dependent on the pressure loss values used at the break. If the pressure loss coefficient at the break is zero, the cladding will melt in less than 4 minutes. If this value is 1.4 or higher the corresponding PCT values remain below the 850 °C limit.

ACKNOWLEDGMENTS

This work has been carried out in the frame of VKSZ_14-1-2015-0021 Hungarian project supported by the National Research, Development and Innovation Fund.

REFERENCES

Bestion D., 1990. The physical closure laws in the CATHARE code, Nuclear Engineering and Design 124, 229-245.

Farkas I., Farkas I. T., 2017. Determination of pressure loss coefficient of the hot duct break of the CEA ALLEGRO 2009 concept using a CFD technique. AEMI-2017-206-3.3-01-M0

Mayer G., Bentivoglio F., 2014. Transient analysis of crossduct break scenarios using the CATHARE2 code for the 75MW ALLEGRO demonstrator. Proceedings of the 2014 22nd International Conference on Nuclear Engineering, ICONE22, July 7-11, 2014, Prague, Czech Republic, ICONE22-31094

Mayer G., Bentivoglio F., 2015. Preliminary study of the decay heat removal strategy for the gas demonstrator ALLEGRO, Nuclear Engineering and Design 286, 67–76.

Mayer G., 2017. Thermohydraulic studies for the ALLEGRO core optimization. AEMI-2017-206-3.2-01-M0

AUTHORS BIOGRAPHY

Dr. Gusztáv Mayer, PhD. Senior researcher at the Hungarian Academy of Sciences Centre for Energy Research (MTA EK). His current research activity is in connection with the European gas cooled fast reactor technology (ALLEGRO, GFR). He has worked on several European projects related to gas fast reactor: GoFastR, ALLIANCE, VINCO. He participated in critical heat flux experiments and two-phase flow thermal hydraulic code development (RETINA). The RETINA code is built into the full scope simulator of Paks Nuclear Power Plant. His previous research area was one- and two-phase flow modeling using the Lattice Boltzmann method (LBM). He has held a PhD degree since 2009 and he has several publications in peer reviewed journals with more than hundred citations.

Attila Guba, senior researcher, Head of Thermohydraulics Department at the Hungarian Academy of Sciences Centre for Energy Research, MTA EK. His current research activity relates to the European gas cooled fast reactor technology (ALLEGRO, GFR), supports the existing and the newbuilt Paks NPP achieving safer operation, reaching higher safety. He has worked on several European projects related PWR safety both on experimental and analytical fields, such as PKL, ATLAS, ROSA, BEMUSE. Takes part in the OECD CSNI WGAMA as the country representative. Previously he participated in several experimental programmes, such as integral test facility PMK-2. His previous research area was one and two-phase flow modeling, thermohydraulics system codes, uncertainty analyses and safety studies.

INFRASTRUCTURE LINKING FOR E-MOBILITY – APPROACH TO INTEGRATIVE TRAFFIC AND ENERGY NETWORK PLANNING

Niels Schmidtke[a], David Weigert[b], Fabian Behrendt[c]

[a] Otto von Guericke University Magdeburg, Magdeburg (Germany)
[a][b][c] Fraunhofer Institute for Factory Operation and Automation IFF, Magdeburg (Germany)
[c] SRH Mobile University, Riedlingen (Germany)

[a] niels.schmidtke@ovgu.de, [b]david.weigert@iff.fraunhofer.de, [c]fabian,behrendt@mobile-university.de

ABSTRACT
This paper gives an introduction to the strategic research field of the cross-infrastructural planning process and the system operation for charging stations from the traffic and energy network view. In the course of the energy turnaround in Germany (grid and plant expansion, liberalization) as well as changes in the transport sector (increasing traffic volume vs. increasing loss of transport infrastructure [Radke 2017; Daehre 2012]) complex cross-infrastructure solutions and tools (simulation systems) will be needed in order to ensure the technical reliability as well as the economic and ecological orientation of these systems. Based on the current stock of charging points and the forecasted total demand, there is a need for the comprehensive construction of charging infrastructure for electric vehicles. This creates user acceptance and lowers the barriers to electric vehicles in the private and commercial sectors.

Keywords: E-Mobility, charging infrastructure, traffic and energy network linking, cross-infrastructural approach

1. INTRODUCTION

In 2009, the EU committed to reduce greenhouse gas emissions by 20% by 2020 [EEA 2017]. This also affects the Federal Republic of Germany: Measures are needed to reduce these emissions in order to achieve the climate protection goals. In addition to actions for traffic avoidance, modal shift and traffic optimization [e.g. Schmidtke et al. 2017; Baumann et al. 2017] the conversion of vehicles with alternative drive technologies is focused. Electromobility is given great potential especially due to its technical maturity [MLV 2018]. For the transport sector, especially for motorized private transport, an increase of more than 10% in terms of traffic volume (pkm) is forecasted by 2030 [Radke 2017]. In order to exploit this potential and to increase the number of registrations for electric vehicles (up to a mass market phase), political incentives must also be created.

So far, battery electric vehicles account for only 0.12% of the total number of passenger cars in Germany (in 2017, approx. 45 million passenger cars in total), although the growth in electric vehicles is currently 33% [KBA 2018]. The (inter-)national political and social aspirations lead to an increase in the attractiveness of electric mobility [NPE 2015] and can lead to a comparably successful market run as in Norway [Bobeth et al. 2016]. The increased promotion programs for electromobility, the distribution of environmental bonuses for the purchase of an electric vehicle, the current discussions about diesel driving bans in Germany and the increasing commitment of the automotive industry to further the development of alternative drive concepts point this out [NPE 2015; VDA 2018]. Already now, this development leads to waiting periods of up to one year when buying an electric vehicle from German manufacturers. For a mass market phase of electromobility, it is therefore essential to implement a cross-infrastructure link between transport and energy networks in order to ensure both the technical availability and the economic and ecological orientation of the system.

2. MOTIVATION AND GOAL

Users and suppliers of such solutions and tools are often narrowly limited to one of the fields of application (traffic or energy technology analysis and planning) (see Chapter 3.1), so that the need arises to realize a model linkage in an interdisciplinary approach (Figure 1). The novelty of the present research approach optimizes the placement of charging infrastructures on the basis of both networks and is thus intended to answer the research question, which interactions exist between the infrastructures and which advantages result from their linking. The development of suitable algorithms and criteria to answer the question of where and how charging infrastructures (placement and prioritization) should be planned is also part of the research work and will be developed in the paper as a concept study. In the long term, the research work will develop a simulation system for multi-scenario analysis for a linked traffic and energy infrastructure. This

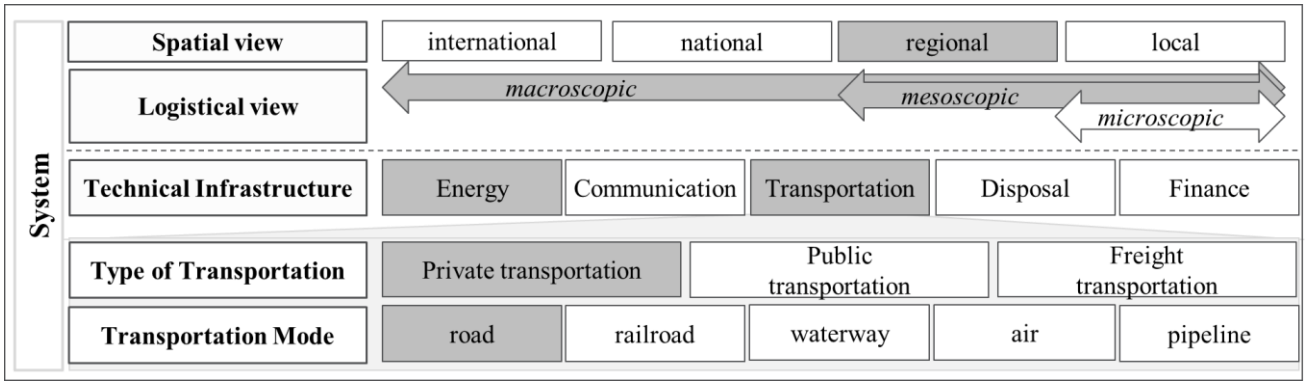

Figure 1 Morphological Box – Research focus [Behrendt 2016]

should make it possible to examine the presented question in an interoperable framework.
On this basis, the objective is to develop optimized strategies for the planning and networked operation of transport and energy infrastructure and to evaluate them simulatively. From the derived results (development of the traffic situation, energetic utilization) a corresponding utilization plan can be represented. In detail, an analysis of the effects on the existing traffic and energy infrastructure (supply bottlenecks, oversupply) as well as their developments (determination of positions for charging infrastructures including design) is to be realized. The research field in this work is limited to the federal state of Saxony-Anhalt, a region in central Germany and home of the authors. Furthermore, the focus is on motorized individual transport (battery electric verhicles (BEV), plug-in hybrid electric vehicles (PHEV)), freight transport (e.g. e-trucks) as well as public passenger transport (e.g. e-buses) take a subordinate role in the first model linking.

3. STATE OF THE ART AND SCIENCE

In the following chapter, the findings of the literature review are described by means of examples of projects already carried out and approaches for the (successive) development of a comprehensive and needs-based charging infrastructure for electric vehicles. The objective is to design a tool-based methodology for the present application, the application of which allows statements about the positioning and design of the charging infrastructure.

3.1. Modeling and simulation of locations for the charging infrastructure

The positioning of charging stations can be defined as a location planning problem. There are various approaches to develop an idealized grid for charging infrastructures. With the aid of algorithms, exact solutions which are increasingly approximated due to the computational effort are sought [Hagg et. al 2015]. Depending on the priority criteria for potential sites for charging infrastructures, the distribution of these can be differentiated in different ways. Overall, this distribution or location problem can be investigated with so-called location-allocation models or flow-based-location models [Hagg et. al 2015; Hoerstebrock 2014]. For the future approach, a multi-part model is to be implemented.

3.1.1. Location-Allocation Models

In the case of location-allocation models, it is assumed that the demand prevails in nodes or areas and should be satisfied with the locations.
As a classic location-allocation model, the Maximum Coverage Location Problem (MCLP) deals with the location of corresponding elements and allocation of demand to locations [Church & Revelle 1974]. On the one hand, only relatively little data is needed for the model, but on the other hand it is a static problem. No queues, capacity limits or dynamic traffic flows are taken into account so that the use of the MCLP is not suitable for the gradual development of charging infrastructures; it is considered separately as a supplementary problem [Hagg et al. 2015].

3.1.2. Flow-Based Location Models

Flow-based location models consider demand as (traffic) flow from origin to destination. Origin and destination points lie within a defined range. Due to flow-related demand, flow-based-location models are better suited for the intended use [Kuby & Lim 2005].
Within a network, the objects flow along links and through nodes. The aim of the model is to place sites on connection-intensive links, which allows the flow to be covered. There are some assumptions in this model, including that the location of a corresponding element has no impact on traffic, each origin-destination relation (OD) has the same route, and the flow is equal in both directions (symmetrical) [Hodgson 1990; Hoerstebrock 2014]. In order to filter out connection intensive links (heavily trafficked roads), data must be available on traffic flows. Furthermore, this method involves a higher computational burden.

The following section provides an overview of previous solutions in which the location problem was addressed.

3.2. Overview of previous solutions

In the field of electromobility there has been increasing research approaches in recent years related to the location problem for charging infrastructure of electric vehicles. A variety of optimization algorithms have been developed and used to address this problem.

[Efthymiou et al. 2017] use OD data (origin-destination) from conventional vehicles to determine the location of charging infrastructure by applying genetic algorithms and making necessary assumptions about the penetration of electric vehicles. [Frade et al. 2011], on the other hand, use socio-demographic data, such as the number of jobs and households, to derive demand per geographic unit. As part of a mixed intergerprogramming algorithm [Chen et al. 2013] aim to minimize travel costs by using parking demand as a proxy for the demand of electric vehicles. [Xu et al. 2013], on the other hand, provide a framework for the optimal design of charging infrastructure (configuration) through a particle swarm optimization algorithm (PSO) with the aim of minimizing transport distances.

In the spatial study area itself (Saxony-Anhalt, see Chapter 4), hardly any strategies for the (successive) development of charging infrastructures have been advanced. In contrast to the algorithmic approaches mentioned (exact or approximated), [MLV 2018] forecasts the electric vehicle numbers on the basis of the current situation and determines the total requirements for charging infrastructure. At this macroscopic level, no exact determination of the location is made, only a recommendation to the maximum catchment area (15km distance) of publicly accessible charging points.

It turns out that previous work often considers the energetic prerequisites in a downstream process. In macro-level studies available in Germany [NPE 2015; Anderson et al. 2016; MLV 2018], the energy network is not included in the calculation. Therefore, the research objective is a methodically linked approach.

4. DESCRIPTION OF THE STUDY AREA

In order to derive the demand for future required charging infrastructure, a description of the traffic structure of Saxony-Anhalt and its existing number of charging points is necessary in the first step. Saxony-Anhalt is located in the center of Germany and represents an appropriate transit state due to the availability of four federal highways (A2, A9, A14, and A38) with a total length of 2,140 km [Radke 2017]. The current situation of electromobility can be illustrated on the one hand by the stock of electric vehicles and on the other hand by the existing charging infrastructure. As of 01/2017, Saxony-Anhalt has approximately 1.2 million registered passenger cars, including 310 BEV and 246 PHEV, so in total there are only 556 externally rechargeable electric cars. Thus Saxony-Anhalt comes last place in the nationwide ranking in relation to the total stock. With the regard to the number of publicly accessible charging points with a total of 211 (08/2017), Saxony-Anhalt also performs poorly compared to the distribution of charging infrastructures in Germany. Although the ratio of electric vehicles per publicly accessible charging point is above average in Saxony-Anhalt, it is continuously rising in Germany [NPE 2015]. To cover the increasing demand – as a result of commuter traffic and increasing leisure traffic in the neighboring federal states [AA 2018] – according to the Ministry of Regional Development and Transport, 1,300 publicly accessible charging points for electric vehicles are planned in Saxony-Anhalt by 2020 [MLV 2018]. Currently there is hardly any charging infrastructure installed, especially in smaller cities and administrative communities, as shown in Figure 2. Taking into account all origin, destination, inland and transit traffic in available OD-matrices (origin-destination), the traffic demand can be determined by daily load curves for any section of the route. As shown in Figure 2 these curves (distinguished by direction) were calculated for selected routes to illustrate the traffic situation. These form the basis for the planning approach of charging infrastructure (see Chapter 5).

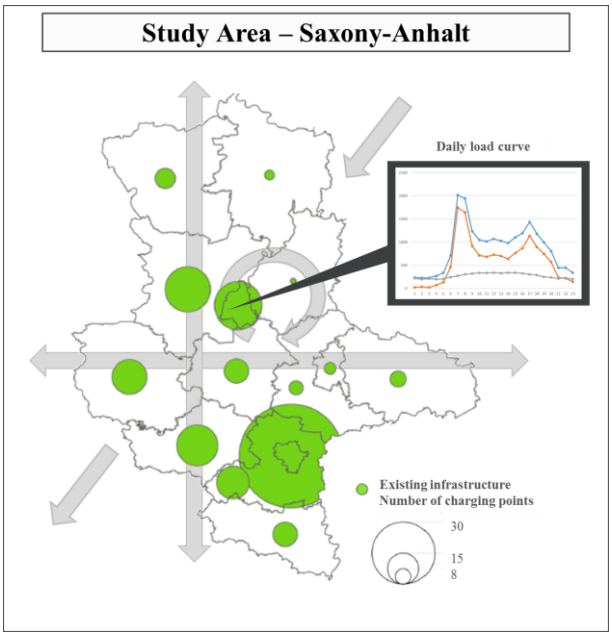

Figure 2 Study Area – Saxony-Anhalt [referring to MLV 2018]

In addition to contributing to the achievement of the climate protection goals, the public perception changes (creation of an incentive system) by an increased demand or the gradual transition to electromobility by new publicly accessible charging infrastructure. The energy transition in Germany has the consequence that the structure of power generation fundamentally changes [AEE 2018]. Saxony-Anhalt is taking a pioneering role in the integration of renewable energies into the electricity supply. In the grid area, the share of electricity generated from renewable energies in terms of network sales is over 180 percent [AEE 2018]. Above all, wind energy plays a key role. Wind turbines installed in Saxony-Anhalt cover around 55 percent of the state's net electricity demand. More than 2,700 wind

turbines with a total capacity of more than 4,700 megawatts are installed. This energy is fed into one of the six switchgears distributed over Saxony-Anhalt in the extra-high voltage network (220kV / 380kV) and transformed into supra-regional distribution grids (high voltage grid - 60kV / 110kV) and regional distribution grids (medium voltage grid - 3kV / 30kV). Above all in the area of local and city grids (low-voltage network - 230V / 400V), corresponding power capacities for the installation of charging infrastructures have to be proved, if necessary a grid expansion to cover the demand is required at certain locations [AEE 2018]. This planning aspect is also taken into account in the present research approach.

5. APPROACH TO INTEGRATIVE TRAFFIC AND ENERGY NETWORK PLANNING

The following chapter describes the conceptual approach for optimal placement and operation of charging infrastructures from the perspective of traffic and energy.

On the one hand, both the transport network model and the energy network model must be developed. To model the transport network, available data sources are analyzed (traffic volume, commuter traffic, etc.) [Radke 2017; KBA 2018], are reviewed with regard to sufficient accuracy and extended. The traffic model is subdivided into traffic cells (OD matrices) and also takes into account socio-demographic data as well as the attitude patterns of citizens towards electromobility (mobility survey in the area under investigation). Based on existing studies [NPE 2015; Anderson et al. 2016], diffusion scenarios (different permeation of electric vehicles) are defined and transferred in the model. The application and adaptation of suitable optimization algorithms (see chapter 3.1) shows the optimal placement of charging infrastructure from a traffic point of view.

To simulate the electrical network, also the network data (in cooperation with the energy network companies of the study area) are analyzed, reviewed with regard to sufficient accuracy and extended. Subsequently, the energy network is simulated in a suitable simulation software in order to carry out corresponding load flow calculations [Hauer 2014]. Furthermore, network scenarios for future development in terms of energy generation and energy consumption are defined [NEP 2018] and transferred in the network model. The network utilization as well as critical network sections can be identified by means of simulations.

Subsequently, the developed models are linked by simulation technology. With the help of traffic flow data and energy network data, it is possible to determine the geographical installation locations of the charging infrastructures. The development of algorithms and criteria for the placement and prioritization of charging infrastructures are crucial, they allow statements about the site selection, the technology choice (DC, AC charging infrastructure) and the number of charging systems. These findings represent the input parameters for the development of algorithms and criteria for the supply of charging infrastructures from the electrical network. The costs of grid expansion, sector linking opportunities and distributed charging strategies are taken into account. The overarching research goal is then the application of the algorithms developed in the linked model to identify suitable charging infrastructure locations and to determine a suitable supply or operating concept from the point of view of the electrical and transport network. Figure 3 illustrates the research design conceptually. After the simulation runs (different permeation of electromobility) the results are visualized and interpreted. In addition to the technological and infrastructural consideration [e.g. Wenge et al. 2010], the selection of suitable methods (algorithms) plays a decisive role. On the basis of the results, a corresponding decision is made on the investment and implementation measures (i.a. construction).

As described, after the development of the single simulators the integrated simulation takes place in a multi-stage process. This is exemplary visualized by a district ("Börde") from the study area Saxony-Anhalt (see Figure 4). The excluded "Greenfield Scenario"

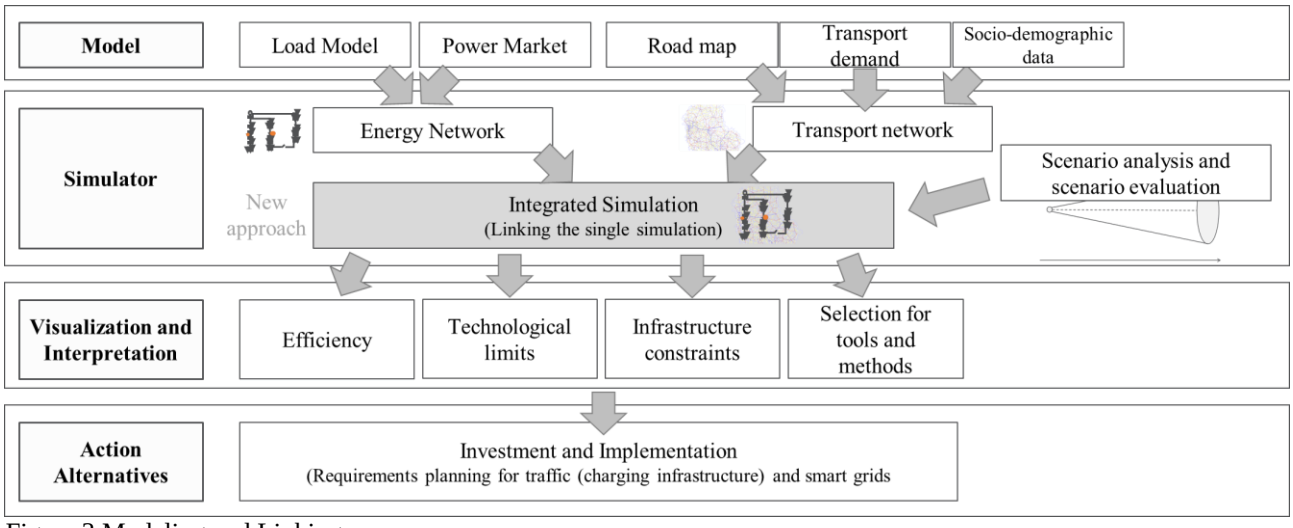

Figure 3 Modeling and Linking

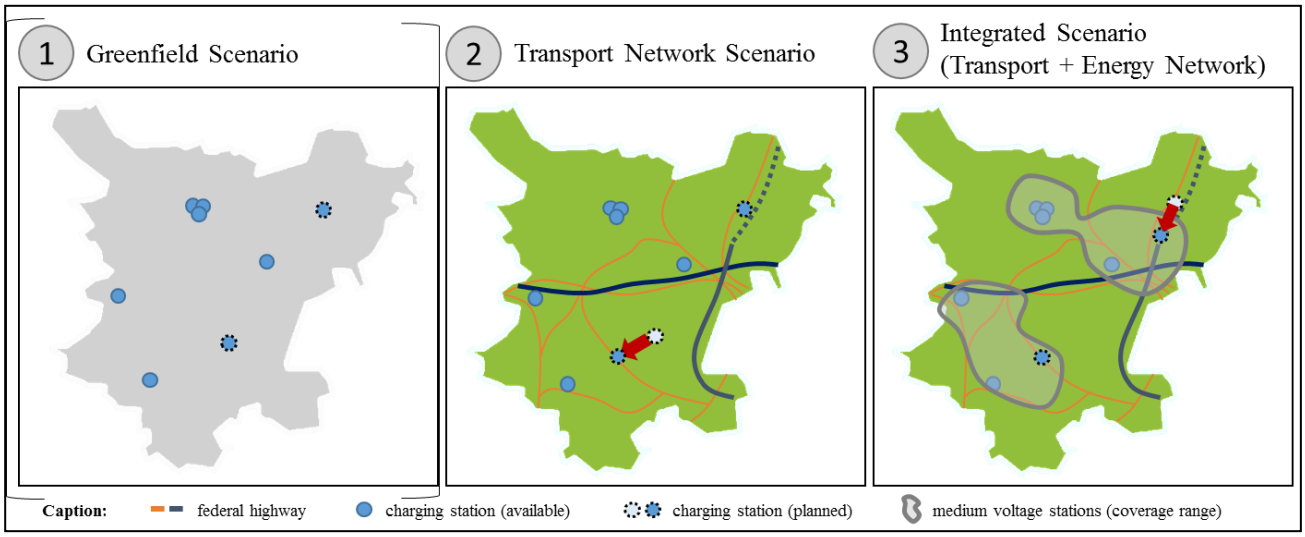

Figure 4 Integrated Simulation

illustrates the prioritization of charging points for a simple location planning problem. However, existing infrastructures, the traffic routes as well as the energy infrastructures are disregarded. Taking into account the transport network as well as the calculated daily load curves (traffic demand) for selected routes, charging points can be prioritized using the models described in chapter 3.1 in the "Transport Network Scenario". These are linked to the existing traffic routes (= edges). In the subsequent “Integrative Scenario”, the energy supply grid (especially the medium and low voltage grid) is also taken into account. As a successive build-up of charging infrastructure is aimed, the goal is to temporarily avoid grid expansion, so that charging infrastructures are placed where appropriate power capacity is available. According to this, the placement of the charging infrastructures is rechecked and, if necessary, adjusted in an integrative planning approach (see red arrow in Figure 4).

The procedure described is applied to the entire study area Saxony-Anhalt. For a sound action recommendation, different diffusion scenarios for electromobility are defined and depicted (see Figure 3). The scenario technique with best-case, worst-case and trend scenarios is used [Göpfert 2012; Decker 2012]. Thus, for example, a permeation of 1-5% electric vehicles is expected for the year 2020, with 2025 already being calculated at 5-25%.

6. SUMMARY AND OUTLOOK

The use of electric vehicles creates a direct link between multiple infrastructures, increasing the flexibility of the systems. Electromobility is seen as one of the flexibility options of the future electric power system [Komarnicki et al. 2018].

The research approach described focuses on linking the energy systems with the transport infrastructures. The model linking should enable optimized strategies for the planning and the networked operation of both infrastructures and be evaluated by the simulation system to be created.

The objective is to answer the question of how the interaction of both infrastructures is formed and what are the benefits of the linking. So far, in addition to the conceptual and formal model, the first scenarios have been defined and also shown as examples. In the further course, the scenarios are differentiated in order to compare the experimental results. The objective is for the entire federal state of Saxony-Anhalt to demonstrate the comprehensive development of charging infrastructures for electric vehicles - against the background of different development scenarios.

The outlook also presents the challenge of broadening the question to another critical infrastructure: information and telecommunications.

REFERENCES

Radke, S.: Verkehr in Zahlen 2017/2018. Hamburg: DIW Berlin, DLR, Verlag: DVV Media Group, 46. Jahrgang, ISBN 978-3-87154-617-4, 2017.

Daehre, K.-H.: Zukunft der Verkehrsinfrastrukturfinanzierung. Magdeburg: Commission report, 2012, p.37.

Schmidtke, N.; Baumann, L; Daehre, K.-H.; Behrendt, F.: Bewertung innovativer Verkehrskonzepte - eine Wirkungsabschätzung für die flächendeckende Einführung des Lang-LKW. München: Internationales Verkehrswesen, Trialog Publishers Verlagsgesellschaft, Bd. 69.2017, 2, p.44-47

Baumann, L.; Behrendt, F.; Schmidtke, N.: Applying Monte Carlo simulation in an indicator-based approach to evaluate freight transportation scenarios. Barcelona: HMS 2017, 09/2017 - Genova: DIME Università, S. 45-52

EEA European Environment Agency: Trends and projections in Europe 2017 – Tracking progress towards Europe’s climate and energy targets. EEA report, No 17/2017, ISSN 1977-8449, p.9

MLV Ministerium für Landesentwicklung und Verkehr (Ministry of Regional Development and Transport): Ladeinfrastrukturkonzept Sachsen-Anhalt. Report of the state government, 06/03/2018, p.5

KBA Kraftfahrtbundesamt (Federal Bureau of Motor Vehicles and Drivers): Bestand an Pkw am 01. Januar 2017, https://www.kba.de/DE/Statistik/Fahrzeuge/Bestand/Umwelt/2017_b_umwelt_dusl.html?nn=, Access on: 14/05/2018

NPE Nationale Plattform Elektromobilität: Ladeinfrastruktur für Elektrofahrzeuge in Deutschland – Statusbericht und Handlungsempfehlungen 2015. AG3 – Ladeinfrastruktur und Netzintegration. Berlin: GGEMO, 2015.

Bobeth, S.; Matties, E.: Elektroauto: Top in Norwegen, Flop in Deutschland? – Empfehlungen aus Sicht der Umweltpsychologie, GAIA 25/1, 2016, p.38-48

VDA Verband der Automobilindustrie: Elektromobilität. https://www.vda.de/de/themen/innovation-und-technik/elektromobilitaet/elektromobilitaet-in-deutschland.html, Access on: 14/05/2018.

Behrendt, F.: Entwicklung eines Vorgehensmodells zur Untersuchung multidimensionaler Einflüsse auf Güterverkehrssysteme. Magdeburg: Dissertation. Otto von Guericke University, 2016, p.59ff, 66.

Hagg, A.; et al.: Methodische Grundlegung für eine Strategie zum sukzessiven Ausbau der Ladeinfrastruktur für Elektromobilität in Bonn und dem Rhein-Sieg-Kreis. Bonn: Report, 30/06/2015.

Hoerstebrock, T.: Strategische Analyse der Elektromobilität in der Metropolregion Bremen/Oldenburg. Doctoral Thesis. Universität Oldenburg, 2014

Church, R; Revelle, C.: The Maximal Covering Location Problem. Emmitsburg, MD: National Emergency Training Center, Print, 1974.

Kuby, M.; Lim, S.: The flow-refueling location problem for alternative-fuel vehicles. Socio-Economic Planning Sciences 39.2, 2005, p.125-145.

Hodgson, M.J.,: A flow Capturing Location Allocation Model. Ohio State University Press, 1990. Available from: https://onlinelibrary.wiley.com/doi/epdf/10.1111/j.1538-4632.1990.tb00210.x Access on: 09/05/18

Efthymiou, D.; Chrysostomou, K.; Morfoulaki, M.; Aifantopoulou, G.: Electric vehicles charging infrastructure location: a genetic algorithm approach. In: Eur. Transp. Res. Rev. (2017) 9:27

Frade, I.; Ribeiro, A.; Gonçalves, G.; Antunes, A.: An optimization model for locating electric vehicle charging stations in central urban areas. Washington DC: Proceedings of the 90th Annual Meeting of the Transportation Research Board, 2011.

Chen, T.; Kockelmand, K.; Khan, M.: The electric vehicle charging station location problem: a parking –based assignment method for Seattle. Washington DC: Proceedings of the 92nd Annual Meeting of the Transportation Research Board, 2013.

Xu, H.; Miao, S.; Zhang, C.; Shi, D.: Optimal placement of charging infrastructures for large-scale integration of pure electric vehicles into grid. Electr Power Energy Syst 53:159–165, 2013.

Anderson, J.E.; et al.: LADEN 2020 – Konzept zum Aufbau einer bedarfsgerechten Ladeinfrastruktur in Deutschland von heute bis 2020. Berlin: Final Report, DLR, 2016.

AA Bundesagentur für Arbeit (Federal Employment Agency): Pendleratlas (Datenbestand Juni 2017), https://statistik.arbeitsagentur.de/Navigation/Statistik/Statistische-Analysen/Interaktive-Visualisierung/Pendleratlas/Pendleratlas-Nav.html, Access on 04/07/2018

AEE Agentur für Erneuerbare Energien (Renewable Energies Agency): Struktur des Stromnetzes. https://www.unendlich-viel-energie.de/english, Access on 04/07/2018

Hauer, I.: Optimale Last- und Erzeugungsanpassung bei kritischen Netzzuständen – Algorithmen und deren Bewertung. Magdeburg: Dissertation, Otto von Guericke University, 2014, ISBN 978-3-944722-18-4

Wenge, C.; Komarnicki, P.; Styczynski, Z. A.: „Models and boundaries of data ex-change between electric-vehicle and charging-point. Example of a practical realization", Modern Electric Power Systems 2010 (MEPS'10), Wroclaw, Poland, ISBN: 978-83-921315-7-1, September 2010.

Göpfert, I.: Logistik der Zukunft – Logisitcs for the Future. 6. Aufl., Springer-Verlag Berlin Heidelberg, Marburg, 2012.

Decker, J.; Krampe, H.; Lucke, H.-J.: Logistikmanagement und Logistikorganisation. In: Krampe, H.; Lucke, H.-J.; Schenk, M. (Hrsg.): Grundlagen der Logistik: Einführung in Theorie und Praxis logistischer Systeme. 4. Aufl., Huss-Verlag, München: 2012, p.131-177.

NEP Netzentwicklungsplan Strom: Szenariorahmen für den Netzentwicklungsplan Strom 2030 (Version 2019) – Entwurf der Übertragungsnetzbetreiber. Berlin: CB.eClausecker, 01/2018.

Komarnicki, P.; Haubrock, J.; Styczynski, Z.: Elektromobilität und Sektorenkopplung – Infrastruktur- und Systemkomponenten. Heidelberg: Springer Vieweg, 2018, ISBN 978-3-662-56248-2

AUTHORS BIOGRAPHY

NIELS SCHMIDTKE after graduating in Industrial Engineering with specialization in Logistics at the Otto-von-Guericke-University Magdeburg he started as a research assistant at its Institute of Logistics and Material Handling Systems. His research focuses on transport logistics and electromobility. Furthermore he works as a research coordinator at the Business Office at "Fraunhofer Group for Production" in Magdeburg. His mayor acitivities are related to the topics Industrie 4.0 and smart logistics processes.

DAVID WEIGERT studied Industrial Engineering with specialization in Logistics at the Otto-von-Guericke-University Magdeburg. He became a research associate at the Chair Logistical Systems at the Otto von Guericke University Magdeburg and scientific project assistant at the Fraunhofer Institut for Factory Operation and Automation IFF. His areas of competence are the analysis and optimization of logistics processes, as well as modelling, simulation and optimization of logistics systems.

FABIAN BEHRENDT is a full professor for Industrial Engineering at SRH Fernhochschule - The Mobile University with focus on distance learning in subject area production and logistics. Moreover he is head of the Business Office at „Fraunhofer Group for Production" of Fraunhofer-Gesellschaft and responsible for management and research strategies. He holds a doctoral degree in engineering and an diploma in industrial engineering. In his research he is dedicated to the study of intelligent logistics zones with the help of new technologies of Industrie 4.0.

MODELING AND SIMULATION OF BLOOD FLOW AND VESSEL STRESS IN HUMAN BRAIN DURING STRENUOUS EXERCISE

Luhan Ma[(a)], Ang Chen[(b)], Yongbo Zhong[(c)], Zhichao Ren [(d)], Ye Lang [(e)], Jiazheng Zhao[(f)], Zhifeng Dong[(g)]
[(a),(b),(c),(d),(e),(f),(g)]Mechanical and Electronic Engineering Dept. of China University of Mining and Tech. (Beijing),
[(a)]m18813093136@163.com, [(b)]chenang19941204@163.com, [(c)]18811228036@163.com,
[(d)]15801260612@163.com, [(e)]langyecumtb@163.com, [(f)]zhaojiazheng1992@126.com, [(g)]dzf@cumtb.edu.cn

ABSTRACT
In order to study the effect of strenuous exercise to human blood flow and vessels stress, the paper takes the central artery in human brain for an example, and carries out a two-way fluid-solid coupling finite element analysis on it. The three-dimensional model is reconstructed, and the calculation was made with Computational Fluid Dynamics software. The simulation results show that, a low velocity vortex region is formed in the sinus of the artery, and the vortex phenomenon is getting weaker with the increase of the acceleration value. The structure shape of blood vessel is the main factor affecting the wall shear stress and Mises stress. With the increase of the exercise acceleration, the maximum of wall shear stress and Mises stress of the vessel wall shows an approximate linear growth.

Keywords: blood vessels stress, fluid-solid coupling, modeling reconstruction, computational fluid dynamics

1. INTRODUCTION
Cardiovascular and cerebrovascular diseases are characterized by high prevalence rate, high disability rate and high mortality rate. The number of deaths caused by cardiovascular and cerebrovascular diseases in the world is as high as 15 million each year, ranking the leading cause of death. A large number of studies show that obtaining mechanical parameters of blood vessel walls and blood is of great significance in the treatment of cardiovascular and cerebrovascular diseases. However, up to now, there is still no effective means to obtain the required data through medical clinical methods or experiments. Therefore considering combining medical science and engineering, the engineering finite element method is used for numerical simulation to obtain the displacement field, the shear stress field and the pressure field (Bracamonte-Baran William and Baritto-Loreto Miguel 2016; Nicolas Moreno and Philippe Vignal 2013).

A large number of scholars have done numerous related researches. Zhaomiao Liu, Changxing Xu and others took the STL file generated by mimics into Geomagic Studio to reconstruct the NURBS surface, and compared the fluid solid coupling model with the rigid vessel wall model. They found that the shear stress, displacement and the location of the maximum stress on the vessel wall are all different (Zhaomiao Liu, Lidan Gao and Yi Shi 2013). Ying Liu , Weizhong Zhang and others, used medical imaging software mimics to establish the real model of blood vessel wall and simplified it. They also considered the constraint effect of brain tissue and apply a inner normal direction force to blood vessel walls to simulate (Ying Liu, Defa Zhang, Yongqiang Bi and Menghong Wang 2015). J. A. MOORE. Annals of Biomedical Engineering, studied the three-dimensional reconstruction method of arterial blood vessels. By comparing several methods of establishing the model of blood vessel wall, a new simplified model is finally provided by using the shape lines that intercept the cross section of blood vessels at a certain distance and then create a curved surface according to these cross section lines (J. A. Moore, D. A. Steinman and D. W. Holdsworth 1998).

Synthesizing the obtained achievements, conclusions are made as follows. Firstly, in considering the constraint effect of brain tissue on vessel walls, the current treatments are too rough to simulate the effect. Secondly, although the nonlinear properties of brain tissue and vessel walls considered as biological soft tissue have been studied, there is still no complete application in the simulation of this problem. Thirdly, the reconstruction method of three-dimensional model is still not perfect. In this paper, the obtained CTA files are introduced into the medical image software mimics, and the real three-dimensional model of the central artery wall is established. While the quality of the obtained model is too low to be used, we reconstruct the model in Geomagic Studio. Then, the around brain tissue and blood models are established on the basis of the model of vessel walls. In the material model, Ogden hyper-elastic model is used to simulate the brain tissue property, and Mooney-Rivlin hyper-elastic model is used to simulate the vessel wall property. The inlet and outlet blood pressure and elastic constraint were applied to the three-dimensional model, and the pressure, shear stress, and Mises stress fields are obtained. Then the calculation and analysis were carried out to simulate under the conditions of the strenuous exercise with three accelerations.

2.THEORETICAL ANALYSIS
The average diameter of the blood vessels analyzed is about 6mm. The blood is taken as Newton fluid with isotropy, incompressibility, constant density and changeless dynamic viscosity. The momentum equilibrium equations of Newton fluid in three dimensional viscous incompressible equations are:

$$\begin{cases} \nabla \cdot \mathbf{U} = 0 \\ \rho \dfrac{\partial \mathbf{U}}{\partial t} + \rho(\mathbf{U} \cdot \nabla)\mathbf{U} = -\nabla \mathbf{P} + \mu \nabla^2 \mathbf{U} \end{cases} \quad (1)$$

ISBN 978-88-85741-16-4; Bruzzone, Janosy, Nicoletti and Zacharewicz Eds.

Where, $\mathbf{U}=(u,v,w)^T$ — velocity of blood flow, $\mathbf{P}$ — blood pressure, ρ — blood density, μ — blood dynamic viscosity.
The mass conservation equation is:

$$\frac{\partial \rho}{\partial t}+\nabla\cdot(\rho\mathbf{U})=0 \tag{2}$$

The energy conservation equations are expressed as three-dimensional unsteady state N-S equation:

$$\begin{cases}\dfrac{\partial(\rho u)}{\partial t}+\dfrac{\partial(\rho uu)}{\partial x}+\dfrac{\partial(\rho uv)}{\partial y}+\dfrac{\partial(\rho uw)}{\partial z}=\dfrac{\partial}{\partial x}\\ (\mu\dfrac{\partial u}{\partial x})+\dfrac{\partial}{\partial y}(\mu\dfrac{\partial u}{\partial y})+\dfrac{\partial}{\partial z}(\mu\dfrac{\partial u}{\partial z})-\dfrac{\partial p}{\partial x}+S_u\\ \dfrac{\partial(\rho v)}{\partial t}+\dfrac{\partial(\rho vu)}{\partial x}+\dfrac{\partial(\rho vv)}{\partial y}+\dfrac{\partial(\rho vw)}{\partial z}=\dfrac{\partial}{\partial x}\\ (\mu\dfrac{\partial v}{\partial x})+\dfrac{\partial}{\partial y}(\mu\dfrac{\partial v}{\partial y})+\dfrac{\partial}{\partial z}(\mu\dfrac{\partial v}{\partial z})-\dfrac{\partial p}{\partial y}+S_v\\ \dfrac{\partial(\rho w)}{\partial t}+\dfrac{\partial(\rho wu)}{\partial x}+\dfrac{\partial(\rho wv)}{\partial y}+\dfrac{\partial(\rho ww)}{\partial z}=\dfrac{\partial}{\partial x}\\ (\mu\dfrac{\partial w}{\partial x})+\dfrac{\partial}{\partial y}(\mu\dfrac{\partial w}{\partial y})+\dfrac{\partial}{\partial z}(\mu\dfrac{\partial w}{\partial z})-\dfrac{\partial p}{\partial z}+S_w\end{cases} \tag{3}$$

Where, S_u、S_v、S_w are generalized source terms. As for the incompressible adiabatic blood, the three parameters are set to be zero.
The initial condition equations are set to be:

$$\begin{cases}\mathbf{U}=0\\ \mathbf{P}_{in}=0\\ \mathbf{P}_{out}=0\end{cases} \tag{4}$$

According to the condition of the analyzed vessel, boundary conditions' equations are shown below.

$$\begin{cases}\mathbf{P}_{in}=\mathbf{P}_1\\ \mathbf{U}(r=R)=0\\ \dfrac{\partial\mathbf{U}}{\partial r}(r=0)=0\\ P_{out}=50Pa\end{cases} \tag{5}$$

Where, $\mathbf{P}_1$ represents the inlet pressure.
The fluid solid coupling surfaces can relate parameters together on the two domains. Equations on the fluid solid coupling surfaces are:

$$\begin{cases}d_s=d_f\\ \tau_s\cdot n_s=\tau_f\cdot n_f\\ u_s=u_f\end{cases} \tag{6}$$

Where, d — displacement, τ — stress, n — normal direction, u — velocity.
Constitutive equations of material of blood vessels: 9 parameters Mooney-Rivlin hyper-elastic model.

$$\begin{aligned}W=&a_{10}(I_1-3)+a_{01}(I_2-3)+a_{20}(I_1-3)^2\\ &+a_{11}(I_1-3)(I_2-3)+a_{02}(I_2-3)^2\\ &+a_{30}(I_2-3)^3+a_{21}(I_1-3)^2(I_2-3)\\ &+a_{12}(I_1-3)(I_2-3)^2+a_{03}(I_2-3)^3\end{aligned} \tag{7}$$

$$I_1=\lambda_1^2+\lambda_2^2+\lambda_3^2 \tag{8}$$

$$I_2=\lambda_1^2\lambda_2^2+\lambda_1^2\lambda_3^2+\lambda_2^2\lambda_3^2 \tag{9}$$

Where, W—strain energy density function, I_1 — the first strain tensor invariant, I_2 — the second strain tensor invariant,λ_i — tensile principal strain.
Constitutive equation of brain tissue materials: Ogden hyper-elastic model

$$W=\frac{2\mu_0}{\mathrm{b}^2}\left(\lambda_1^{\mathrm{b}}+\lambda_2^{\mathrm{b}}+\lambda_3^{\mathrm{b}}-3\right) \tag{10}$$

Where, μ_0 — initial shear modulus, b — hardening parameter.
Based on Newton second law, we deduce the motion equation of vessel walls as:

$$\rho_s\mathbf{a}_s=\nabla\cdot\boldsymbol{\delta}_s \tag{11}$$

Where, ρ_s -vessel density, δ_s - Cauchy stress tensor, $\mathbf{a}_s$-vessel acceleration.

3.ESTABLISHMENT OF THE FINITE ELEMENT MODEL

3.1 Establishment of the Three-dimensional Model

The obtained CTA data file from the hospital will be introduced into the medical modeling software **Mimics** to create a real three-dimensional model of the blood vessel, and the central section part of the model is extracted for analysis. As the blood model obtained in mimics is too rough to analyze, it can not meet the requirements of the finite element pre-processing for the model. In 3-matic post-processing modular of mimics we extract center lines and form an equivalent section model. Based on the equivalent section model the generated rough model is introduced to Geomagic studio for surface reconstruction, repairing, and smoothing, and then is transformed into STL file. Based on the reconstructed blood model, a vessel wall model is established, and the thickness of the vascular wall is determined by empirical data 1mm.

3.2 Material Model

Both the blood vessel wall and the brain tissue belong to the category of human soft tissue, and have hyper-elastic and visco-elastic properties (Yuanzhen

Feng 1984). Ogden hyper-elastic model is used to simulate the material properties of brain tissue, and Mooney-Rivlin hyper-elastic model is used to simulate the properties of vascular wall materials (J. A. Moore, D. A. Steinman, D. W. Holdsworth 1998). Based on the experimental data from current documents, the fitted stress-strain curves of the brain tissue and the blood vessel are shown in Figure 1 and 2 (Gerhard A. Holzapfel, Ray W. Ogden 2010; Fan Wu 2016; Albert Y. Chong, Barry J. Doyle, Shirley Jansen 2017).

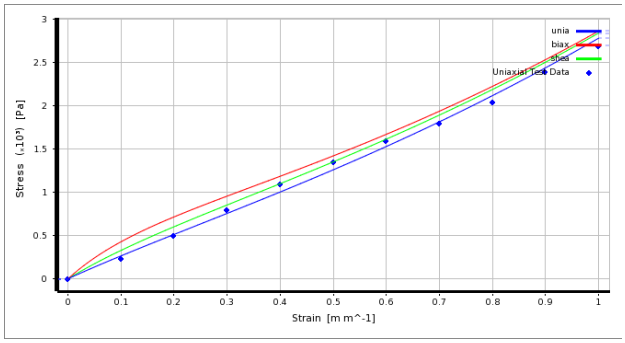

Figure 1: The Stress-strain Curve Of Brain Tissue

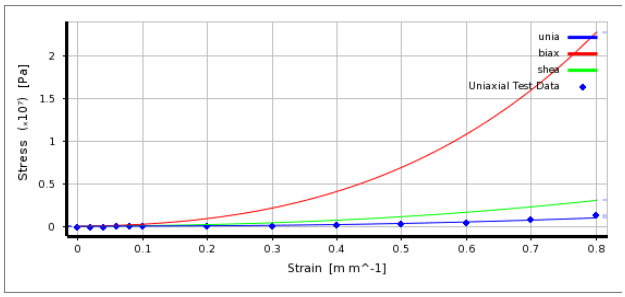

Figure 2: The Stress-strain Curve Of Blood Vessel

Because the characteristic scale of the flow field is far larger than the cell scale, the blood is taken as Newton fluid with isotropy, incompressible, constant density and dynamic viscosity. The density of blood is set to be 1060kg/m^3 and the dynamic viscosity is set to be 3.5e~3kg.m/s (Cristian C. Botar 2017; Mathias Baumert, Michal Javorka 2013; Christian Vergara, Davide Le Van 2017).

3.3 Boundary Conditions

The constrained boundary conditions are as follows: Elastic supports are applied to the outer surfaces of the brain tissue model to simulate the restraint effect on the around part of brain tissue. Fixed constraints are applied to the end surfaces of the vessel model to simulate the restraint effect exerted by the unconsidered adjacent vessels. The models of blood vessels and brain tissue are established as a multi-body component and share topological to transfer loads. Fluid-solid coupling surfaces are established on the inner walls of blood vessels.

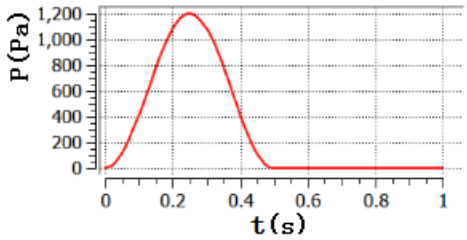

Figure 3: The Curve Of The Pressure Of Inlet

The load boundary conditions are as follows: In solid domain, a standard acceleration of gravity is applied to the model. In fluid domain, the pressure in the outlet is set to be 50Pa, the curve of the pressure in the inlet is shown in figure 3 and an acceleration of gravity is applied (Albert Y. Chong, Barry J. Doyle, Shirley Jansen 2017).

3.4 Meshing

Because the models are composed of numbers of spline surfaces and their shapes are quite complex, models are divided into blocks to be meshed in ICEM. In order to improve the calculation precision on vessel walls, hexahedron grid dominant elements are used on the parts near vessel walls and the elements are refined. Inflation layers are set to make the coupling easier. Finally, 17829 nodes and 103582 elements are obtained in the solid domain and 22232 nodes and 69436 elements are formed in the fluid domain.

4. MOTIONLESS STATE CALCULATION AND RESULTS

The calculation was made with CFX software. The calculation data of the Mises stress and shear stress on vessels reach the maximum value at the moment 0.25s when the pressure of the blood was at peak, which was the key points to be carried out detailed analysis.

4.1 Streamline

Figure 4 presents the flow state of blood at the moment 0.25s in a cardiac cycle. It shows that, the blood forms a low-speed vortex zone in the arterial sinus, and the blood velocity keeps increasing and reaches the maximum value at the entrance of the arterial sinus. Then one part of the blood enters the vortex zone and flow into the left branch vessel with an almost constant velocity. While the other part of blood that does not flow into the vortex area flows a little slower after entering the sinus and then flows into the right branch vessel. Its speed increases first and then decreases. The inlet and outlet of the sinus are areas where the blood flow velocity is larger.

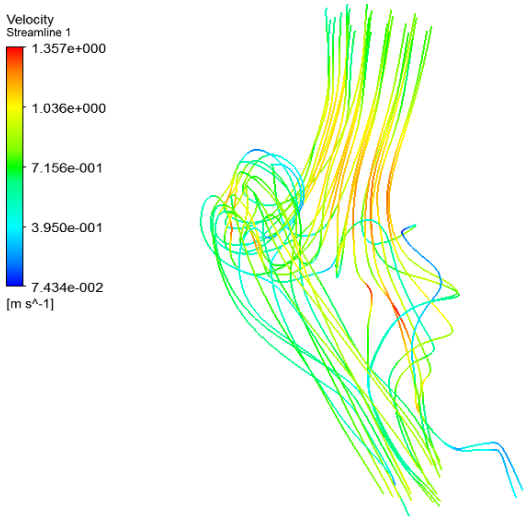

Figure 4: Streamlines Of Blood At 0.25s

From the above analysis, it is shown that the arterial sinus is a place with complex blood flow, and it is easy to cause the problem of large value or complex change of stress. Therefore, we extract several points on this area to carry out detailed analysis of parameters and positions of these points are shown in Figure 5.

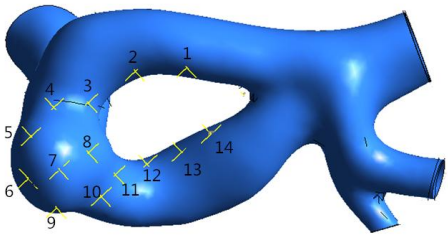

Figure 5: The Locations Of The 14 Points

4.2 Wall Pressure

Low wall pressure can lead blood flow lacking of power to cause histanoxia and atherosclerosis, and too high wall pressure can destroy the structure of blood cells and the lipid in the cells will deposit and form atherosclerosis.

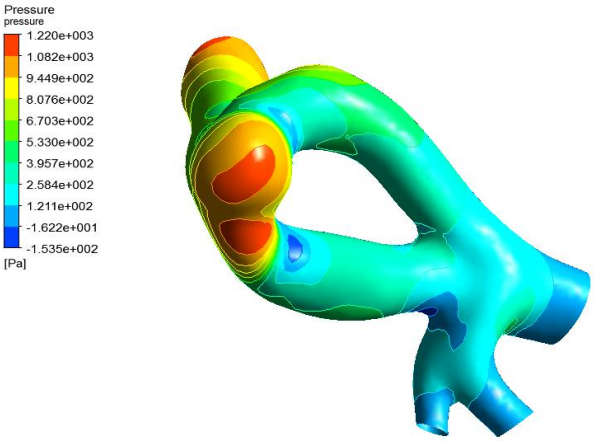

（a）Pressures On Vessel Walls At 0.25s

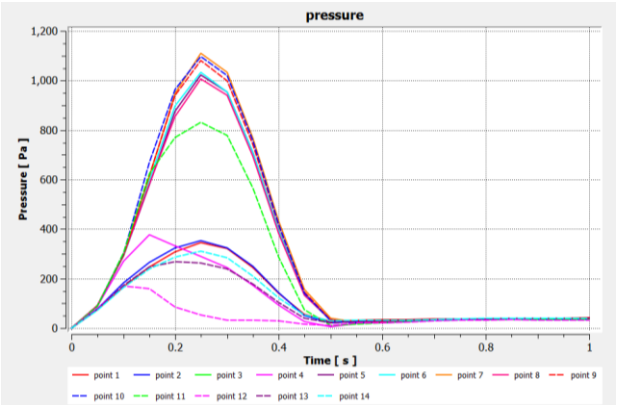

（b）Pressure Curves Of The Extracted Points

Figure 6: Pressures On Vessel Walls

From figure 6(a), we can see that the maximum pressure on vessel walls reaches 1220Pa in a cardiac cycle, and the maximum pressure appeares in the arterial sinus and the inlet of the left branch vessel. The general rule of the pressure distribution is that the pressure level on the wall of the main vessel is generally higher than that of the branch vessels, the pressures on the outer lateral of two branch vessels are higher than those on the inner lateral, and the wall pressure in the sunken part of the vessel conjunction suddenly decreases. The reason of the phenomenon is that there is not much energy loss in the main blood vessel and the flow velocity is relatively large, so the pressure on the main vessel is high. And the pressure on the arterial sinus is high because of the accumulation of blood in the vortex region.

Figure 6(b) presents the time-variation curves of pressure on the extracted points. From the obtained curves, we can see that variation trends of all curves are in accordance with the trend of pressure placed on the inlet. While among the points, three of them vary with a little difference. Observing the figure 6(b), we can find that the three points are placed on parts close to the arterial sinus and caved in. So the difference may be caused by the consumption of blood flow energy by vortex and the shape change of vessels.

4.3Wall Mises Stress

The vessel wall as a kind of biological soft tissue belongs to the elastic-plastic material, so the fourth strength theory is used to judge whether the material is valid. So the Mises stress is extracted and its equation is shown as follows.

$$\sigma_{Mises} = \sqrt{\frac{1}{2}((\sigma_1 - \sigma_2)^2 + (\sigma_2 - \sigma_3)^2 + (\sigma_3 - \sigma_1)^2)} \quad (12)$$

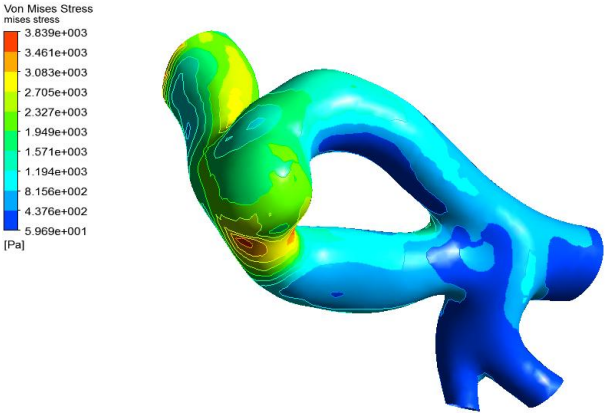

（a）Mises Stresses On Vessel Walls At 0.25s

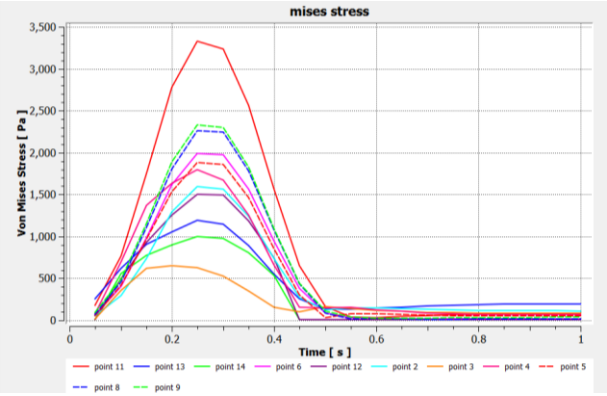

（b）Mises Stress Curves Of The Extracted Key Points

Figure 7: Mises Stresses On Vessel Walls

As shown in figure 7(a), the maximum value of Mises stress on vessel walls in a cardiac cycle is 3839Pa, and the maximum stress appears on the arterial sinus and the inlet part of the left branch vessel. The overall stress distribution trend is that the stress near the arterial sinus reaches the maximum, the stress level of each vessel in the high part is higher than that in the low part in the vertical direction, and the overall stress level of the main vessel is higher than that of the branch vessel, and the stress change is relatively gentle in general. The reasons are as follows. The blood accumulation in the vortex area is the main cause of the high stress level near the arterial sinus. The gravity acceleration causes the stress different in the vertical direction, and the blood flow velocity affects the overall level of the main vascular and branch vascular stress to a certain extent.

As shown in figure 7(b), we can see that the variation trend of the Mises stress on each point is basically the same as the pressure applied on the inlet vessel. Stress curves of points on sunken places near the arterial sinus vary a little different. It's peak slightly advance and the curve changes slowly after the peak. The reason should be accordance with the previous pressure curve, and is still caused by vortex and wall shape changes.

4.4Wall Shear Stress

It is found that when the wall shear stresses are high, and it can cause intima damage to form thrombus. While low shear stresses or excessive shear stress shake and gradient may cause thickening the intima to form atherosclerotic plaque.

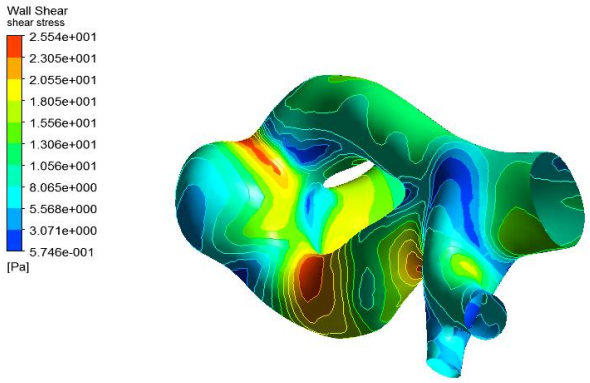

（a）Shear Stresses On Vessel Walls At 0.25s

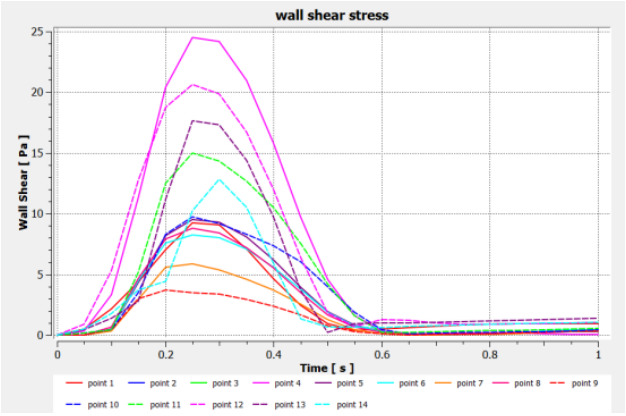

（b）Shear Stress Curves Of The Extracted Key Points

Figure 8: Shear Stresses On Vessel Walls

According to the figure 8(a), we can see the maximum value of shear stress reaches 25.54Pa in a cardiac cycle and the high values appear on the sunken parts of vessel intersections. The general rule of its distribution is that the value of shear stress is higher in the sunken parts of the vessels' intersection, the value of the shear stress is smaller in the wider parts of the blood vessels, and the value of the shear stress varies greatly in the complex part of the blood vessels. So the shape of blood vessels is the main factor affecting the numerical value of wall shear stress. The reason may be as follows. The flow field is less homogeneous and the blood flow velocity is faster on the sunken narrow places which leads to turbulent shear stress higher than that of other areas. While the velocity of blood flow is slow in the wide part of the blood vessel, especially in the low-speed vortex area. So shear stresses on these places are low.

From figure 8(b), we can see that the variation trend of shear stress on each key point is roughly the same as that of the pressure on the inlet, the peaks of shear stress curves on the arterial sinus are slightly forward comparing with the pressure curve on the inlet and after peaks curves change slowly. This phenomenon may be caused by the consumption of blood flow energy by vortex.

5. EXERCISE STATE CALCULATION AND RESULTS

Strenuous exercise or acceleration movement is likely to cause the stress variation of human vessels. The simulates for three jumping states under the vertical upward accelerations 5m/s^2, 10m/s^2 and 15m/s^2. The simulation results show that the vortex in the arterial sinus gradually weaken with the increase of the acceleration, and distributions of wall pressure, wall Mises stress and wall shear stress during exercise state are basically the same as the static state. Only the high value area expanded slightly and the value of parameters change greatly. Data of variations are also basically the same as the stationary state, and are similar to the pressure curve applied at the inlet. It can be seen that the pressure exerted on the inlet has a great effect on the distribution and variation of parameters. As the parameters vary greatly under different conditions, the results of each state analysis are listed in Table 1.

With the increase of the acceleration value, the maximum value of four parameters basically increases. An 5m/s^2 acceleration increase is lead to about 0.24m/s maximum flow velocity increase, 380Pa maximum pressure increase, 1500Pa maximum Mises stress increase and 5Pa maximum shear stress increase. The acceleration is an important factor affecting the numerical value of each parameter. Mises stress increases a little faster in the later stage. This may be caused by the nonlinearity of vascular wall materials.

Table 1: Maximum Values Of Four Parameters

state	parameter	maximum value
stationary state	blood flow velocity	1.357m/s
	wall pressure	1220Pa
	wall Mises stress	3839Pa
	wall shear stress	25.54Pa
vertical upward 5m/s^2	blood flow velocity	1.588m/s
	wall pressure	1622Pa
	wall Mises stress	5716Pa
	wall shear stress	29.85Pa
vertical upward 10m/s^2	blood flow velocity	1.848m/s
	wall pressure	2001Pa
	wall Mises stress	7138Pa
	wall shear stress	34.36Pa
vertical upward 15m/s^2	blood flow velocity	2.160m/s
	wall pressure	2378Pa
	wall Mises stress	8831Pa
	wall shear stress	38.88Pa

5.CONCLUSIONS

(1) The calculation results shows that a low velocity vortex region is formed in the sinus of the artery, and the vortex phenomenon is getting weaker with the increase of the acceleration value. The blood velocity keeps increasing and reaches the maximum value at the entrance of the arterial sinus. Then one part of the blood enters the vortex zone and flows into the left branch vessel with an almost constant velocity. While the other part of blood flows a little slower after entering the sinus and then flows into the right branch vessel. Its speed increases first and then decreases.

(2) The arterial sinus is the place where the Mises stress of vessel wall reaches the maximum. The wall pressure decreases sharply in the sunken area on the vessel intersection while the wall shear stress increases sharply. The overall level of wall pressure and Mises stress on the main vessel are greater than that on branch vessels. The structure shape of blood vessel is the main factor affecting the wall shear stress and Mises stress.

(3) With the increase of the exercise acceleration, the maximum of wall shear stress and Mises stress of the vessel wall shows an approximate linear growth. A 5m/s^2 acceleration increase is lead to about 0.24m/s maximum flow velocity increase, 380Pa maximum pressure increase, 1500Pa maximum Mises stress increase and 5Pa maximum shear stress increase.

REFERENCE

Albert Y. C., Barry J. D., Jansen S., etc, 2017. Blood Flow Velocity Prediction in Aorto-iliac Stent Grafts Using Computational Fluid Dynamics and Taguchi Method. Computers in Biology and Medicine, 84, 235-246.

William B., Miguel B., etc, 2016. Computational Fluid Dynamics Applied to the Study of Blood Flow in the Human Aortic Arch and its Main Branches. Ingenieria Investigacion y Tecnologia, 10, 45-60.

Vergara C., Davide L. V., etc, 2017. Large eddy simulations of blood dynamics in abdominal aortic aneurysms. Medical Engineering and Physics, 000, 1-9.

Cristian C. B., etc, 2017. Dynamic simulation and Doppler Ultrasonography validation of blood flow behavior in Abdominal Aortic Aneurysm, Physica Medica, 37, 1-8.

Gerhard A. H., Ray W. O., 2010. Modelling the Layer-specific Three-dimensional Residual Stresses in Arteries, with an Application to the Human Aorta,23(7),787-799.

Moore J. A., Steinman D. A., Holdsworth D. W., 1998. Accuracy of Computational Hemodunamics in Complex Arterial Geometries Reconstructed from Magnetic Resonance Imaging. Annals of Biomedical Engineering, 32(4), 104-117.

Baumert M., Javorka M., etc, 2013. Joint symbolic analyses of heart rate, blood pressure, and respiratory dynamics. Journal of Electrocardiology, 46,569-573.

Moreno N., Vignal P., etc, 2013. Multiscale modeling of blood flow: Coupling finite elements with smoothed dissipative particle dynamics. International Conference on Computational Science, ICCS, 18, 2565-2574.

Liu Y., Zhang D. F., Bi Y. Q., Wang M. H., 2015. Analysis of Unstable Blood Flow in Aortic Arch and Branch Vessels. Applied Mathematics and Mechanics, 36(4), 432-438.

Liu Z. M., Gao L. D., Shi L.，2013. Fluid-Solid Coupling Analysis of Coronary Artery bypass Graft Based on CT Imaging. Journal of Beijing University of Technology, 39(8), 1255-1260.

ACKNOWLEDGEMENTS

This research is supported by "Foundation of Central Universitys of Education Department of China" No. 2010YJ04. Authors would like to acknowledge and express their thanks for the support.

CORPORATE SUSTAINABILITY ASSESSMENT THROUGH FUZZY TOPSIS

Eleonora Bottani[(a)], Marta Rinaldi[(b)], Federico Solari[(c)]

Department of Engineering and Architecture, University of Parma, Viale delle Scienze 181/A – 43124 Parma, Italy

[(a)]Eleonora.bottani@unipr.it; [(b)]marta.rinaldi@unipr.it; [(c)]federico.solari@unipr.it

ABSTRACT

The aim of this paper is to propose a decision-making methodology that enables the analysis and evaluation of sustainability at the corporate level. The proposed methodology grounds on two tools, namely the technique for order preference by similarity to ideal solution (TOPSIS) approach and fuzzy logic. The integration of these tools offers an effective way to deal with two typical issues of sustainability assessment, i.e.: 1) the fact that the company's performance should be frequently evaluated against qualitative key performance indicators; and 2) the fact that to be meaningful, the company's sustainability performance needs to be compared to a reference value, e.g. a threshold or benchmark, to evaluating how the company is distant from a target.

The proposed approach has been applied to a real firm, operating in the food machinery industry, for testing purpose. The main pros and cons of the approach are described.

Keywords: sustainability assessment, fuzzy logic, TOPSIS, triple bottom line approach.

1. INTRODUCTION

1.1. Background

The term "sustainability" is derived from the Latin verb *sustinere*, composed of *tenere* ("to hold"), and *sub* ("up"). This term has been used since 1980s referring to human sustainability and has resulted in the most widely quoted definition of sustainable development, i.e. "the development that meets the needs of the present generations, without compromising the ability of the future generations to meet their own needs", according to the World Commission on Environment and Development (1987).

It is nowadays acknowledged that sustainability should embrace three main perspectives, i.e. the economic, environmental and social ones (Harris & Kennedy, 1999; Goldman & Gorham, 2006; Colla et al. 2008; Dyllick & Hockerts, 2002), in line with the triple bottom line (TBL) approach. TBL, originally introduced by Elkington (1997), provides a framework for measuring the performance of the business and the success of the organization using the economic, social, and environmental lines (Goel, 2010). In essence, TBL expresses the expansion of the environmental agenda in a way that integrates the economic and social lines (Elkington, 1997). Despite the three-dimensional nature of the TBL, scientific literature often focused on only one aspect of sustainability. For example, Yan, Chen, & Chang, (2009) studied the environmental perspective, while Bibri (2008) evaluated the social one only. Few studies refer to all three perspectives of sustainability (e.g. Marcus & Fremeth, 2009).

1.2. Sustainability evaluation

Several authors pointed out the importance of measuring the company's performance in terms of sustainability (Seuring & Gold, 2013). The purpose of sustainability assessment is to provide the decision-makers (DMs) with an evaluation of a system's global (or local) perspectives, to assist them to determine which actions to undertake in an attempt to make the system more sustainable (Kates et al., 2001). Searcy (2016) highlighted that sustainability performance measurement requires a systematic, structured and integrated approach that considers all facets of the problem. However, it is also known in literature that there are some challenges related to the evaluation of sustainability. First, identifying all the key aspects of sustainability is not trivial (Bossel, 1999). Second, even if all of the relevant aspects have been considered in the evaluation, it is often difficult to measure all them in a meaningful way (Singh et al., 2009). This is often the case for the social sustainability perspective, which still lacks specific and quantitative indexes (Colla et al., 2008). Sometimes, more metrics are available for a similar performance; hence, a further issue is that different companies might decide to use different indexes to measure the same performance (Hervani et al., 2009), making the comparison between companies ineffective. This happens because the relevance of each index could depend on the specific company evaluated or on the market segment where this company operates. Third, to derive an overall evaluation of the system's sustainability, the performance obtained against each index need to be aggregated into a composite score. As a matter of fact, although the combination of more metrics in a composite index involves losses of information, composite indicators are increasingly

adopted in the context of sustainable development, as they allow for the simultaneous evaluation of multiple aspects, which can then be summarized into a single comparable index (Singh et al., 2009). However, the aggregation can be difficult if different measurement units are used when evaluating different indicators, which is typical in the context of sustainability because of the evaluation of different perspectives. Furthermore, some indicators may have a qualitative/subjective nature, while other ones can be measured in quantitative terms (Singh et al., 2009). Finally, to be meaningful, indicators often need to be compared to a reference value, e.g. a threshold or benchmark, because of the need for assessing how a company is distant from a target (Lancker et al., 2000; Sadler, 1999; Pope et al., 2004). Indeed, the absolute numerical value of a key performance indicator (KPI) can obviously change depending on the company examined or the industry field, and therefore, it tells very little about the sustainability level of a company (Ugwu & Haupt, 2007). This is, for instance, the case for the company's turnover: a turnover of, e.g., 1,000,000 €/year can be judged as high in a specific market and low in a different one, with a different impact on the economic sustainability.

1.3. Contribution of the paper

In the attempt to solve some of the issues described above, this paper proposes an evaluation model for sustainability, grounded on the technique for order preference by similarities to ideal solution (TOPSIS) (Chen & Hwang, 1992). TOPSIS is based on the logical consideration that the most suitable result of a problem should be as closest as possible to the *Positive Ideal Solution* (PIS) and as far as possible from the *Negative Ideal Solution* (NIS). The corresponding computational procedure is therefore effective in evaluating how far the sustainability performance of a company is from the ideal situation of a fully sustainable company and to the negative situation of a poorly sustainable company. This automatically determines a benchmark for the assessment and solves one of the issues related to the evaluation of sustainability. In the proposed approach, TOPSIS is also integrated with fuzzy logic, with the purpose of overcoming the issue of subjectivity in the evaluation of corporate sustainability and the difficulty of providing a quantitative assessment to some of the sustainability KPIs. The use of fuzzy logic for the assessment of sustainability was originally suggested by Phillis and Andriantiatsaholiniaina (2001) and Andriantiatsaholiniaina et al. (2004), although not at the company's level. Examples of the evaluation of the company's sustainability through fuzzy logic can be found in Böhringer & Jochem (2007), Kouikoglou & Phillis, (2011), Philips & Davis (2009), Bottani et al. (2017).

1.4. Organization of the paper

The remainder of the paper is organized as follows. Section 2 details the methodologies used in this paper, including fuzzy logic, TOPSIS and the definition of the KPIs used for sustainability assessment. Section 3 describes the application of the approach to a sample company, taken as a case study for testing purpose. Section 4 concludes by indicating the main pros/cons of the proposed approach, the implications and limitations of the tool and identifying future research activities.

2. MATERIAL AND METHODS

This section introduces some fundamentals of fuzzy sets theory (Zadeh, 1965) and operations of fuzzy numbers are introduced, as well as the basic of the TOPSIS approach (Chen and Hwang, 1992; Hwang and Yoon, 1981).

2.1. Fuzzy logic

A fuzzy set A in the universe of discourse X is characterised by a membership function $\mu_A(X)$ ranging in the interval [0,1], which measures the grade of membership of a generic element $x \in X$ to the fuzzy set A. The closer the membership value to 1, the higher the grade of membership of x to A.

In a crisp approach, an element x either belongs to or does not belong to a generic crisp set A, and thus a sharp distinction exists between members and non-members of this set. Conversely, in a fuzzy approach, the definition of a membership function implies that the distinction between members and non-members is not so clear-cut. In other words, the same element x may belong to distinct fuzzy sets A and B, with different degrees of membership. Yet, this type of reasoning is typical of human beings, who do not fix sharp borders between members and non-members of sets.

Two important additional concepts in fuzzy reasoning are convexity and normality.

A fuzzy set A is defined as convex if and only if:

$$\mu_A(\lambda x_1 + (1-\lambda)x_2) \geq min\{\mu_A(x_1); \mu_A(x_2)\}$$
$$\forall \lambda \in [0,1], \forall x_1, x_2 \in X$$

A fuzzy set A is defined as normal if and only if

$$\exists x_i \in X | \mu_A(x_i) = 1$$

A fuzzy number n is defined as a fuzzy subset in the universe of discourse X that is both normal and convex, and whose membership function is continuous. A triangular fuzzy number a is defined by a triplet of values (l_a, m_a, u_a), which denote its lower, modal and upper value. Tts membership function should satisfy the following set of formulae:

$$\mu_A(x) = \begin{cases} \dfrac{x - l_a}{m_a - l_a} & for\ x \in [l_a, m_a] \\ \dfrac{u_a - x}{u_a - m_a} & for\ x \in [m_a, u_a] \\ 0 & otherwise \end{cases}$$

Operations with triangular numbers were firstly introduced by Zadeh, (1965); however, an exhaustive review of properties when operating with fuzzy

numbers can be found in Zimmermann, (1991). For the sake of clarity, some of the fundamentals are:

$$a \oplus b = (l_a + l_b, m_a + m_b, u_a + u_b)$$
$$a \otimes b = (l_a l_b, m_a m_b, u_a u_b)$$
$$-a = (-u_a, -m_a, -l_a)$$
$$\frac{1}{a} \cong \left(\frac{1}{u_a}, \frac{1}{m_a}, \frac{1}{l_a}\right)$$
$$\ln(a) \cong (\ln(l_a), \ln(m_a), \ln(u_a))$$

where $a = (l_a, m_a, u_a)$, and $b = (l_b, m_b, u_b)$, are triangular fuzzy numbers with lower, modal and upper values equal to l, m, u, respectively.
Finally, the distance $d(a,b)$ between two triangular fuzzy numbers $a = (l_a, m_a, u_a)$, and $b = (l_b, m_b, u_b)$, can be calculated as follows:

$$d(a,b) = \sqrt{\frac{1}{3}[(l_a - l_b)^2 + (m_a - m_b)^2 + (u_a - u_b)^2]}$$

It can be seen that $d(a,b)$ is a crisp, real positive number.
The definition given implies that a approaches b when $d(a,b) \cong 0$, while $a = b$ if and only if $d(a,b) = 0$. Moreover, given three fuzzy numbers $a = (l_a, m_a, u_a)$, $b = (l_b, m_b, u_b)$ and $c = (l_c, m_c, u_c)$, b is closer to a than the other fuzzy number c if and only if $d(a,b) < d(a,c)$.

2.2. Fuzzy TOPSIS

The TOPSIS method is a linear weighting technique which was first proposed in its crisp version by Chen and Hwang (1992), with reference to Hwang and Yoon (1981). Since then, this method has been widely adopted to solve multi-criteria decision making (MCDM) problems in many different fields. Its general extension for group decision making problems under fuzzy environment was elaborated by Chen (2000).
TOPSIS has some important characteristics which have led to its choice as a suitable tool for sustainability assessment. First, TOPSIS is the unique MCDM method that approaches the evaluation issue on the basis of the logical consideration that the most suitable solution should be the closest to the PIS and the farthest from the NIS. The distances may be either summed up in the Euclidean sense or pondered, hence prioritizing one of the two distances. In the specific case of sustainability evaluation, the computational procedure is effective in evaluating how far the sustainability performance reached by a company is from the ideal situation of a fully sustainable company or to the negative situation of a poorly sustainable company. This automatically determines a benchmark for the assessment and therefore solves one of the typical issues of sustainability assessment.
Second, the method is intuitive, easy to understand and to implement. All these issues are of fundamental importance for a direct field implementation of the any evaluation methodology. Moreover, it allows the straight linguistic definition of weights and ratings under each criterion, without the need of pairwise comparisons and the risk of inconsistencies.
On the other hand, TOPSIS requires the evaluation criteria to be monotonic. A criterion is monotonic if and only if an alternative which scores more (less) versus a criterion is preferable to the one which scores less (more). Monotonic criteria could be classified either as benefits *(B)* or costs *(C)*: a criterion can be classified as a benefit if the more desirable the candidate, the higher its score versus this criterion. On the contrary, cost criteria see the most desirable candidate scoring at the lowest.
The application of the TOPSIS approach follows the steps listed below.

Step 1. The first step consists in pooling the performance judgements and the weights given by p DMs $(k = 1, \dots, p)$. The following equations can be applied to obtain the aggregate fuzzy decision matrix $X\ [x_{i,j}]_{mxn}$ and the aggregate fuzzy weight vector $W\ [w_j]_{1xn}$

$$x_{i,j} = \frac{1}{p}\left(x_{i,j,1} \oplus \dots \oplus x_{i,j,k} \oplus \dots \oplus x_{i,j,p}\right)$$
$$w_j = \frac{1}{p}\left(w_{j,1} \oplus \dots \oplus w_{j,k} \oplus \dots \oplus w_{j,p}\right) \quad (1)$$

Step 2. Once weights and performance have been pooled, the aggregate fuzzy decision matrix X is then normalized and the fuzzy normalized decision matrix $R\ [r_{i,j}]_{mxn}$ is obtained.

$$R = \begin{array}{c|ccc} & C_1 & C_j & C_n \\ \hline A_1 & r_{1,1} & r_{1,j} & r_{1,n} \\ A_i & r_{i,1} & r_{i,j} & r_{i,n} \\ A_m & r_{m,1} & r_{m,j} & r_{m,n} \end{array} \quad (2)$$

The aim of normalization is twofold: on the one hand, normalization is necessary to compare heterogeneous criteria, on the other, normalization ensures that triangular fuzzy numbers all range within the interval [0,1].
In the normalization process, different equations have to be applied to benefit criteria and to cost criteria. The following formulae are used respectively:

$$r_{i,j} = \frac{x_{i,j}}{u_j^+} = \left(\frac{l_{x_{i,j}}}{u_j^+}; \frac{m_{x_{i,j}}}{u_j^+}; \frac{u_{x_{i,j}}}{u_j^+}\right) \; for\ j \in B$$
$$r_{i,j} = \frac{l_j^-}{x_{i,j}} = \left(\frac{l_j^-}{u_{x_{i,j}}}; \frac{l_j^-}{m_{x_{i,j}}}; \frac{l_j^-}{l_{x_{i,j}}}\right) \; for\ j \in C$$

where
$$u_j^+ = max\{u_{i,j}, i = 1, \dots m, j \in B\}$$
$$l_j^+ = min\{l_{i,j}, i = 1, \dots m, j \in C\} \quad (3)$$

Step 3. The third step requires the fuzzy normalized decision matrix R to be weighted. A fuzzy weighted normalized decision matrix V $[v_{i,j}]_{mxn}$ is obtained

$$V = \begin{array}{c|ccc} & C_1 & C_j & C_n \\ \hline A_1 & v_{1,1} & v_{1,j} & v_{1,n} \\ A_i & v_{i,1} & v_{i,j} & v_{i,n} \\ A_m & v_{m,1} & v_{m,j} & v_{m,n} \end{array} \quad (4)$$

where $v_{i,j} = r_{i,j} \otimes w_j \; \forall i = 1,\dots,m; \; \forall j = 1,\dots,n$ this matrix, each element $v_{i,j}$ is a fuzzy normalized number which ranges within the interval [0,1].

Step 4. The fourth step is aimed at determining the fuzzy positive ideal solution A^+ and the fuzzy negative ideal solution A^-. The following equations are used:

$$A^+ = \left(v_1^+, \dots v_j^+, \dots v_n^+\right)$$
$$A^- = \left(v_1^-, \dots v_j^-, \dots v_n^-\right)$$

Where

$$v_1^+ = \begin{cases} (1,1,1) \; for \; j \in B \\ (0,0,0) \; for \; j \in C \end{cases}$$
$$v_1^- = \begin{cases} (0,0,0) \; for \; j \in B \\ (1,1,1) \; for \; j \in C \end{cases} \quad (5)$$

Step 5. The n-dimensional separation distances of each alternative $i = 1, \dots, m$ to the fuzzy PIS A^+ $(d_{i+}) \in R$ and to the fuzzy NIS A^- $(d_{i-}) \in R$ are computed:

$$d_{i+} == \sum_{j=1}^{n} d(v_1^+; v_{i,j}) == \sum_{j=1}^{n} \sqrt{\frac{1}{3}\left[(l_{i,j} - l_j^+)^2 + (m_{i,j} - m_j^+)^2 + (u_{i,j} - u_j^+)^2\right]}$$

$$d_{i-} == \sum_{j=1}^{n} d(v_1^-; v_{i,j}) == \sum_{j=1}^{n} \sqrt{\frac{1}{3}\left[(l_{i,j} - l_j^-)^2 + (m_{i,j} - m_j^-)^2 + (u_{i,j} - u_j^-)^2\right]} \quad (6)$$

Step 6. Finally, for each alternative A_i, a closeness index $C_{index} \in [0,1]$ is computed as follows:

$$C_{index} = \frac{d_{i-}}{d_{i+} + d_{i-}} \quad (7)$$

C_{index} scores 0 if and only if $d_{i-} = 0$, i.e. $A_i = A^-$; in the same way, C_{index} scores 1 when $d_{i+} = 0$, i.e. that is $A_i = A^+$. In a MCDM problem, whose goal is to identify the best alternative $A_{optimal}$, this latter is the one whose C_{index} is closest to 1.

2.3. Sustainability KPIs

No matter the computational procedure used, evaluating the sustainability level of a company requires the following preliminary steps:

Step 1. Choice of the appropriate key performance indicators (KPIs).

Step 2. Identification of an appropriate measure for each KPI

Step 3. Identification of a benchmark (if required) for the evaluation of the company's performance

The identification of KPIs for the evaluation of sustainability is not straightforward. Hassini et al. (2012) reviewed the available literature on sustainability assessment, to derive appropriate indices for measuring the performance of each business process, providing a quantitative assessment of sustainability in a real context. Ahi and Searcy (2015) have carried out a detailed review of 445 articles, with the aim of identifying the main indices for sustainability assessment, according to its 3 perspectives. They identified 2555 unique metrics, most of which appeared only once in the literature, thus demonstrating that there is no consensus about indexes for sustainability assessment. Tajbakhsh and Hassini (2015) proposed a data envelopment analysis (DEA) to assess the sustainability of supply chain operations, related to economic, social and environmental perspectives. In general terms, from an economic point of view researchers have focused mainly on the total supply chain cost, while from an environmental point of view, the typical approach is to use appropriate methodologies that evaluate the environmental impact of a company or product. The social perspective, on the other hand, is the youngest in the context of sustainability and there is a lack of specific indicators for its assessment. Identifying the benchmark is not trivial too. In sustainability assessment, benchmarks are required to rate the total cost or environmental impact of a company compared to a target value.

For the purpose of this study, the list of suitable KPIs for sustainability assessment was adapted from Bottani et al. (2017), who also proposed a set of possible benchmark values for these KPIs.

3. MODEL APPLICATION

3.1. The context

The application of the TOPSIS approach was carried out in a real company, referred to as Company A for the sake of confidentiality. The company is an Italian manufacturer of plants for the food industry and exports its products to more than 147 countries. The company operates on an engineer-to-order (ETO) basis: any new product starts with the design of the plant and includes assembly, installation, civil works, test of the equipment at the customer's site and staff training. In Italy, Company A is leader in its market segment while, on a global basis, it ranks second among the top producers of milling plants.

3.2. Implementation and results

The list of KPIs elaborated by Bottani et al. (2017) was screened to evaluate the suitability of each KPI to evaluate sustainability in the targeted company. Then, the chosen KPIs were reorganized following into the three sustainability perspectives, i.e. economic, environmental and social, and identifying the cost (C)

and benefit (B) indexes. Overall, 37 KPIs were used in the evaluation ($j = 37$), including 7 costs and 30 benefits. The full list of KPIs, their description and the related benchmark is provided in Appendix.

The scores of Company A against each KPIs were derived during an interview with company's managers operating in different business units. The numerical values of these KPIs are not reported in this paper, as many data are economic and therefore subject to confidentiality.

The scores were translated into linguistic judgements according to a 5-point scale, from very low – VL to very high – VH. Four DMs were involved in the evaluation ($p = 4$). Triangular fuzzy numbers were used to express the judgement, using the scale proposed below:

VL: (0; 0.1; 0.25)
L: (0.1; 0.25; 0.4)
M: (0.4; 0.5; 0.6)
H: (0.6; 0.75; 0.9)
VH: (0.75; 0.9; 1).

The same scale was used to express the relative importance of each KPI. w_j and $x_{i,j}$ were then obtained applying eq.1.

The $x_{i,j}$ values were normalized following the computational procedure described in eq.3 and distinguishing among cost and benefit indexes, thus obtaining the $r_{i,j}$ values. Then, the $v_{i,j}$ values were computed by multiplying the $r_{i,j}$ values and the weight of each KPI, as expressed in eq.4.

The positive A^+ and negative A^- ideal solutions were easily defined for each KPI on the basis of eq.5. to be more precise, for the KPIs that do not require a benchmark (e.g. delivery flexibility or product customization), the PIS is obviously determined as 100% (1,1,1 in terms of fuzzy numbers) while the negative ideal solution is 0% (0,0,0 in terms of fuzzy numbers). For those KPIs for which an absolute benchmark does not exist (e.g., sales growth), the best competitor (Company B) is used as the benchmark. Under this circumstance, the performance of the best competitor was also retrieved. The AIDA database was used to derive the most recent economic figures of Company B. For social or environmental KPIs, the performance of Company B was derived from direct contacts with the company. Again, the performance values of Company B are not reported in this paper, for confidentiality. The PIS and NIS are determined by comparing the score of Company A and of its best competitor. For those KPIs for which an official benchmark exists, this latter is taken as the PIS.

Using eq.6, the distance between Company A and the positive and negative ideal solutions was determined. Finally, eq.7 was applied to derive the C_{index}, which summarizes the distance between the sustainability performance of Company A and that of the positive/negative ideal solutions. To be more effective, the computation was made separately for the economic, environmental and social perspectives, so as to highlight the performance of Company A against the three sustainability pillars.

The results in table 1 were obtained.

Table 1: results of TOPSIS implementation

Perspective	d_{i+}	d_{i-}	C_{index}
Economic	6.004	11.516	0.657
Environmental	1.476	3.039	0.673
Social	3.985	7.375	0.649
Total	*11.465*	*21.930*	*0.657*

3.3. Discussion

The results proposed above show that Company A has achieved a good level of sustainability. Indeed, its distance from the PIS is always lower than the distance from the NIS.

The closeness index is similar across the three perspectives, although it is slightly higher for the environmental perspective (67.3%) and lower for the social one (64.9%). This result suggests that, to improve its sustainability level, Company A should primarily enhance its performance against the social KPIS; more precisely, Company A should look at those KPIs for which the distance from the PIS is higher, should be improved. These KPIs are: work schedule ($d_{i+} = 0.458$) and amount of local suppliers ($d_{i+} = 0.412$). Improvements in this KPIs should be privileged for implementation.

4. CONCLUSIONS

This paper has proposed a fuzzy TOPSIS model for evaluating the corporate sustainability according to the TBL approach. The use of fuzzy logic for sustainability evaluation is not new and has been proposed by researchers to overcome the issue of assessing the company's performance against qualitative sustainability KPIs. Conversely, the use of TOPSIS in the context of sustainability is original and is particularly useful to handle with the issue of comparing the company's performance with a benchmark. This is a crucial point for sustainability evaluation because, to be meaningful, the performance of a company needs to be compared to a reference value, e.g. a threshold or benchmark, to assess how the company is distant from a target. Conversely, absolute performance values are often meaningless as they can significantly vary depending on the context or other variables (e.g. the company's size) and therefore tell very little about the sustainability level of the company. The structure of TOPSIS, which is grounded on the identification of a positive ideal solution and a negative ideal solution, automatically offers a suitable benchmark to evaluated the sustainability performance of a company.

The proposed approach has been tested on a real firm, operating in the food machinery industry. The application has shown that the proposed approach has some strong points but also some limitations. These latter mainly refer to the need for preliminary identifying the meaningful KPIs and their measurement

unit, and the need for a wide amount of data e.g. (company's performance, benchmark…), which are required for the application of the proposed approach. These issues are actually the typical concerns to be faced when trying to evaluate the sustainability level of a company. On the contrary, an interesting strong point is that the proposed approach allows the computation of a normalized synthesis index (i.e. the closeness index), which summarizes the sustainability level reached by a company. At the same time, the closeness index can also be computed separately for the economic, environmental and social perspectives, which is important to prioritize interventions for improving the sustainability level of the company.

Starting from this paper, future research activities should be directed towards the creation of an intelligent tool, for instance in Microsoft Excel, that allows automating the computational procedure proposed in this paper, so as to facilitate the practical application of the model developed. Moreover, the results returned by the proposed approach could be compared with other approaches available in literature (e.g. Bottani et al. 2017), for a better evaluation of the potential of the proposed approach.

ACKNOWLEDGMENTS

This research was supported by the research Grant No. D92I15000210008 (project code RBSI14L97M), called "ESCALATE—Economic and Environmental Sustainability of Supply Chain and Logistics with Advanced Technologies", funded by the Italian Ministry of University and Research under the SIR (Scientific Independence of young Researchers) 2014 program (decree of 23 January 2014, No. 197) and awarded to the first author.

REFERENCES

Andriantiatsaholiniaina, L.; Kouikoglou, V.; Phillis, Y. Evaluating strategies for sustainable development: Fuzzy logic reasoning and sensitivity analysis. Ecol. Econ. 2004, 48, 149–172.

Associazioni Sindacali, Contratto Collettivo Nazionale di Lavoro (CCNL) Settore Metalmeccanico per le Lavoratrici & i Lavoratori addetti all'industria metalmeccanica privata & alla installazione di impianti. 2016. Available online: http://www.contrattometalmeccanici.it (accessed on 9 February 2017)

Böhringer, C.; Jochem, P. Measuring the immeasurable—A survey of sustainability indexes. Ecol. Econ. 2007, 63, 1–8.

Bossel, H. Indicators for Sustainable Development: Theory, Method, Applications; Balaton Group (International Institute for Sustainable Development): Winnipeg, MB, Canada, 1999. Available online: http://publ.ext.zalf.de/web/lsa_ergebnisse_agstruk_indikatoren/pdfs%5Cbalatonreport.pdf (accessed on 28 January 2017)

Bottani, E.; Gentilotti, M.C., Rinaldi, M. A fuzzy logic-based tool for the assessment of corporate sustainability: a case study in the food machinery industry. Sustainability, 2017, 9(4), DOI: 10.3390/su9040583

Chen, S.J.; Hwang, C.L. Fuzzy Multiple Attribute Decision Making: Methods and Applications. Springer-Verlag, Berlin, 1992

Colla, V.; Branca, T.; Vannucci, M.; Fornai, B.; Amato, A. Quantitative sustainability assessment through key performance indicators in ULCOS project. In Proceedings of the 2nd International Seminar on Society & Materials (SAM2), Nantes, France, 24–25 April 2008.

CSR Manager Network Italia & Istat, Oltre il Dato Finanziario: Imprese & Benessere Collettivo. 2013. Available online: http://download.terna.it/terna/0000/0064/05.pdf (accessed on 9 February 2017)

Dyllick, T.; Hockerts, K. Beyond the business case for corporate sustainability. Bus. Strategy Environ. 2002, 11, 130–141

Fraunhofer Institute for Reliability and Microintegration, Energy-Using Product Group Analysis—Lot 5: Machine Tools and Related Machinery. 2012. Available online: http://www.eupnetwork.de/fileadmin/user_upload/Produktgruppen/Lots/Final_Documents/EuP_Lot5_Task3_March2012 .pdf (accessed on 31 January 2017).

Goldman, T.; Gorham, R. Sustainable urban transport: Four innovative directions. Technol. Soc. 2006, 28, 261–273.

Harris, J.; Kennedy, S. Carrying capacity in agriculture: Global and regional issues. Ecol. Econ. 1999, 29, 443– 461.

Health and Safety Executive, European Comparison. 2016. Available online: http://www.hse.gov.uk/statistics/european/european-comparisons.pdf?pdf=european-comparisons (accessed on 31 January 2017).

Hervani, A.; Helms, M.; Sarkis, J. Performance measurement for green supply chain management. Benchmarking 2005, 12, 330–353

Istat, "Nero a Metà": Contratti Part-Time & Posizioni Full-Time fra i Dipendenti delle Imprese Italiane. 2014. Available online: http://www.istat.it/it/files/2014/09/IWP-n.-3-2014.pdf (accessed on 14 October 2016)

Kates, R.; Clark, W.; Corell, R.; Hall, M.; Jaeger, C.; Lowe, I.; McCarthy, J.; Schellnhuber, H.; Bolin, B.; Dickson, N.; et al. Sustainability science. Science 2001, 292, 641–642.

Kouikoglou, V.; Phillis, Y. Application of a fuzzy hierarchical model to the assessment of corporate social and social sustainability. Corp. Soc. Responsib. Environ. Manag. 2011, 18, 209–219.

Lancker, E.; Nijkamp, P. A policy scenario analysis of sustainable agricultural development options: A

case study for Nepal. Impact Assess. Proj. Apprais. 2000, 18, 111–124.
Phillis, Y.; Andriantiatsaholiniaina, L. Sustainability: An ill-defined concept and its assessment using fuzzy logic. Ecol. Econ. 2001, 37, 435–456.
Phillis, Y.; Davis, B. Assessment of Corporate Sustainability via Fuzzy Logic. J. Intell. Robot. Syst. 2009, 55, 3–20.
Pope, J.; Annandale, D.; Morrison-Saunders, A. Conceptualising sustainability assessment. Environ. Impact Assess. Rev. 2004, 24, 595–616.
Sadler, B. A framework for environmental sustainability assessment and assurance. In Handbook of Environmental Impact Assessment; Blackwell: Oxford, UK, 1999; pp. 12–32.
Searcy, C. Measuring enterprise sustainability. Bus. Strategy Environ. 2016, 25, 120–133
Seuring, S.; Gold, S. Sustainability management beyond corporate boundaries: From stakeholders to performance. J. Clean. Prod. 2013, 56, 1–6.
Singh, R.; Murty, H.; Gupta, S.; Dikshit, A. An overview of sustainability assessment methodologies. Ecol. Indic. 2009, 9, 189–212
Ugwu, O.O.; Haupt, T.C. Key performance indicators and assessment methods for infrastructure sustainability—a South African construction industry perspective. Build. Environ. 2007, 42, 665–680.

AUTHOR BIOGRAPHY

Eleonora BOTTANI is Associate professor in Mechanical Industrial Plants at the Department of Engineering and Architecture of the University of Parma. She graduated (with distinction) in Industrial Engineering and Management in 2002, and got her Ph.D. in Industrial Engineering in 2006, both at the University of Parma. During the studies, she was awarded as the best student of the Industrial Engineering and Management class for 4 subsequent academics years, from 1998/1999 to 2001/2002. Her research activities concern logistics and supply chain management issues. She is author (or co-author) of more than 160 scientific papers, referee for more than 60 international journals, editorial board member of five scientific journals, Associate Editor for one of those journals, and editor-in-chief of a scientific journal.

Marta RINALDI is a Research Fellow at the Department of Engineering and Architecture of the University of Parma. She graduated (with distinction) in Industrial Engineering and Management in 2011 and got a Ph.D. in Industrial Engineering in 2015. From 2011 to 2014, she was scholarship holder at the Interdepartmental Center CIPACK. She currently works on discrete event simulation and its application to industrial plants, manufacturing systems and business processes, and is author of more than 20 papers in this field.

Federico SOLARI is a Research Fellow at the Department of Engineering and Architecture of the University of Parma. He got a Ph.D. in Industrial Engineering at the University of Parma with a thesis entitled “Advanced approach to the design of industrial plants by means of computational fluid dynamics”. He previously got a Master Degree in Food Industry Mechanical Engineering at the same University, discussing a thesis related to the design of a plant for the volatile compounds extraction. He achieved his Ph.D. He attended several conferences related to food process, modelling and simulation. He published several papers on the same topics on international journal and conferences.

APPENDIX

Table A1: details of KPIs, benchmark, performance and weights for TOPSIS implementation.

KPI	Definition	Benchmark type	Type of KPI	Perspective	w_j	$x_{i,j}$	Benchmark	d_{i+}	d_{i-}
Delivery flexibility	Ratio between the number of times the request to change the date for delivery is satisfied and the total requests	the higher the better	benefit	economic	VH	H	VH	0.320	0.721
Customization	Ratio between the number of times the request of personalization is satisfied and the total requests	the higher the better	benefit	economic	H	L	VH	0.549	0.365
Warehouse turnover rate	Number of times per months where the items rotates, i.e. they are replaced in the warehouse. The higher the number of rotations, the higher the capacity of the company to recover the financial resources invested in the production of the good	best competitor	benefit	economic	H	H	VH	0.370	0.647
Rate of multiple sourcing	Percentage of supplies for which a multiple-sourcing strategy is adopted. This KPI evaluates the risk of a supplier's failure: the higher is the number of different suppliers, the lower is the risk of supplier's failure	the higher the better	benefit	economic	VH	M	VH	0.362	0.545
Sale growth	The increase in the company's sale compared to the previous year	best competitor	benefit	economic	VH	VH	VL	0.275	0.811
Market share	The share of the company's sales compared to the total market's sales	best competitor	benefit	economic	VH	H	M	0.320	0.721
ROI	A financial performance referred to the company's balance sheet, computed as the ratio between the net income and the amount of capital invested	best competitor	benefit	economic	H	H	H	0.370	0.647
Cost of sales/Turnover	Ratio between the total cost of the items manufactured and sold (from the company's balance sheet) and the company's turnover	best competitor	cost	economic	VL	H	H	0.000	0.577
Inventories/Turnover	Ratio between the economic value of the amount of stocks (from the company's balance sheet) and the company's turnover	best competitor	benefit	economic	H	M	VH	0.412	0.496
Net profit	A measure of the company's profitability and is taken from the company's balance sheet	best competitor	benefit	economic	H	H	VH	0.370	0.647
Fill rate	The number of units filled as a percentage of the total ordered	best competitor	benefit	economic	VL	L	VH	0.592	0.183
Unitary labour cost	Average cost of a standard employee	best competitor	cost	economic	VL	M	M	0.000	0.577
ROE	The amount of net income returned as a percentage of shareholders' equity.	best competitor	benefit	economic	H	H	M	0.370	0.647
Net working capital	The aggregate amount of all current assets and current liabilities	best competitor	benefit	economic	H	H	VH	0.370	0.647
ROS	The percentage of total revenue that is converted into operating profits	best competitor	benefit	economic	VH	H	VH	0.320	0.721
Production cost	The costs incurred by a business when manufacturing a good or providing a service	best competitor	cost	economic	VL	M	L	0.000	0.577
Asset value	The value of an entity's assets minus the value of its liabilities	best competitor	benefit	economic	VH	H	VH	0.320	0.721
Total cash and cash equivalents	The most liquid current assets found on a business's balance sheet.	best competitor	benefit	economic	M	VH	M	0.362	0.545
Net equity	The difference between the fair market value of business assets and its liabilities.	best competitor	benefit	economic	VH	H	M	0.320	0.721
Carbon footprint	Amount of greenhouse gas emission of the products manufactured by the company	official benchmark: EPD certification of food machines (e.g. Fraunhofer Institute for Reliability and Microintegration, 2012).	cost	environmental	VL	M	H	0.000	0.577
Eco-design	Percentage of products realized applying environmentally sustainable design concepts	the higher the better	benefit	environmental	M	L	VH	0.556	0.293
Packaging recycling rate	Percentage of packaging material recycled	the higher the better	benefit	environmental	VH	H	VH	0.320	0.721
Packaging non-	Percentage of packaging material disposed in landfill	the higher the better	cost	environmental	VH	H	VH	0.000	0.577

recycling rate									
Unitary emissions for transport	Unitary emissions associated to the transport activities	best competitor	cost	environmental	M	H	H	0.000	0.577
Investments in R&D for environment	Amount of capital invested in R&D for environmental efficiency	best competitor	benefit	environmental	VH	VL	L	0.599	0.293
Number of employees	Percentage of full-time workers out of the total amount of employees	best competitor	benefit	social	VH	H	M	0.320	0.721
Profit per employee	Ratio between the amount of sales and the cost of the employees	best competitor	benefit	social	H	H	VH	0.370	0.647
Work injury	Ratio between the number of days in which work injuries occurred and the total number of working days	official benchmark: standardised accident rates of Europe (Health and Safety Executive, 2016).	cost	social	VL	M	M	0.000	0.577
Employment gender ratio	Percentage of female workers respect to the male workers	official benchmark: average percentage of women at work in Italy (CSR Manager Network Italia & Istat, 2013)	benefit	social	VH	H	H	0.320	0.721
Work schedule	Average number of hours worked per week by an employee	official benchmark: collective labour agreement for the mechanical industry (Associazioni Sindacali, 2016)	benefit	social	M	M	M	0.458	0.386
Salary	Average annual cost per employee	official benchmark: collective labour agreement for the mechanical industry (Associazioni Sindacali, 2016)	benefit	social	VH	M	M	0.362	0.545
Safety training	Percentage of workers who attend training courses on safety and emergency procedures	the higher the better	benefit	social	VH	H	H	0.320	0.721
Full-time workers	Percentage of full-time workers out of the total amount of employees	official benchmark: average percentage of full-time workers in Italy (Istat, 2014)	benefit	social	H	H	VH	0.370	0.647
Temporal working continuity	Ratio between the number of new hired workers and of layoffs in one working year	best competitor	benefit	social	VH	M	H	0.362	0.545
Local suppliers	Ratio between the number of local suppliers and the total number of suppliers	best competitor	benefit	social	H	M	H	0.412	0.496
Local workers	Ratio between the number of local workers and the total number of employees	best competitor	benefit	social	VH	H	VH	0.320	0.721
Sustainable suppliers	Percentage of suppliers that are evaluated and selected taking into account their orientation towards sustainability	best competitor	benefit	social	H	H	M	0.370	0.647

MODELLING AND CONTROL OF A PHOTOVOLTAIC ENERGY SYSTEM WITH BATTERY STORAGE

Carlos Y. García-Ramos[(a)], Jose M. González-Cava[(a)], José F. Gómez González[(b)], Sara González Pérez[(b)], Benjamín González Díaz[(b)], Juan Albino Méndez-Pérez[(a)]

[(a)] Dep. of Computer Science and Systems Engineering, Universidad de La Laguna. APDO. 456, 38200 La Laguna, Tenerife, SPAIN
[(b)] Dep. of Industrial Engineering, Universidad de La Laguna. APDO. 456, 38200 La Laguna, Tenerife, SPAIN

[(a)]jamendez@ull.edu.es

ABSTRACT
This work presents a simulated study of the energy management of an energy system connected to the grid with photovoltaic generation and battery storage. The work proposes a energy management system based on fuzzy logic. It is intended to be used in the hotel industry. The objective of the proposed controller is to maximise the renewable power source but including also economic criteria in the management. The proposal was implemented in simulation considering a 5,1kW peak photovoltaic installation and a set of batteries with a capacity of 384Ah. First results obtained show that the system achieves the specifications proposed. Thus, the study evidences the potential of the proposed control algorithm and demonstrate the suitability of the use of intelligent techniques for the energy management in hotels.

Keywords: fuzzy logic, simulation, energy management, renewable energy

1. INTRODUCTION

The complexity of the services and resources in the hotel industry makes necessary the use of specific tools for the energy management. This type of tools apart from achieving the objective of improving the profitability of the whole installation, allows to increase its environmental sustainability.
The introduction of renewable energy requires advanced control systems to efficiently integrate these resources in the system. Thus, Energy Management Systems (EMS) arise to monitor , control and optimise the energy generation, transmission, distribution and microgrid management. accomplish this task.
For grid connected systems EMS are also responsible for controlling the power flow from and to the grid (to improve the energy self-comsumption), monitoring the network, peak shaving and economic management (Olatomiwa, Mekhilef, Ismail, & Moghavvemi 2016).
Many of the existing EMS use optimization techniques based on linear programming (Comodi, Renzi, Cioccolanti, Caresana, & Pelagalli 2015). Other methods are based on predictive control (Serale, Fiorentini, Capozzoli, Bernardini, & Bemporad, 2018). Due to the complexity of the problema, strategies based on intelligent techniques (Real-Calvo et al. 2017) have been also proposed. Among them, fuzzy logic techniques have proven to be adequate for these applications (Mohamed & Mohammed 2013; Ruban, Rajasekaran, Pasupathi, & Rajeswari 2016).
For the hotel industry, there are also specific tools for energy analysis and management as proposed in (Cabello Eras et al., 2016). In this work, a discussion about the indicators for prediction and control of the hotel energy consumption. A new proposal for an indicator is also presented to efficiently detect anomalies in the energy management. In (Mardani et al. 2016) a new decision making taking tool based on fuzzy logic is presented. Its aim is the evaluation of energy saving technologies in luxury hotels. These examples highlight the importance of advanced control algorithms to improve energy savings and efficiency in hotels.

This work intends to take a first step in the development of an integral energy management system in hotels. The framework in which this study is presented refers to energy management in hotels considering a grid-connected system, a photovoltaic generation (PV) plant and a battery energy storage system. The study will focus on the development of an intelligent system that allows to manage the flow of power in the system and properly manage the storage resource in batteries to optimize the operation of the system. The criteria with which the system will be developed focus on the maximum use of the renewable resource, trying to minimize the energy cost for the hotel. The proposal for this energy management system will be based on the use of techniques based on fuzzy logic. The study presented here is therefore intended to be a first step towards the introduction of intelligent control techniques in the field of hotel energy management.
The work begins by describing the system and the modelling aspects. Then the control system and the solution adopted for the problem is described. Finally,

the first results of this study are presented and the most important conclusions about them and future perspectives are extracted.

2. SYSTEM MODELLING

This work is intended as a first step towards the intelligent energy management in hotels. The common energy profile in hotels has some peculiarities. It presents an important energy demand during the night period and two consumption peaks at noon and late afternoon. Also, hotel consumption has a great dependency on the season. Thus, the use of EMS plays an important role in the energy management. The main variables involved are depicted in Figure 1.

As observed, the management of the system is done using information of the system state, using prediction variables (forecasts of consumption and energy generation) and taking into account the cost of energy according to the market tariifs.

The study proposed in this work considers a small-scale installation as a test bench for the design of an EMS. First results presented here do not use information of prediction variables. In future works, the design proposed will be translated to a real scale hotel.

2.1. Description of the plant components

For the simulation, a simplified model of a small-scale micro grid using Phasor solution is considered. This kind of solution, provided by specialized technology of Simscape Power Systems™ from Mathworks, allows to accelerate the simulation speed. The model employed in this paper is a modification of Hiroumi Mita's Model (https://es.mathworks.com/help/physmod/sps/examples/simplified-model-of-a-small-scale-micro-grid.html).

As well as the original model, the micro-grid is a single-phase AC network, where all the energy sources are divided in an electricity network, an array of photovoltaic panels and a battery, employed to provide and storage energy. This battery is controlled by a fuzzy controller that will be described in the next section. The interconnection between components is shown in Figure 2.

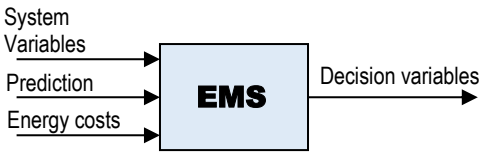

Figure 1: Input/output variables in the Energy Management System (EMS)

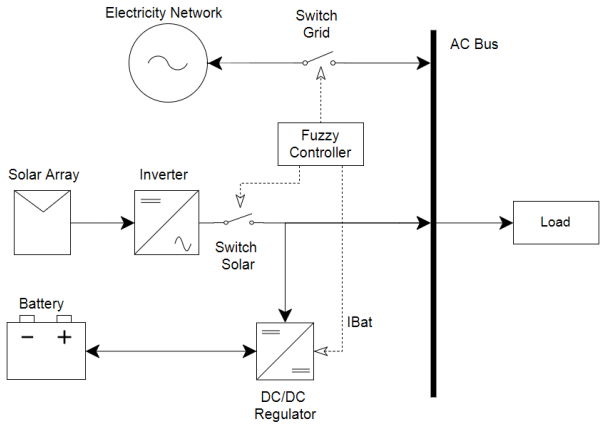

Figure 2. Schedule of the proposed system, detailing all the components and the flow power.

In contrast to the original model, our proposal includes an option to change the initial state of charge and limits the maximum and minimum state of charge. The battery, then, supplies the remaining current when the power of the micro-grid is insufficient and/or the economic conditions are favorable to do it. If there is a surplus of solar power and the price of network consumption is lower than the price of battery usage, the charge operation will be allowed.

Like the Hiroumi Mita's model, the micro-grid is connected to the power network through a transformer mounted on a post which lowers the voltage from 6.6 kV to 200 V. The solar power generation is modeled employing a 1-Dimension lookup table, whose values are 0 from 20h to 4h and reaches its peak amount (5 kW) from 14h to 15h. Data provided by this table is used to control a current source connected to the micro-grid and to a snubber resistance in parallel. This model also fits the generated current to the maximum requested current. In other words, if the load is disconnected from the micro-grid, the array of photovoltaic panels only generates the requested current by the load and the battery. The load is also modeled employing a lookup table, where the amount of electric power load reaches peak consumption at 9h (6,500 W), 19h and 22h (7,500 W). Both solar and load data used in this simulation are shown in Figure 3.

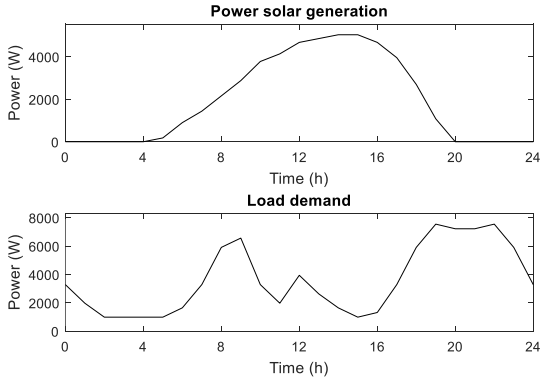

Figure 3. PV generation and load demand employed in the simulation.

3. CONTROL SYSTEM

The electrical system is managed by a fuzzy logic based controller that will be in charge of choosing the energy source to meet the demand and to define the flow rate of energy from or to the battery system.

3.1. Fuzzy notations

Artificial intelligence and, in particular, soft computing techniques have become an important tool for decision taking. Its use is not only limited to the industrial field but to other areas (González Rodríguez, Méndez, Batista, & Gonzalez-Cava 2018; Mendez et al. 2018).

In general, fuzzy logic refers to the fuzzy set theory, where object classes have limits that are not clearly defined (fuzzy). The membership of one variable to these sets is defined through membership degrees (from 0 to 1). In this way, fuzzy logic has become an important tool to exploit the tolerance to vagueness, uncertainty and partial truth to achieve robustness and find low cost solution (Lotfi a. Zadeh 1994).

For the decision taking in this work, a fuzzy controller based on Mamdani inference was considered (Passino & Yurkovich 1998). Consider the fuzzy system defined by n input variables u_i, $i = 1, 2, \ldots, n$ and m output variables y_i with $i = 1, 2, \ldots, m$, expressed by the linguistic variables. Each linguistic variable takes values from the linguistic set $(\tilde{A}_i, \tilde{B}_i)$ denoted, for each input and output, respectively as:

$$\tilde{A}_i = \{\tilde{A}_i^j : j = 1,2, \ldots N_i\}, \quad (1)$$

$$\tilde{B}_i = \{\tilde{B}_i^p : p = 1,2, \ldots M_i\} \quad (2)$$

Each variable relates to a linguistic value by means of the membership function $\mu(u_i)$ that takes values between 0 and 1 according to the degree of membership to corresponding set. The relation between inputs and outputs is given by the inference system consisting of a set of IF-THEN rules:

$$\boldsymbol{If}\ \tilde{u}_1 is\ \tilde{A}_1^j\ \boldsymbol{and}\ \tilde{u}_2 is\ \tilde{A}_2^k, \boldsymbol{and}, \ldots\ \boldsymbol{and}, \tilde{u}_n is\ \tilde{A}_n^l$$
$$\boldsymbol{then}\ \tilde{y}_q\ is\ \tilde{B}_q^p$$

The last part of the fuzzy system is the defuzzification stage, where fuzzy variables are converted to crisp values. The method considered here for defuzzification is the center of gravity method (COG) defined by:

$$y_q^{crisp} = \frac{\sum_{i=1}^{R} b_i^q \int_{y_q} \mu_{\hat{B}_q^i}(y_q) dy_q}{\sum_{i=1}^{R} \int_{y_q} \mu_{\hat{B}_q^i}(y_q) dy_q}, \quad (3)$$

where R is the number of rules. This expression represents the center of the area defined by the membership function associated to the implicit fuzzy set of the i-th rule. The integral term refers to the area under $\mu_{\hat{B}_q^i}(y_q)$.

3.2. Fuzzy controller

As commented, the implementation of the EMS is done using fuzzy logic models. The proposed system will be responsible to select the best energy source according to the state of the system and to economical criteria. Also battery charge management is defined by the fuzzy inference system.

To cope with the intervariability of the hotels (according to the different characteristics of each specific hotel), the inputs were defined as normalized ratio variables. This will make easier the use of the controller in different scenarios. its own characteristics.

Three input variables were considered in the controller:

- ***SOCr***: ratio between the state of charge of the battery and a reference value for the charge percentage. In this work, the reference value was fixed to 70% to minimize battery damages and to increase the life cycle of the battery.
- ***Pr***: ratio between power generated by the PV system and the power demand of the hotel.
- ***ECr***: ratio between the cost of the energy obtained from the grid and the energy produced by the battery. The cost of the energy directly obtained from the PV system was neglected as it is much lower than the other sources of energy.

The membership functions of the input variables are depicted in Figure 4.

The output variables considered in this work are related to the selection of the source of energy and the charge rate of the battery. Four variables were considered:

- ***BPS***: battery power source (from the PV system or from the electrical grid). The universe of discourse is defined between -1 and 1. Positive values will charge from the grid, negative values will charge from the PV system.
- ***Gb***: grid breaker. Depending on the state of the system and the prices, grid can be used or not.
- ***PVb***: photovoltaic breaker. When production is too low, the breaker is activated.
- ***Ibat***: charge rate of the battery. The universe of discourse is defined between -1 and 1. Positive values will charge the battery while negative values will discharge the battery. Charge values can have asymmetric values, that according to recent studies increase the battery life as discharge currents can be greater than charge currents (Geaney & O'Dwyer 2017).

The membership functions of the output variables are depicted in Figure 5.

Concerning the inference system, the rules where obtained by means of the information of an expert and by simulation. Figure 6 show some of the decision surface curves of the resulting fuzzy inference system.

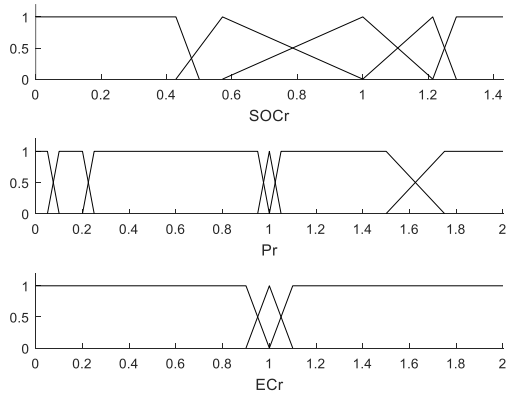

Figure 4. Input membership functions of the proposed fuzzy controller.

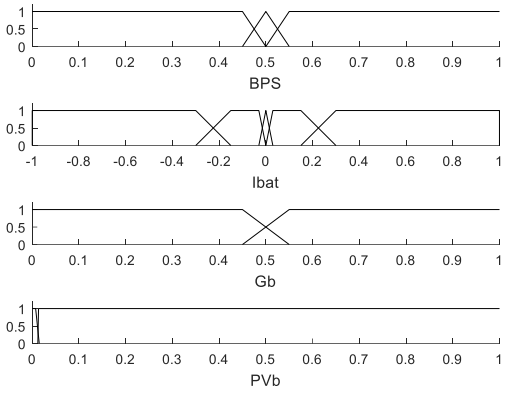

Figure 5. Output membership functions of the proposed fuzzy controller.

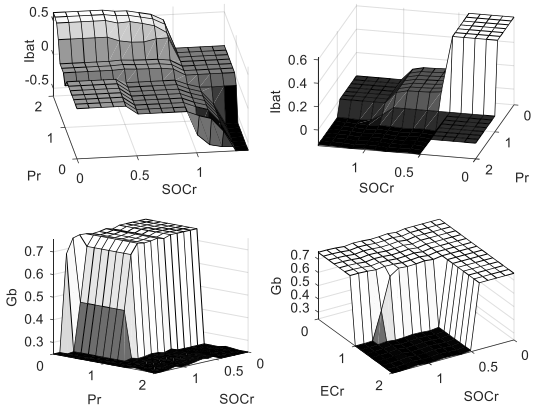

Figure 6. Some of the decision surfaces curves of the proposed fuzzy controller.

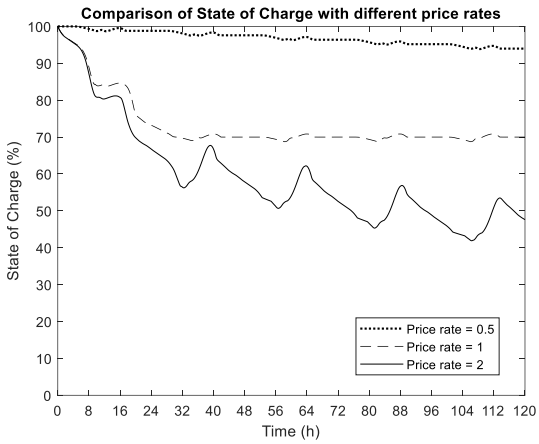

Figure 7. Battery state of charge with different ECr and initial state of charge 100%.

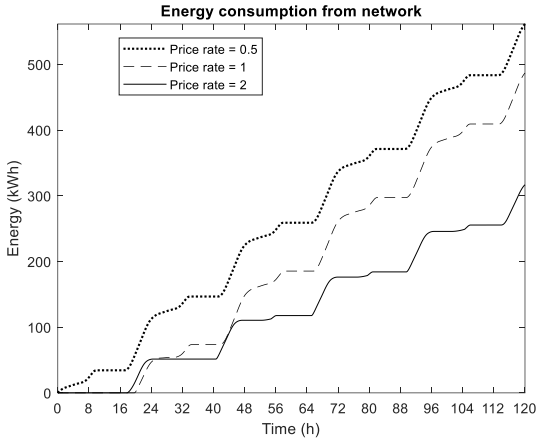

Figure 8. Energy consumption from the network with different ECr and initial state of charge 100%.

4. RESULTS

The proposal is to simulate an energy management system based in fuzzy logic and to evaluate its performance. The proposed controller was evaluated in different scenarios where variations in the meteorological conditions, initial state of charge of the battery and cost of energy was considered.

In a first experiment, a 5 days simulation interval was considered. During this interval, solar radiation has the same characteristics every day. The cost of energy ratio varies between three different tariffs: 0,5, 1,0 and 1,5. For the initial state of charge, two scenarios were considered. First scenario (scenario 1) considers an initial state of charge of 100%. In the second scenario (scenario 2) the initial state of charge is 30%. These values were considered as they are the limit values allowed for the state of charge.

Figure 7 shows the simulation of the system in scenario 1. As can be observed, according to the state of charge, this value varies significantly between the three ECr proposed. Only when the battery price and the grid price are equal, the controller tries to reach the setpoint (70%). In the other two cases, when the ECr is 0.5 the controller tries to avoid the usage of the battery, ignoring the setpoint. Finally, when the ECr has the value 2, the controller employs the battery more frequently to save economic resources, without considering the achievement of the setpoint its main goal.

This effect is also viewed in Figure 8 when the energy consumption is compared. In this case, the system generally tries to avoid the energy consumption from the network when its value is higher than the battery's one. Finally, the PV energy surplus is supplied to the network

In Figure 9 the power flow through the battery is shown. In that case, positive values refer to discharge operation, while negative values refer to charge operation. The power supplied by the battery differs greatly according to ECr. The peaks that are reached by the power flow through the battery are continuously decreasing as soon as the state of charge is being closer to the setpoint. However, the peaks that corresponds to charge operation are always constant because of the usage of the same PV data for each day.

Figure 10 shows the simulation of the system in scenario 2 (30% initial estate of charge). Likely the scenario 1, the state of charge, the power flow through the battery and the energy consumption varies according to ECr. However, the results obtained when ECr is equal to 0.5 and 1 are similar. In those cases, the controller tries to reach the setpoint charging the battery from the PV surplus and the network. In addition, it could be seen that when ECr is equal to 2, the setpoint seems to be reached in a bigger simulation interval and the battery is charged only with the PV surplus energy.

It is important to mention the difference between the energy consumption during night periods, being bigger in scenario 2 than in scenario 1 and whose aim is charging the battery. This effect is clearly visible in the first hours of simulation in Figures 8 and 11. The energy consumption also reaches a bigger value, without matter the ECr than in scenario 1.

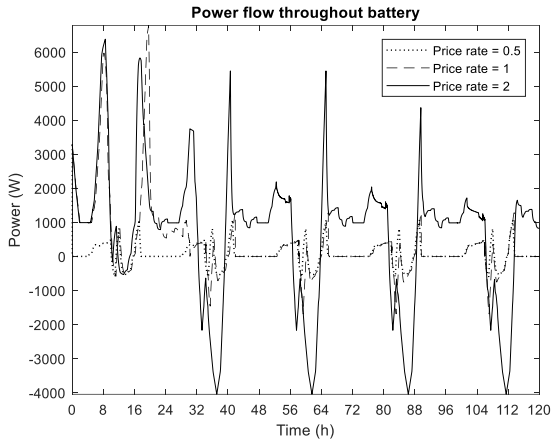

Figure 9. Power flow throughout battery with different ECr and initial state of charge 100%.

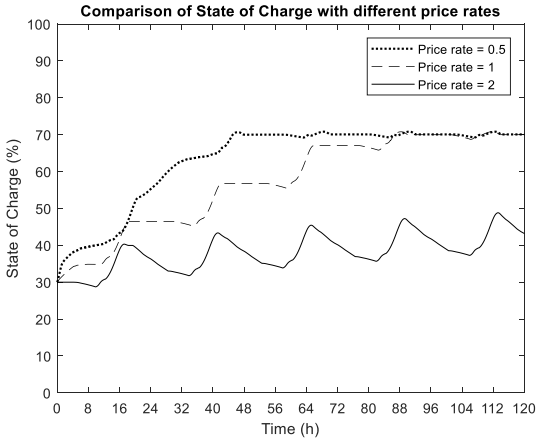

Figure 10. Battery state of charge with different ECr and initial state of charge 30%.

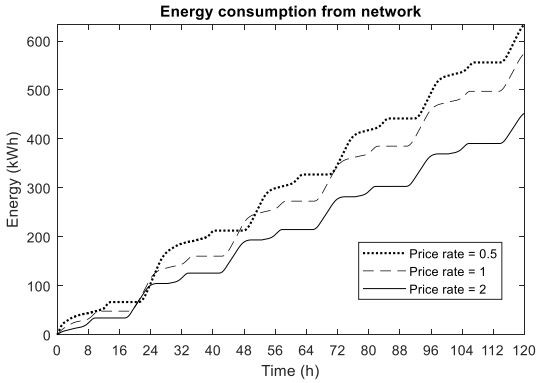

Figure 11. Energy consumption from the network with different ECr and initial state of charge 30%.

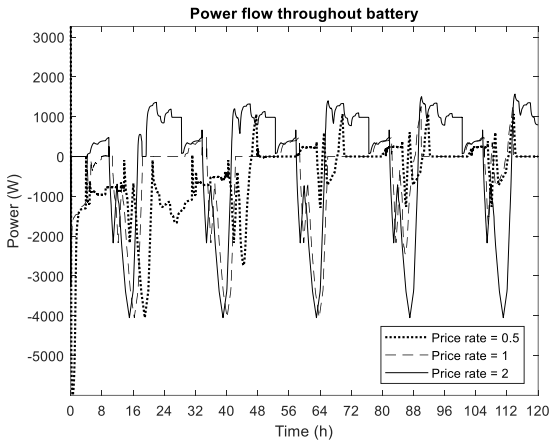

Figure 12. Power flow through the battery with different ECr and initial state of charge 30%.

Finally, in Figure 12 the power flow through the battery is shown. Positive values are much smaller in scenario 2 than in scenario 1, which means that the discharge current is lower and the remaining current is consumed from the network. The positive peaks seem to be continuously increasing their value as the state of charge increases too.
As can be seen, in both simulation scenarios the battery tries to reach the reference value when ECr is equal to 1 and has different results when ECr is 0.5, being closer to the setpoint when the initial state of charge is 30% than in the scenario 1, when the initial state of charge is 100%. When ECr is equal to 2, a more aggressive answer is shown by the system. In that case, reaching the setpoint seems more difficult, even in a bigger time interval. However, the system tries to minimize the global cost of energy consumption in every scenario and not only to reach a setpoint employed to extend battery life.

5. CONCLUSIONS

A simulation study of an energy management system was proposed. The control system designed meets the basic design specification: to optimize the management of the energy system considering economic criteria. The final system is intended to be applied in hybrid energy systems in hotels.
The controller based in fuzzy logic focuses in achieving the setpoint of the battery state of charge by selecting the best charge/discharge operation. Different simulations with two scenarios have been done with satisfactory results.
The simulation has been designed so that the power generated with the PV system is not enough to meet the demand of the proposed plant during the whole simulation period. When this happens, the system activates the grid or the battery system to meet the demand. This operation is done according to economic criteria and taking into account the state of charge of the battery.
In this work, the potential use of energy management systems based on fuzzy logic is presented. The future perspectives indicate that artificial intelligence techniques will play a central role in energy management.

ACKNOWLEDGMENTS

This work is under the auspicious of the research Project GREENTOURIST (2016TUR17) supported by Fundación CajaCanarias.

José M. González Cava has received financial support for the development of this study through the program "Formación del Profesorado Universitario" (FPU15/03347) of the Ministerio de Educación, Cultura y Deportes of the Spanish Government.

REFERENCES

Cabello Eras, J. J., Sousa Santos, V., Sagastume Gutiérrez, A., Guerra Plasencia, M. Á., Haeseldonckx, D., & Vandecasteele, C., 2016. Tools to improve forecasting and control of the electricity consumption in hotels. *Journal of Cleaner Production*, *137*, 803–812. https://doi.org/10.1016/j.jclepro.2016.07.192

Comodi, G., Renzi, M., Cioccolanti, L., Caresana, F., & Pelagalli, L., 2015. Hybrid system with micro gas turbine and PV (photovoltaic) plant: Guidelines for sizing and management strategies. *Energy*, *89*, 226–235. https://doi.org/10.1016/j.energy.2015.07.072

Geaney, H., & O'Dwyer, C. (2017). Tailoring Asymmetric Discharge-Charge Rates and Capacity Limits to Extend Li-O2 Battery Cycle Life. *ChemElectroChem*, *4*(3), 628–635. https://doi.org/10.1002/celc.201600662

González Rodríguez, G. C., Méndez, J. A., Batista, B. M., & Gonzalez-Cava, J. M., 2018. A Fuzzy Modelling Approach to Laundry Industry. In J. Kacprzyk, E. Szmidt, S. Zadrożny, K. T. Atanassov, & M. Krawczak (Eds.), Advances in Fuzzy Logic and Technology 2017: Proceedings of: EUSFLAT 2017 Springer International Publishing. https://doi.org/10.1007/978-3-319-66824-6_14.

Mardani, A., Zavadskas, E. K., Streimikiene, D., Jusoh, A., Nor, K. M. D., & Khoshnoudi, M., 2016. Using fuzzy multiple criteria decision making approaches for evaluating energy saving technologies and solutions in five star hotels: A new hierarchical framework. *Energy*, *117*, 131–148. https://doi.org/10.1016/j.energy.2016.10.076

Mendez, J. A., Leon, A., Marrero, A., Gonzalez-Cava, J. M., Reboso, J. A., Estevez, J. I., & Gomez-Gonzalez, J. F., 2018. Improving the anesthetic process by a fuzzy rule based medical decision system. *Artificial Intelligence in Medicine*, *84*, 159–170. https://doi.org/10.1016/j.artmed.2017.12.005

Mohamed, A., & Mohammed, O., 2013. Real-time energy management scheme for hybrid renewable energy systems in smart grid applications. *Electric Power Systems Research*, *96*, 133–143. https://doi.org/10.1016/j.epsr.2012.10.015

Olatomiwa, L., Mekhilef, S., Ismail, M. S., & Moghavvemi, M., 2016. Energy management strategies in hybrid renewable energy systems: A review. *Renewable and Sustainable Energy Reviews*, *62*, 821–835. https://doi.org/10.1016/j.rser.2016.05.040

Passino, K. M., & Yurkovich, S., 1998. Fuzzy Control. Addison-Wesley (Vol. 163). https://doi.org/10.3233/978-1-60750-706-2-39

Real-Calvo, R., Moreno-Munoz, A., Pallares-Lopez, V., Gonzalez-Redondo, M. J., Moreno-Garcia, I. M., & Palacios-Garcia, E. J., 2017. Sistema Electrónico Inteligente para el Control de la Interconexión entre Equipamiento de Generación Distribuida y la Red Eléctrica. *RIAI - Revista Iberoamericana de Automatica e Informatica Industrial*, *14*(1), 56–69. https://doi.org/10.1016/j.riai.2016.11.002

Ruban, A. A. M., Rajasekaran, G. M., Pasupathi, T., & Rajeswari, N., 2016. A fuzzy-logic based management system in smart-microgrid for residential applications. *1st International Conference on Emerging Trends in Engineering, Technology and Science, ICETETS 2016 - Proceedings*. https://doi.org/10.1109/ICETETS.2016.7603096

Serale, G., Fiorentini, M., Capozzoli, A., Bernardini, D., & Bemporad, A., 2018. Model Predictive Control (MPC) for enhancing building and HVAC system energy efficiency: Problem formulation, applications and opportunities. *Energies*, *11*(3). https://doi.org/10.3390/en11030631

Zadeh, L. A., 1994. Soft computing and fuzzy logic. *Software, IEEE*, (November), 48–56. https://doi.org/10.1109/52.329401

Author's index

ISBN 978-88-85741-16-4; Bruzzone, Janosy, Nicoletti and Zacharewicz Eds.